DISS. ETH NO. 22228

LEAD BIOAVAILABILITY AND EFFECTS TO PERIPHYTON

A thesis submitted to attain the degree of

DOCTOR OF SCIENCE of ETH ZURICH

(Dr. sc. ETH Zurich)

presented by

THEODORA JANINA STEWART

MSc ETH Umweltnaturwissenschaften, ETH Zürich

Born on 13.09.1985

Citizen of the United States of America

accepted on the recommendation of

Prof. Dr. Laura Sigg, examiner
Dr. Renata Behra, co-examiner
Dr. Maarten Nachtegaal, co-examiner
Prof. Dr. Bernhard Wehrli, co-examiner
Prof. Dr. Vera Slaveykova, co-examiner

2014

Table of Contents

Summary

To understand toxic biological effects of non-essential trace metals to organisms in the aqueous environment, one must be able to follow a series of complex metal interactions, both abiotic and biotic in nature, which ultimately lead to the internalization of a metal and its binding to sensitive cellular targets. We chose to work with periphyton, natural biofilm communities composed of algae, bacteria, fungi and protozoa held together in a matrix of extracellular polymeric substances (EPS). Periphyton is an important primary producer in freshwater ecosystems, which contribute to nutrient cycling and also accumulate both essential and non-essential trace metals, often reflecting dynamic fluctuations of metals in the overlying water. Using natural communities colonized with water from a small Swiss stream, the goal of this doctoral work was to understand the relationship between lead (Pb) accumulation and distribution in periphyton and the subsequent biological effects to overall community functions, as well as to understand intracellular Pb speciation upon internalization.

As the EPS is thought to have a protective mechanism against toxicity to periphytic organisms, it was of interest to develop both an EPS extraction technique and characterization method to analyze the EPS composition, as well as to determine if this composition significantly varied with season, thus possessing potentially different metal binding capacities. An extraction technique was developed that targeted the more loosely bound EPS, prevented cell lysis, and which would be amenable to later metal distribution studies. The extracted EPS from seven different communities were analyzed using liquid chromatography – organic carbon detection – organic nitrogen detection (LC-OCD-OND), a method based on size exclusion chromatography coupled with detection and quantification of organic carbon and nitrogen in the separated fractions. Four fractions were observed in all extracts: high molecular weight (M_r) biopolymers, building blocks of humic acids, low M_r acids, and low M_r neutral compounds, however no humic substances were detected. Low C/N ratios of the biopolymer fraction indicated the presence of high M_r proteins, which can provide additional functional groups (i.e. amines and thiols) for Pb binding. Small variations were observed in the relative amounts of these fractions in the different communities, but no clear seasonal trends were observed. Therefore, large seasonal variations in the Pb - EPS binding capacity would not be expected.

To assess the link between Pb distribution and impacts to important community functions such as photosynthesis, respiration and extracellular enzymatic activities, three-week chronic microcosm exposure studies to 210 nM Pb^{2+} were carried out on two different periphyton communities. Average total accumulation normalized to dry weight (DW) (11 ± 4 μmol Pb/g DW) was approximately three orders of magnitude higher than controls (60 ± 20 nmol Pb/g DW). Distribution results showed that little Pb was associated with EPS loosely associated to biomass (9% ± 3%). The majority of Pb was either sorbed to biomass (EDTA-exchangeable) (60% ± 7 %) or intracellularly accumulated (non-EDTA exchangeable) (30% ± 6 %). However, no significant biological effects were observed in any of the endpoints measured, indicating low bioavailability of Pb to periphytic organisms. High ratios of Fe:C and Mn:C of the operationally defined intracellular fraction indicated the presence of Fe and Mn inorganic material, which have been shown to scavenge Pb in periphyton. It is plausible that Pb toxicity is mitigated in periphyton through its binding to inorganic Fe and Mn precipitates. However, it is likely that Pb is also taken up into organisms, whereby intracellular defense mechanisms may also explain the lack of toxic effects observed.

To gain insight into the question intracellular defense responses, we moved from distribution of Pb within the periphyton community to the chemical distribution of Pb at the cellular level to better understand what intracellular processes take place to mitigate Pb toxicity. Temporal dynamics of intracellular Pb speciation were measured using synchrotron resonant x-ray emission spectroscopy (RXES) in model green alga, *Chlamydomonas reinhardtii*, upon exposure to 0.1 nM and 25 nM Pb^{2+} for up to 24 hours. Intracellular Pb speciation changes were detected at 3, 5, 10 and 24 hours of exposure. Initial inorganic precipitation in the form of $PbO_{(s)}$ and $Pb_3(PO_4)_{2(s)}$ shifted towards complexation with organic phosphate and formation of tridentate thiol complexes upon longer exposure times to 0.1 nM Pb^{2+}. Upon 25 nM Pb^{2+} exposure, formation of $PbS_{(s)}$ was also observed. These results indicate that, although Pb is initially sequestered in intracellular precipitates, over time redistribution may occur to either phytochelatins (PCs) and other thiol based peptides involved in detoxification, or to sensitive cellular targets such as proteins, ATP, nucleic acids, and sugar phosphates, which could lead to toxic effects upon longer exposure times.

Interference in periphyton community functions as a result of Pb toxicity would be detrimental to the role of periphyton as a primary producer in freshwater ecosystems.

However, the results from this doctoral work suggest that what is of ecological concern is not the direct toxicity of Pb to periphytic organisms and community structure and function. Rather, with its ability to accumulate and sequester Pb, periphyton can act as a concentrated source of Pb to grazers and may contribute to biological effects in these organisms through chronic dietary exposure.

Zusammenfassung

Um biologisch-toxische Auswirkungen von nicht-essentiellen Spurenmetallen auf Organismen (Lebewesen) in der aquatischen Umwelt zu verstehen, ist es wichtig komplexe abiotische und biotische Wechselwirkungen von Metallen nachzuvollziehen, die zur Aufnahme von Metallen und ihrer Bindung an sensitiven zellulären Targets (Zielobjekten) führen. Periphyton, eine Biofilmgemeinschaft, welche aus Algen, Bakterien, Pilzen und Protozoen in einer Matrix aus extrazellulärer polymerer Substanz (EPS) besteht, wurde für diese Untersuchung ausgewählt. Periphyton ist ein wichtiger Primärproduzent in Süsswasser-Ökosystemen, das zum Nährstoffkreislauf beiträgt und ebenfalls grosse Mengen essentielle und nicht-essentielle Spurenmetalle akkumulieren kann, und dadurch oft Schwankungen der Metallkonzentrationen im darüberliegenden Wasser widerspiegelt. Das Ziel dieser Dissertation war es, den Zusammenhang zwischen der Akkumulation und der Verteilung von Blei (Pb) in Periphyton sowie die biologischen Auswirkungen anhand natürlicher Gemeinschaften zu verstehen. Dafür wurden Biofilme mit Wasser eines Schweizer Baches gezüchtet, um die intrazelluläre Pb-Speziierung durch die Aufnahme von Pb und die nachfolgenden Auswirkungen bis zu generellen Funktionen der Biolfilmgemeinschaft zu verstehen.

Da die EPS eine schützende Funktion von periphytischen Organismen vor Toxizität haben soll, war es von Interesse eine Methode zur EPS Extraktion und Charakterisierung zur Analyse der Zusammensetzung zu entwickeln sowie nachzuweisen, ob sich die Zusammensetzung wesentlich mit den Jahreszeiten verändert und sie dadurch potentiell andere Metallbindungskapazitäten aufweist. Eine Extraktionsmethode, die Zellauflösung verhindert und dadurch für Metallverteilungsstudien anwendbar ist, wurde für die schwach gebundene EPS entwickelt.

Die von sieben verschiedenen Biofilmgemeinschaften extrahierte EPS wurde mit Flüssigchromatographie – organischer Kohlenstoff Detektor – organischer Stickstoff Detektor (LC-OCD-OND) analysiert. Diese Methode basiert auf Gel-Permeations-Chromatographie gekoppelt mit dem Nachweis und der Quantifizierung von organischem Kohlenstoff und Stickstoff in getrennten Fraktionen. Vier Fraktionen wurden in allen Extrakten betrachtet: Biopolymere mit grossem Molekulargewicht (M_r), Bausteine der Huminsäuren, low M_r acids, and low M_r neutral compounds.

Huminstoffe wurden nicht gefunden. Kleine C/N-Verhältnisse in der Biopolymerfraktion wiesen auf die Anwesenheit von Proteinen mit hohem M_r hin, welche zusätzliche funktionelle Gruppen (d.h. Amine und Thiole) zur Bindung von Pb bereitstellen können. Kleine Veränderungen wurden in den relativen Mengen dieser Fraktionen für die verschiedenen Biofilmgemeinschaften gefunden, aber keine klaren jahreszeitlichen Trends beobachtet. Aus diesem Grund werden keine grossen jahreszeitlichen Veränderungen in der Pb-EPS-Bindungskapazität erwartet.

Um die Verbindung zwischen der Pb-Verteilung und dem Einfluss auf wichtige Funktionen der Biofilmgemeinschaft, wie z.B. Photosynthese, Atmung und extrazelluläre enzymatische Aktivitäten zu untersuchen, wurden zwei Biofilmgemeinschaften drei Wochen lang in Mikrokosmen 210 nM Pb^{2+} ausgesetzt. Die durchschnittliche, auf das Trockengewicht (DW) normalisierte, Gesamtakkumulation (11 ± 4 µmol Pb/g DW) war ungefähr drei Grössenordnungen höher als die Kontrollen (60 ± 20 nmol Pb/g DW). Die Ergebnisse der Pb-Verteilung zeigten, dass wenig Pb an der EPS an schwach gebundener Biomasse gebunden war (9% ± 3%). Der grösste Teil des Pb war entweder an der Biomasse sorbiert (EDTA austauschbar) (60% ± 7 %) oder intrazellulär akkumuliert (nicht EDTA austauschbar) (30% ± 6 %). Dennoch wurden keine wesentlichen biologischen Auswirkungen an den gemessenen Endpunkten beobachtet. Dies deutet auf eine geringe Bioverfügbarkeit des Pb für periphytische Organismen hin. Hohe Fe:C- und Mn:C-Verhältnisse in der als intrazellulär definierten Fraktion deuteten auf das Vorhandensein von anorganischen Fe- und Mn-Phasen hin, für die eine Pb-Festlegung in Periphyton gezeigt wurde. Es ist daher möglich, dass die Pb-Toxizität in Periphyton durch die Bindung an anorganischen Fe- und Mn-Präzipitaten abgeschwächt wird. Trotzdem wird Pb wahrscheinlich in Organismen aufgenommen, wodurch intrazelluläre Abwehrmechanismen erklären können, dass keine toxischen Auswirkungen nachgewiesen werden konnten.

Um dieser Frage nachzugehen haben wir, anstatt der Verteilung von Pb innerhalb der Biofilmgemeinschaft, die chemische Verteilung von Pb auf zellulärer Ebene angeschaut, um die auftretenden intrazellulären Prozesse zur Abschwächung der Pb-Toxizität besser zu verstehen. Die zeitliche Dynamik der intrazellulären Pb-Spezierung wurde mittels Synchrotron Resonanz-Röntgenemissionsspektroskopie (RXES) anhand des Modellorganismus der Grünalge, *Chlamydomonas reinhardtii*, bei Exposition von 0.1 nM bis 25 nM Pb^{2+} für 24 Stunden gemessen. Veränderungen

der intrazellulären Pb-Speziierung wurden über eine Zeitreihe von 3, 5, 10 und 24 Stunden gemessen. Anfängliche anorganische Präzipitate in Form von $PbO_{(s)}$ and $Pb_3(PO_4)_{2(s)}$ wurden über längere 0.1 nM Pb^{2+} Exposition zu Pb komplexiert an organischem Phosphat und tridentaten Thiolkomplexen. Bei Konzentrationen von 25 nM Pb^{2+} wurde die Bildung von $PbS_{(s)}$ beobachtet. Diese Ergebnisse deuten darauf hin, dass obwohl Pb zuerst in intrazellulären Präzipitaten gebunden war, es über die Zeit zu einer Neuverteilung des Pb kommen kann. Dort wird Pb an Phytochelatinen (PC) und anderen thiol-basierten Peptiden gebunden, welche an der Detoxifizierung beteiligt sind oder an sensitiven zellulären Zielen wie Proteinen, ATP, Nukleinsäuren und Zuckerphosphaten, so dass es bei langer Exposition zu toxischen Effekten kommen kann.

Eine Beeinträchtigung der Funktionen der Biofilmgemeinschaft durch Pb-Toxizität wäre für die Aufgabe des Periphytons als Primärproduzent in Süsswasser-Ökosystemen schädlich. Allerdings deuten die Ergebnisse dieser Dissertation darauf hin, dass nicht die direkte Pb-Toxizität auf periphytische Organismen und Struktur und Funktion der Gemeinschaft bedenklich sind, sondern vielmehr die Fähigkeit Pb zu akkumulieren und sequestrieren. Dadurch kann Periphyton eine Quelle von Pb für Weidegänger darstellen und zu biologischen Auswirkungen auf diese Organismen durch chronische Exposition während der Nahrungsaufnahme führen.

1 Introduction

1.1 Trace metals in the environment

Trace metals in aquatic environments are grouped into two classes: essential metals (i.e. Cu, Zn, Mn, Fe), which are crucial for the functioning of metalloenzymes, redox processes, and electron transport, and non-essential metals (i.e. Pb, Cd, Ag, Hg) which have no known essential biological functions. Over the centuries human activity has led to a large redistribution of metals in the environment, overwhelming biogeochemical cycles and placing pressure on organisms to cope with fluctuating concentrations of potentially toxic metals.[1] When an essential metal is either below or above a certain optimal concentration range for an organism, deficiencies or toxicity can occur, respectively. However, for non-essential metals, toxicity can occur at lower concentrations and are concentration dependent, where increasing concentrations often lead to increasing adverse biological effects due to either direct metal binding to sensitive cellular targets that disrupt normal functions of biomolecules[2] or through the induction of reactive oxygen species (ROS).[3]

1.2 Lead

The biogeochemical cycles of lead (Pb) have been largely affected by anthropogenic activities as a result of its great natural abundance and use over the centuries.[4,5] Until its phasing out in North America (late 1970s) and Western Europe (early 1990s), the most significant source of Pb in the environment came from the combustion of leaded gasoline,[6] which resulted in an anthropogenic input 30 times greater than the natural background emission.[7] Currently, the most significant inputs of Pb into the environment come from airborne particulates released from ore and metal processing plants as well as industrial processes.[8]

Although Pb levels in the environment have decreased after the phasing out of leaded gasoline, Pb persists in the aquatic environment as a result of strong adsorption to particulates.[9] Under most natural freshwater conditions, the dominant dissolved inorganic Pb species are $Pb(CO)_{3(aq)}$, $PbOH^+$, and Pb^{2+}.[10] However, Pb can form strong complexes through coordination with both oxygen and sulfur[11] originating from both inorganic and organic ligands that possess varying degrees of binding strength, thus influencing Pb bioavailability. Dissolved Pb concentrations tend to be low, in the pico to low nanomolar range for uncontaminated sites.[12] At sites more strongly impacted by urbanization[13] and mining,[14] Pb is found at high nano to low

micromolar concentrations, where the colloidal and particulate fractions can represent a large percentage of total Pb.[14] This is particularly relevant for benthic communities, which collect particulate and colloidal matter.[14] As Pb can be toxic to aquatic organisms under chronic exposure conditions[15,16] it is important to understand the relationship between metal speciation, bioavailability and toxic effects of Pb.

1.3 Metal Speciation and Bioavailability

The bioavailabilty, or the availability of a metal to be intracellularly accumulated, and its uptake in aquatic organisms is dependent not only on the total metal concentration, but more importantly on metal speciation, which refers to the chemical form of a metal.[17] This distinction is important when trying to understand metal-organism interactions in freshwater ecosystems, which are inherently complex and dynamic in their physical characteristics, water chemistry, and biological diversity. The truly dissolved fraction (< 1kDa) contains free ions and metals bound to both inorganic and organic ligands, such as hydroxide, carbonate and chloride,[18] and carboxylic acids, amino acids, small peptides, and to some extent humic and fulvic acids.[19] Additionally, exudates from microorganisms can contribute to the organic ligand pool,[20] which is relevant in the context of metal accumulation in periphyton. The colloidal fraction / macromolecules (1 nm – 1 μm), of particular importance for Pb speciation in freshwaters, includes humic substances (HS) and HS aggregates, polysaccharides, proteins, Fe oxyhydroxides, Mn oxides, metal sulfides, carbonates and phosphates, as well as cellular debris.[21] As a result of metal complexation to these different ligands, metal species vary in both their thermodynamic stability as well as kinetic lability. These two properties, which influence the likelihood and rate of metal dissociation, strongly affect the bioavailability of metals, and thus the uptake into aquatic organisms.

With respect to metal uptake, observations that the free metal ion often dictates intracellular accumulation have led to the development of models such as the free ion activity model (FIAM) and its derived biotic ligand model (BLM), which relate metal uptake in organisms to the free ion concentration. The FIAM predicts that metal uptake and subsequent biological effects are related to the activity of the free metal ion in solution, whereas the BLM goes a step further by taking into account

competition from other cations for membrane bound uptake sites as well as including the influence of natural organic ligands on the speciation of metals in water.[22] Although these models have predicted the uptake of various metals in different algal species under defined laboratory conditions,[23,24] they both assume that the organism is in equilibrium with the surrounding environment, and have, under certain conditions, failed to accurately predict metal uptake in the presence of dissolved organic matter (DOM).[25,26] In the case of the BLM, ligands only serve as metal complexing agents, thereby reducing the concentration of surface bound metals and decreasing uptake and toxic effects.[27] This assumption does not take into account the importance of metal complexes themselves in the intracellular accumulation of metals. Exceptions have been reported whereby organic metal complexes have had a direct influence on intracellular metal accumulation. Higher accumulation of Ag in the presence of thiosulfate was measured in the alga *C. reinhardtii* relative to what was expected from the free ion concentration,[28] uptake of Cu, Cd and Pb was related to the passive diffusion of lipophilic metal-organic complexes across the plasma membrane in the diatom *Thalassiosira weissflogii*,[29] and studies conducted with Pb uptake in *Chlorella kesslerii* showed although NOM decreased Pb uptake, the uptake was higher than expected for measured Pb^{2+} concentrations and demonstrated the importance of ternary complexation of Pb – NOM with cell surfaces.[25,30] Additionally, Pb uptake in *C. reinhardtii* was enhanced in the presence of carbonate under diffusion limiting conditions, indicating the influence of inorganic complexes in Pb uptake under environmentally relevant concentrations.[31]

1.4 Metal toxicity & intracellular speciation

Organisms have developed mechanisms, including sequestration and excretion, to prevent metal toxicity and maintain physiologically required cellular concentrations of essential metals.[2,32] When internalized, essential metals are bound and actively transported to specific subcellular organelles and incorporated into the required biomolecules. Toxicity can occur when either too high concentrations of essential metals or relatively lower concentrations of non-essential metals are intracellularly accumulated. In the case of Pb, toxicity can occur from the replacement of essential metals with Pb, as has been demonstrated with the exchange of Zn from the family of Zn finger proteins.[33] Lead has also been reported

to interfere in electron transfer reactions in mitochondria[34] and chloroplasts,[35] affecting respiration and photosynthesis,[15] and other physiological disruptions have been observed in algae.[36] In addition to these direct effects, indirect effects can occur through an increase in metal induced reactive oxygen species (ROS) via a Fenton type reaction. These ROS lead to the radical attack of proteins, lipids and nucleic acids, ultimately leading to cell death if antioxidant mechanisms are unable to scavenge ROS.

Algae avoid direct toxic effects through metal sequestration either by complexation with phytochelatins (PCs), important peptides in metal detoxification,[15,37,38] or through metal immobilization in intracellular precipitates, such as polyphosphate vacuolar granules,[39,40] as presented in Figure 1.4.1. The PCs, with an amino acid composition of $(\gamma\text{-Glu-Cys})_n$-Gly (n = 2 – 11), have a high affinity to metals due to their thiol and carboxylic acid groups. Rapid induction of PCs in *C. reinhardtii* was measured upon both short and long term Pb exposures (down to 1 nM Pb^{2+}),[15] and several other studies have also indicated that Pb is able to induce PCs.[37,41] Yet, in a study conducted by Scheidegger et al., it was observed that although Pb induced the production of PCs, the amount was not high enough to bind all intracellular Pb.[42] As no observable toxic effects were present under these conditions, other sequestration processes were assumed to be present to mitigate toxicity. Indeed, studies have indicated that, in addition to phytochelatin induction, polyphosphate containing vacuoles appear to serve an important role in intracellular metal sequestration.[39,40]

Antioxidant mechanisms are critical in mitigating the indirect effects of metal toxicity brought upon by ROS. Glutathione (GSH) is one of the most abundant cellular thiols found in millimolar concentrations.[15] In addition to being a precursor for PC production, GSH plays an integral role in cellular antioxidant responses. As part of these antioxidant mechanisms, GSH is oxidized by ROS to prevent the oxidation of sensitive cellular targets, but is then quickly reduced again by glutathione reductase, resulting in a highly reduced intracellular pool of GSH.[43] Additionally, within the ascorbate - glutathione cycle responsible for scavenging ROS, specifically H_2O_2, GSH aids in the reduction of oxidized ascorbate.[44]
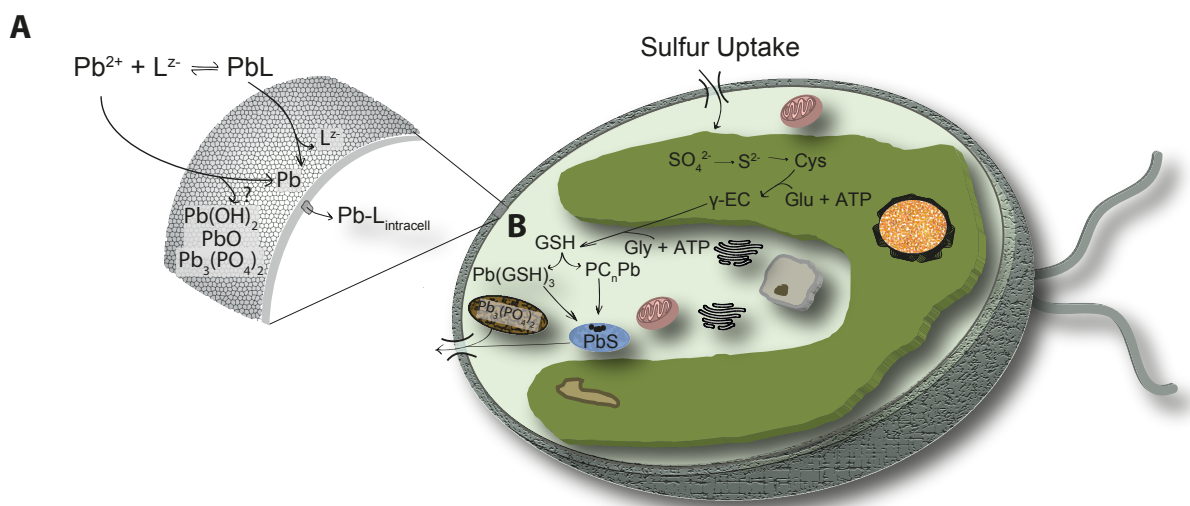
Figure 1.4.1: Scheme of possible Pb sequestration mechanisms. (A) Precipitation of Pb in the forms $Pb(OH)_{2(s)}$, $PbO_{(s)}$ and $Pb_3(PO_4)_{2(s)}$ within the cell wall. (B) Uptake of Pb^{2+} through membrane transporters, binding to GSH or to PCs, and subsequent transport to vacuoles with possible formation of $PbS_{(s)}$ precipitates. Additional sequestration of Pb in polyphosphate granules is possible.

Intracellular speciation is clearly important to understand such metal detoxification responses and potential modes of toxicity. The importance of metal solution chemistry in accurately assessing metal bioavailability and uptake in organisms has long been established.[17] However, the missing link in understanding the relationship between metal uptake and toxicity is the ability to accurately measure intracellular metal speciation. Therefore, a fundamental necessity for better understanding biological responses to metal toxicity is the determination of intracellular metal speciation, which identifies specific cellular metal-ligand interactions.

1.4.1 X-ray spectroscopy for intracellular metal speciation

Non-destructive metal specific techniques with low detection limit capabilities that are able to provide chemical and structural information on the complexation of a metal are required to determine metal speciation within the cell. With this information, metal uptake can be better linked to cellular responses so that a more complete understanding of metal – organism interactions in the aquatic environment is achieved. Techniques for intracellular metal speciation often involve homogenization of cells, sonication, separation of specific fractions of interest using ultracentrifugation, and the subsequent analysis using a variety of available

techniques, such as high-performance liquid chromatography (HPLC) coupled to inductively coupled plasma – mass spectrometry (ICP-MS)[45] to quantify metals in specific eluted fractions. Electrospray ionization mass spectrometry (ESI-MS) has been used to detect and identify specific metal complexes, such as PCs.[46] However, steps must be taken to prevent metal redistribution during fractionation processes[47] and to prevent oxidation of sensitive metal complexes.[48] Furthermore, these targeted techniques do not allow for an analysis of all dominant intracellular metal species of a specific metal of interest.

Synchrotron based x-ray spectroscopy, which includes both absorption (XAS) and emission spectroscopy (XES), allows for the determination of metal speciation in hydrated biological samples both in bulk, and now increasingly at the subcellular level at ~100 nm scale resolution.[49] In XAS, elemental speciation is obtained when a monochromatic X-ray beam, scanned across an energy range, interacts with a sample. As shown in Figure 1.4.2, when the incident energy corresponds to the binding energy of a core electron of a specific element of interest, a sharp increase of the absorption coefficient is measured and produces a feature called an absorption edge. The region around the absorption edge is referred to as the X-ray absorption near edge structure (XANES) and reflects the empty density of states. When the incident energy provides enough kinetic energy for a core electron to leave the atom, a core electron is ejected with a specific kinetic energy. The ejected photoelectron wave is scattered by surrounding atoms and, depending on the kinetic energy of the ejected photoelectron, the outgoing and backscattered waves constructively or destructively interfere and result in what is referred to as the extended X-ray absorption fine structure (EXAFS). With XAS, the unoccupied density of electronic states of an element is probed, where spectra can be divided into two main parts: XANES, providing information on the oxidation state and molecular geometry, and EXAFS, providing information on the identity of neighboring atoms and coordination geometry, as well as bond distances. XAS is typically measured in transmission mode by measuring the ratio of the incoming intensity to intensity transmitted through the sample. However, XAS can also be performed in fluorescence mode for dilute non - strongly absorbing samples, often the case for biological material. In fluorescence mode, emitted X-ray fluorescence, produced from outer shell electrons filling core hole vacancies, is measured. Because fluorescence is directly proportional to the absorption coefficient ($\mu(E)$) and collected at 90° relative to the

incident energy where elastic scattering is suppressed, increased signal to noise ratio is achieved, enhancing sensitivity.
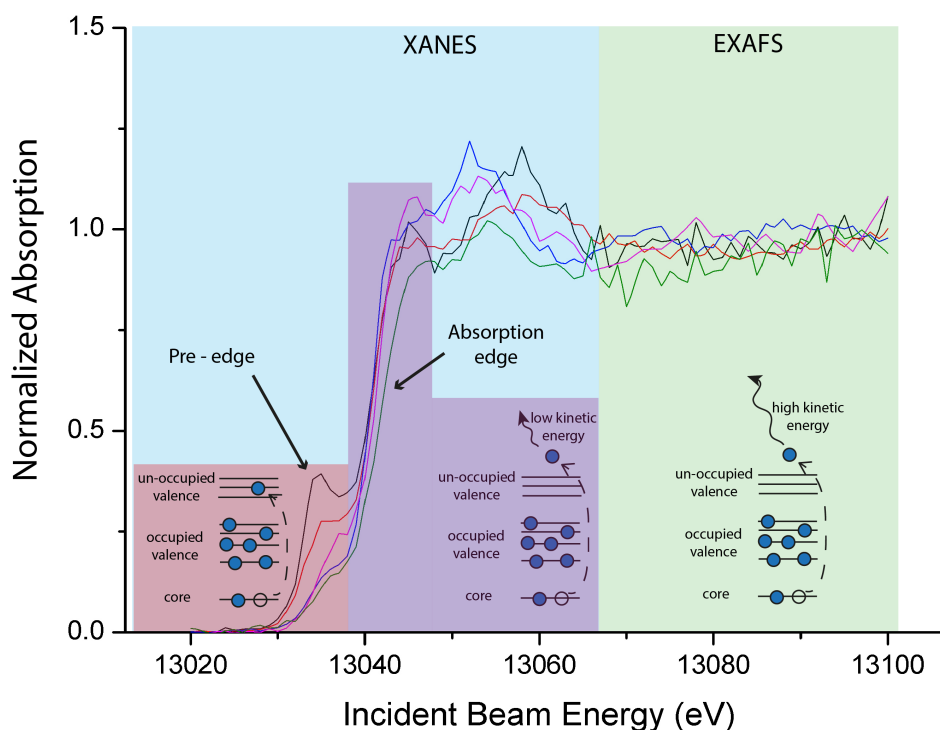
Figure 1.4.2: Scheme of X-ray absorption process.Core electrons are excited to un-occupied valence states at energies corresponding to the pre-edge (red). Electrons are ejected into the continuum at energies corresponding to the absorption edge (purple). At higher incident energies these electrons are ejected with a higher kinetic energy and scatter off of neighboring atoms, producing constructive and destructive interference patterns see in the EXAFS region (green).

Using X-ray absorption spectroscopy one can probe the local chemical environment of a metal at the atomic level, thereby gaining information on the speciation of the metal in its natural state. XAS has been used for probing metal speciation in biological samples,[50,51] ranging from fungal cell walls[52] and bacterial biofilms[53] to metal hyper accumulating plants.[54] However, distinguishing between different types of organic ligands that scatter only lightly is virtually impossible with XAS. Furthermore, with respect to Pb, distorted geometries of Pb complexes, due to a lone electron pair, lead to poorer resolution and make it challenging to go beyond identification of the direct coordination and thus ligand identification.[55]

X-ray emission spectroscopy (XES) is a secondary process that probes the occupied density of electronic states in a sample (Figure 1.4.3C). Resonant X-ray emission spectroscopy (RXES) (also referred to as resonant inelastic X-ray

scattering (RIXS)) and used in the work presented in Chapter 4, combines both XAS and XES, providing a complete picture of the electronic structure of a metal complex. As illustrated in Figure 1.4.3, RXES is a photon – in / photon – out process, in which a *ground state* absorbs an incoming photon in resonance with a specific absorption edge (Figure 1.4.3A), resulting in an excited *intermediate state*, which contains a core hole (Figure 1.4.3B). The subsequent emission of a photon leads to the *final state*, which possesses a higher energy, relative to the initial state and contains a core hole (Figure 1.4.3C) with a longer lifetime than in XAS, thereby decreasing the core hole broadening of spectral lines and increasing spectral resolution. The energy transfer of the system is the difference in energy between the ground and final states, which exists from the change in energy and momentum of the scattered photon, and when plotted against the incident energy allows for the separation of pre-edge structures from the main absorption edge (Figure 1.4.3E).
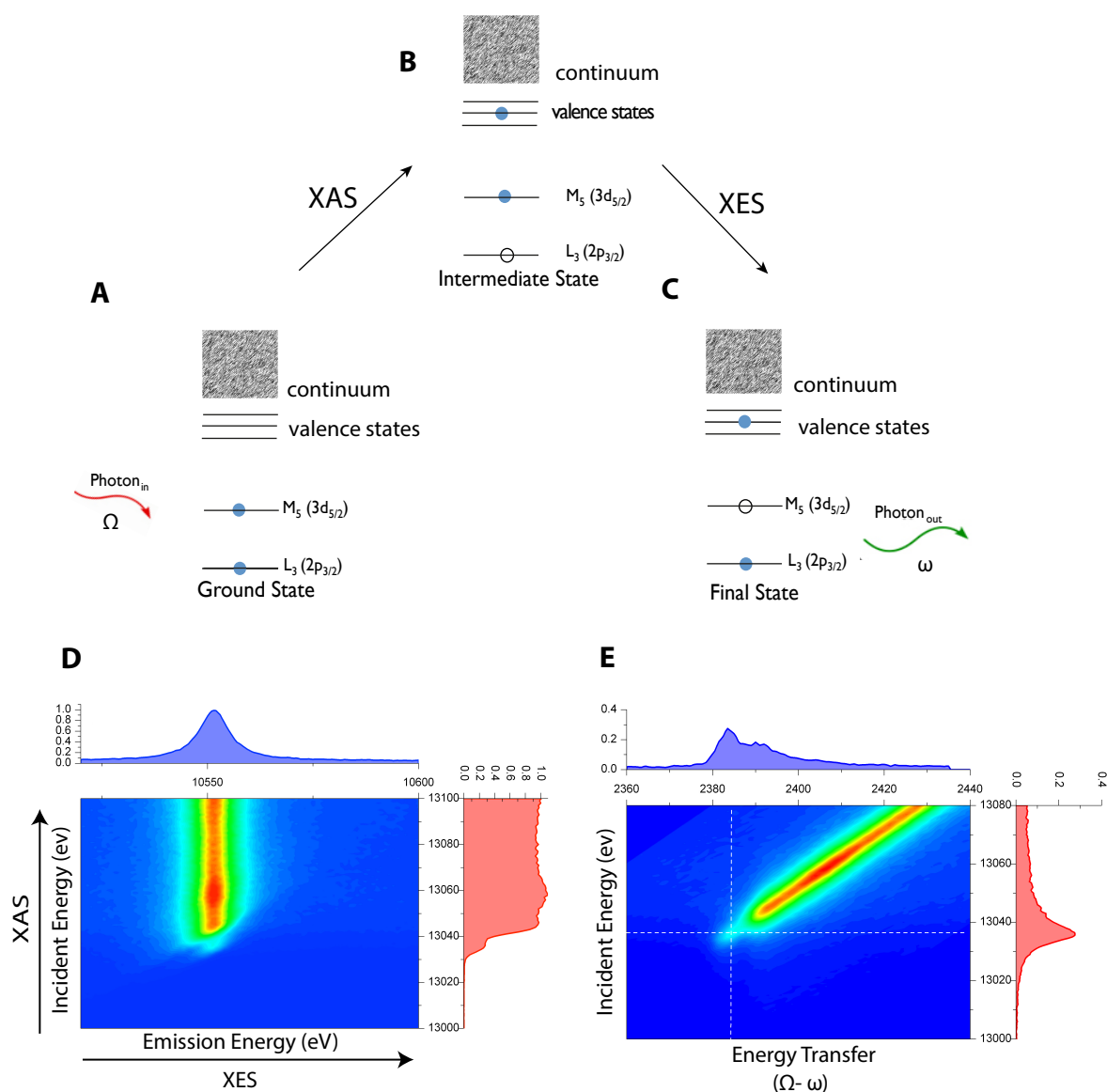
Figure 1.4.3: Scheme of resonant inelastic X-ray scattering for L edge of Pb. (A) Core 2p electron in the ground state is excited to an unoccupied valance state by an incoming photon in resonance with the energy required for this transition. (B) An intermediate state is created with a core hole. (C) Emission of a photon resulting from the electronic transition 3d → 2p is measured and (D) the incident energy is plotted as a function of the emission energy or (E) as a function of the energy transfer.

With synchrotron-based RXES, highly resolved 2D spectra of metal complexes can be obtained (Figure 1.4.3D,E), where RXES planes (Figure 1.4.3D) are analogous to a metal-ligand fingerprint, and in the case of Pb, allow for discernment between different types of oxygen and sulfur ligand bound Pb complexes. Obtaining this degree of detailed metal speciation is not possible with XAS or any other technique.[56] Thus, RXES provides a new ability to identify and track changes in intracellular metal-ligand complexes.

1.5 Periphyton

The term periphyton refers to a community of both autotrophic and heterotrophic organisms, specifically algae, bacteria, fungi, and protozoa, embedded in extracellular polymeric substances (EPS) produced from the organisms themselves. These photosynthetic benthic communities are found in both freshwater and marine ecosystems within the photic zones in both running streams and rivers, as well as ponds and lakes.[57] Periphyton is one of the most important primary producers in rivers and streams,[58] has shown to play an important function in the cycling of organic carbon[59] as well as inorganic nutrients,[60] and is an important food source for grazing organisms.

1.5.1 EPS Composition

The EPS from biofilms are composed of secreted organic polymers, typically polysaccharides, proteins, glycoproteins, glycolipids, nucleic acids, amphiphilic compounds, and can also include larger compounds such as humic substances and colloids.[61-65] All components of the EPS are held together in a hydrogel like network. It is the three-dimensional structure of the EPS that contributes to physico-chemical nature of the biofilm,[66,67] and protects organisms against toxicity from both inorganic and organic pollutants.[68,69] The types of polysaccharides found in EPS depend on their microbial origin and can be used for attachment to surfaces or excreted from the organisms once attached to a surface.[64] Although less understood, proteins can comprise a significant percentage of the EPS composition and extracellular enzymes serve an important role in hydrolyzing large organic matter to assimilable molecules that can be taken up and used for cellular metabolism.[70]

There are two types of operationally defined EPS fractions based upon extraction techniques: easily extractable soluble compounds and those compounds that are more difficult to extract based on physical extraction techniques. Soluble compounds include any soluble macromolecules or colloids, whereas the fraction more strongly bound to cell walls of embedded organisms or to other organic material is considered to contain the less easily extracted compounds of the EPS.[71]

1.5.2 Metal Binding

Metal accumulation in biofilms can occur via four main processes: sorption to ionisable functional groups from EPS, sorption to cellular surfaces of organisms embedded within the EPS, sorption to inorganic material, and the intracellular uptake

by these organisms. The EPS contain important metal binding functional groups, which can influence the bioavailability of potentially toxic metals to periphytic organisms. The abundance of carboxylic groups in the polysaccharide fraction of the EPS has been proposed to both help bind toxic metal cations[72] as well as be important in acquiring Fe and Mn for cyanobacteria growth.[73] It has also been hypothesized that proteins containing exposed carboxylic or amino side groups may also be involved in metal binding.[65]

Metal binding to EPS is not only dependent on the composition of the EPS, but is also metal specific. It was observed that in EPS of different composition isolated from bacteria, binding of Mo was preferred over Ni and Cr,[74] another study showed that Pb binding to EPS was preferred over Cd and Zn,[75] and Pb has been shown to bind preferentially to the more strongly associated EPS fraction relative to other metals.[76] Reported accumulation of Pb in periphyton from field studies normalized to dry weight (DW) is often on the order of nmol Pb/g DW,[13,14,77] but accumulation in the μmol/g DW range has also been reported at certain sites.[14,78] Where some studies have focused exclusively on metal binding of the EPS,[79,80] others have measured accumulation and toxicity in whole biofilms.[81-84] However, results linking metal distribution and biological effects are still lacking.

1.6 Significance of Work

Periphyton is a main primary producer and food source in freshwater systems, but also able to accumulate non-essential metals, which pose both a direct threat to organisms within the periphyton community as well as to those organisms dependent on periphyton as a food source. In both microcosm and field studies, work on metal accumulation in periphyton in relation to aquatic speciation of non-essential metals has been conducted, as well as studies to determine biological effects of non-essential metals on periphyton under various exposure conditions. However, this work attempts to fill a gap between metal speciation in natural waters and biological effects by determining and linking the distribution and bioavailability of Pb in periphyton to potential effects on important ecosystem functions provided by periphyton. Moving from metal distribution within the community to the cellular level, this work takes our understanding of intracellular speciation a significant step further with the determination of temporal Pb speciation dynamics at the cellular level, which

provides chemical insight into possible detoxification and toxic modes of action of internalized Pb.
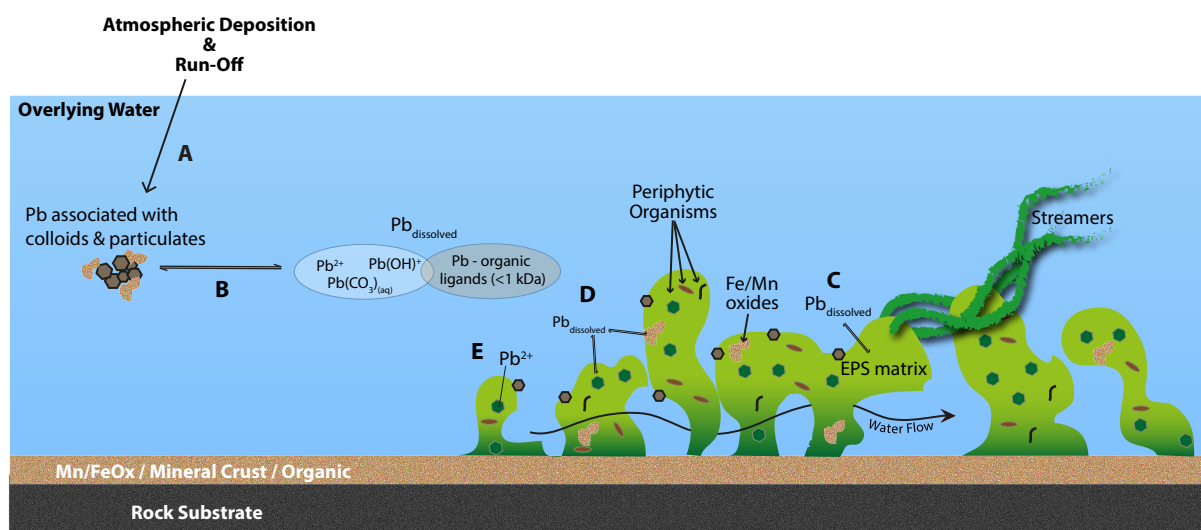
Figure 1.6.1: Biogeochemistry of Pb in freshwater and interactions with periphyton. Introduction of Pb into the freshwater aquatic environment via atmospheric deposition or runoff (A) results in Pb sorbed to both inorganic and organic colloids and particulates as well as dissolved Pb species (B). Both dissolved and colloidal/particulate Pb can be accumulated in periphyton through immobilization in EPS (C), sorption to metal oxides within periphyton and to cell surfaces of periphytic organisms (D) and intracellularly accumulated (E).

1.7   Outline of Thesis

In Chapter 2, work is presented on both the development of an EPS extraction protocol amenable for metal distribution analysis, and the characterization of seasonal variations in EPS composition using liquid chromatography – organic carbon detection – organic nitrogen detection (LC-OCD-OND). The extracted EPS from communities sampled within a six month period were analyzed using LC-OCD-OND and four fractions were quantified: high M_r biopolymers, building blocks of humic acids, low M_r acids, and low M_r neutral compounds. Slight variations were observed in the relative amounts of these fractions, but no clear seasonal trends were observed. The implications of using LC-OCD-OND as a useful analytical tool for EPS composition are presented and discussed. This chapter was published in *Environmental Science and Pollution Research.* Additional results on Pb binding to EPS as a function of Pb^{2+} concentration and pH is provided in Supplementary Chapter 2. Results indicated an excess of binding sites upon Pb exposure up to 1 μM

Pb^{2+}, but approximate calculations of conditional stability constants revealed relatively weak Pb binding to EPS, independent of the pH tested.

In Chapter 3, the study linking Pb distribution in periphyton with biological effects is presented. In this work, chronic three-week microcosm Pb exposures to 210 nM Pb^{2+} were conducted. Subsequently, Pb as well as Cu, Mn and Fe distributions were quantified in the total periphyton, the EPS, and operationally defined sorbed and intracellular fractions. In agreement with calculated Pb-EPS conditional stability constants, the EPS does not seem to play a significant role in decreasing bioavailabilty of Pb, as little Pb was associated with the EPS fraction. Although the majority of Pb was either sorbed to biomass or intracellularly accumulated fraction, no significant biological effects were observed in any of the biological endpoints tested, indicating decreased bioavailability of Pb to periphytic organisms, whether by extracellular sequestration by Fe and Mn oxides or by the intracellular sequestration of Pb. This chapter is submitted to *Environmental Science and Technology*.

In Chapter 4 we transition to cellular level and work is presented on the intracellular temporal dynamics of Pb speciation in a model green alga *C. reinhardtii* using resonant x-ray emission spectroscopy (RXES), a technique sensitive to functional group chemistry of metal complexes. *C. reinhardtii* was exposed for 24 hours to 0.1 nM and 25 nM Pb^{2+} and speciation measurements were taken as function of time. Previous work on Pb induction of PCs in *C. reinhardtii* indicated that not enough PCs were induced to sequester all intracellular Pb. We observed that inorganic oxides and phosphate initially sequestered Pb, but upon longer exposure times organic complexation with phosphates and thiols increased. At the higher exposure concentration formation of $PbS_{(s)}$ was observed. The increasing organic complexation may indicate early signs of toxicity that are not measureable using standard endpoints such as photosynthesis and growth. This chapter is submitted to *PNAS*.

Characterization of Extracellular Polymeric Substances (EPS) from Periphyton Using Liquid Chromatography-Organic Carbon Detection – Organic Nitrogen Detection (LC-OCD-OND)

Stewart, T. J., Traber, J., Kroll, A., Behra, R., Sigg, L. Characterization of extracellular polymeric substances (EPS) from periphyton using liquid chromatography-organic carbon detection-organic nitrogen detection (LC-OCD-OND). *Environ Sci Pollut Res* 20, 3214–3223 (2013).

2.1 Abstract

A protocol was developed to extract, fractionate, and quantitatively analyze periphyton extracellular polymeric substances (EPS), which obtains both information on the molecular weight (M_r) distribution and protein and polysaccharide content. The EPS were extracted from freshwater periphyton between July and December 2011. Organic carbon (OC) compounds from different EPS extracts were analyzed using liquid chromatography-organic carbon detection–organic nitrogen detection (LC-OCD-OND), and total protein and polysaccharide content were quantified. Four distinct OC fractions, on the basis of M_r, were identified in all extracts, corresponding to high M_r biopolymers (≥80–4 kDa), degradation products of humic substances (M_r not available), low M_r acids (10–0.7 kDa), and small amphiphilic/neutral compounds (3–0.5 kDa). Low C/N ratios (4.3 ± 0.8) were calculated for the biopolymer fractions, which represented 16–38 % of the measured dissolved organic carbon (DOC), indicating a significant presence of high M_r proteins in the EPS. Protein and polysaccharide represented the two major components of EPS and, when combined, accounted for the measured DOC in extracts. Differences in specific OC fractions of EPS extracts over the course of the study could be quantified using this method. This study suggests that LC-OCD-OND is a new valuable tool in EPS characterization of periphyton.

2.2 Introduction

Phototrophic biofilms, also commonly referred to as periphyton, are communities of hetero- and autotrophic organisms held together by a network of extracellular polymeric substances (EPS). The excreted EPS, typically composed of polysaccharides, proteins, glycoproteins, glycolipids, nucleic acids, and amphiphilic compounds,[61,63,65] provide both biofilm structure and a nutrient source for periphytic organisms, but also may serve as a protective barrier against toxic compounds, such as nonessential trace metals.

Methods of EPS characterization have largely relied on techniques for quantification of total proteins and polysaccharides in EPS, using assays, such as the Bradford and Lowry, and the DuBois methods.[85,86] Despite the relative ease of standard assays, these methods only provide information on total concentrations in a sample. More detailed characterization techniques, such as HPLC, have been used

to determine the monosaccharide composition in both bacterial and phototrophic biofilms,[87-89] coupled mass spectrometry (MS) techniques, such as LC- MS/MS, have been used to identify specific proteins in bacterial biofilms,[90] and confocal scanning laser microscopy has been used to study the exopolysaccharide composition of biofilms using fluorescently labeled lectins.[91] These methods have the advantage of targeting and identifying specific types of extracellular compounds. However, what is needed is a comprehensive and quantitative approach, able to simultaneously fractionate and characterize EPS.

Liquid chromatography-organic carbon detection–organic nitrogen detection (LC-OCD-OND) is a technique based on size-exclusion chromatography (SEC), which is able to provide quantitative information regarding organic carbon (OC) compounds, such as polysaccharides and proteins found in EPS. Although SEC has been previously used for the separation of compounds in bacterial EPS,[92-94] LC-OCD-OND provides additional information by the online coupling of SEC to OC, organic nitrogen (ON), and ultraviolet (UV) detectors. The total (TOC) and dissolved organic carbon (DOC) are measured, and DOC is further separated and quantified in six separate fractions: biopolymers (high M_r polysaccharides and proteins), humic substances (HS), building blocks of HS, low M_r acids, and amphiphilic/neutral compounds (alcohols, aldehydes, ketones, and amino acids). This technique has been used in the drinking and groundwater monitoring sectors, and there is a collection of work that has studied different fractions of EPS from bacterial biofilms, with respect to assessing membrane fouling.[95-97] However, LC-OCD-OND has never been used as a tool to characterize EPS from periphyton.

The aim of this work was twofold: to develop an extraction protocol for EPS from periphyton suitable for metal analysis and to obtain M_r and protein and polysaccharide content of different OC fractions of EPS using LC-OCD-OND. The EPS was extracted from biofilms, colonized between July and December 2011. Chromatograms from this 6-month period were compared to determine if differences in EPS composition could be observed and quantified using this technique. Results were compared with total polysaccharide and protein quantification. The application of LC-OCD-OND for the characterization of periphyton EPS is assessed.

2.3 Materials and Methods

2.3.1 Periphyton colonization

All periphyton was colonized on glass microscope slides, previously acid soaked in 0.03 M HNO_3 and washed with nanopure water (Ω 18, Milli-Q), which were placed in Plexiglas flow-through channels with continuous pumping of natural stream water from the Chriesbach (Dubendorf, Switzerland).[98] Each channel contained four rows of eight paired glass slides (76 × 26 mm, Thermo Scientific), amounting to a total of 64 slides per channel. Larger-sized sediment was removed from the water before entering colonization channels by using a sediment trap (51 × 70 × 260 cm) with an average residence time of 20 min. Flow rate was maintained at approximately 1 cm/s and monitored with a Schildknecht MiniAir2 flow meter. Illumination was provided by BioSun fluorescent tubes (MLT Moderne Licht-Technik AG, ML-T8 36W/965/ G13B), mimicking the natural sunlight spectrum. Light/dark cycles, each 12 h, were maintained with electronically controlled timers (Demelectric AG). Slides were transferred to a plastic box containing stream water, so that drying of the biofilms was avoided during transport, prior to extraction.

2.3.2 Periphyton EPS extraction

Glass slides were taken from flow-through channels after 25 days of colonization. Biomass was gently scraped off with a clean glass slide into a 100-mL muffled glass beaker placed on ice containing the extraction solution composed of $NaNO_3$ (10 mM, pH 7.4) and a 1 µg/mL protease inhibitor cocktail, with equal amounts of Aprotinin, Leupeptin, and Pepstatin A (AppliChem AG). The 10 mM $NaNO_3$ was chosen, as it is a chemically inert salt with an ionic strength similar to the stream water used to colonize the periphyton. A volume of 60 mL was used for the extraction of 32 slides. The biofilm slurry was resuspended in the solution by gentle pipetting and then further resuspended using a water sonication bath (45 kHz 60 W, VWR Ultrasonic Cleaner) for 30 s. Fine sediment and larger biomass was allowed to settle, and the solution was removed and centrifuged at 1,880 × g for 10 min. Biomass was resuspended a second time in fresh solution and treated as described above. In a separate series of extractions, $NaHCO_3$ (2 mM, pH 7.6) was used as an extraction solution.

To determine if agitation of the solution over time yielded higher EPS extraction efficiencies, two different physical methods were compared, referred to as shaking

and stirring methods. A biofilm slurry was obtained according to the above protocol and a control sample, representing t_0, was taken before the remaining slurry was separated into separate aliquots. Half of the aliquots were placed on a shaker at 90 rpm, whereas the remaining aliquots were stirred at 300 rpm. Samples were taken after 30, 60, 90, and 120 min from each type of extraction method and centrifuged at 1,880 × g for 10 min. The resulting biomass pellet was lyophilized overnight, and dry weight measurements were taken. All supernatants were filtered through 0.22 μm PES Millipore filters, which were previously flushed with 1 L of nanopure water (Ω 18, Milli-Q) to prevent OC contamination of the sample. Filtered samples were stored in muffled 100-mL glass Schott flasks at 4 °C and treated with a final concentration of 0.02 % (w/v) NaN_3 to prevent bacterial growth and subsequent degradation of EPS.

2.3.3 Glucose-6-phosphate dehydrogenase assay

Activity of glucose-6-phosphate dehydrogenase (G6P-DH), an intracellular enzyme, was measured in extracts according to Esposito et al., to determine the degree of cell lysis resulting from the extraction technique used in this study.[99] At each step of the extraction (i.e., scraping of biofilms from slides, sonication, centrifugation, and filtration), samples were taken in triplicate and transferred to a 96-well plate. Upon addition of 180 μL of reaction mixture (50 mM Tris Base, 0.15 mM NADP, 10 mM $MgCl_2$, and 3 mM glucose-6-phosphate), absorption of NADPH (formed during the conversion of glucose-6- phosphate) was measured at 340 nm at 30 °C over 30 min. A standard curve was generated using G6P-DH in both water and in the EPS extract to verify that the EPS did not interfere with the detection of G6P-DH activity. The limit of detection in both cases was 0.00125 U/mL (U is the amount of enzyme that reduces 1.0 μmol NADP/min at 30 °C, pH 7.8). To measure total activity of the biomass, cell lysis was induced by combining 1 mL of the biomass suspension with the same volume of extraction solution containing 0.1 % SDS. The sample was sonicated for 15 min, centrifuged, and the supernatant was used as a representation of total G6P-DH activity. A known amount of G6P-DH was also treated as described above to verify that the procedure did not inhibit G6P-DH activity.

2.3.4 LC-OCD-OND characterization of extracted EPS

To characterize the OC compounds found in the extracted EPS, LC-OCD-OND was used. Samples were diluted (1:50) with nanopure water (Ω 18, Milli-Q) in muffled assimilable organic carbon-free 20-mL glass vials. Compounds were separated using a size exclusion column (250 × 20 mm, Toyopearl TSK HW-50S) able to separate both polysaccharides (0.1–18 kDa) and proteins (0.5–80 kDa for globular proteins), as reported by the manufacturer. A handling control, in which the extraction solution was treated like the periphyton EPS extract, was performed to assess the carbon contamination associated with the extraction protocol. In all cases, OC coming from the handling control accounted for less than 2 % of DOC in extracts and, therefore, was negligible for the quantification of OC compounds in EPS. Phosphate buffer (24 mM, pH 6.6) was used as the mobile phase and phosphoric acid solution (60 mM, pH 1.2) was used as an acidification solution to aid in the removal of inorganic carbon prior to analysis. The limit of quantification was 10 µg/L for both OC and ON.

The TOC and DOC, as well as specific OC compounds, were identified and quantified using FIFFIKUS, a software quantification method (DOC-Labor Dr. Huber, Germany). Distinguishable fractions can include mineral colloids, polysaccharides, HS, building blocks of HS, low M_r acids, and amphiphilic/neutral compounds. The software uses information obtained from the isolation of polysaccharides, and other fractions from EPS, and their subsequent measurement using ion chromatography and amperometric detection for sugars.

2.3.5 LC-OCD-OND calibration

Protein and polysaccharide standards were measured to create a calibration curve for the M_r determination of peaks from extracts. BSA (66.5 kDa), ovalbumin (44 kDa), Carbonic Anhydrase (29 kDa), Ribonuclease A (13.7 kDa), Aprotinin (6.5 kDa), and Pepstatin A (0.686 kDa) were used as protein standards. Thyroglobulin (669 kDa) was used to determine the void volume of the column and for the calculation of retention factors. Protein standards were measured both individually and in mixtures in phosphate buffer, $NaNO_3$, $NaHCO_3$, and spiked in EPS extracts so as to rule out matrix effects on elution times. As no significant effects were observed, the standard calibration curve in phosphate buffer was used for M_r calculations (Figure 2.8.1). Mixtures of protein standards (Thyroglobulin (669 kDa), BSA (66.5 kDa), Ovalbumin (44 kDa), and Pepstatin A (0.686 kDa)), corresponding to retention times of peaks

seen in EPS extracts, were analyzed (Figure 2.8.2) to determine the resolution of M_r separation in these mixtures. Polyethylene glycol (PEG) standards ranging from 0.106 to 21.030 kDa were used as polysaccharide standards and measured in nanopure water (Ω 18, Milli-Q), $NaNO_3$, $NaHCO_3$, and spiked in EPS extracts. The standard calibration curve in nanopure water was used for M_r calculations.

2.3.6 Protein and polysaccharide quantification

The Bradford assay was conducted on the whole extract to quantify total protein.[85] BSA was used for standard calibration, and extracts were diluted with nanopure water to fall within the calibration range. Bradford dye reagent (Bio-Rad) was used for the analysis. Absorbance was measured at 595 nm, and samples were measured in triplicate. Protein was converted from micrograms of protein to milligrams of carbon, assuming an average carbon content of 0.53 g C/g protein.[100]

The phenol-sulfuric acid method (DuBois method) was used on the whole extract to determine total polysaccharide content.[86] Glucose was used as a calibration standard. Equal volumes of sample or glucose standard were mixed with phenol (500 μL, 2% (w/v), Fluka) in glass vials and then 2.5 mL of concentrated sulfuric acid (95–97%, Sigma-Aldrich) was added, and the solution was mixed via gentle vortex. After allowing the sample to cool for 30 min, absorbance of solutions was measured at 490 nm. Polysaccharide was converted from micrograms of polysaccharide to milligrams of carbon, assuming 0.4 g C/g polysaccharide.[100]

2.4 Results

2.4.1 Extraction method

The EPS extraction efficiencies of the shaking and stir methods were evaluated with respect to TOC and DOC. The amount of extracted TOC and DOC are shown in (Figure 2.7.1) as a function of extraction time. No significant differences were observed between these two methods over the course of 120 min nor were differences observed over time within a single type of extraction technique. No differences were observed between $NaNO_3$ and $NaHCO_3$ as extraction solutions (Figure 2.8.3). Results from the G6P-DH assay indicated no detectable G6P-DH activity during any step of the EPS extraction, as measurements were all below the limit of detection of the assay (Table 2.8.1).

2.4.2 EPS characterization

In all LC-OCD-OND chromatograms (Figure 2.7.2A), four distinct fractions were observed corresponding to biopolymers, building blocks of HS, low M_r acids, and neutral/amphiphilic compounds. No HS were present in any EPS extracts measured, as HS typically elute at approximately 45 min and would display a distinct signal in the UV spectra.[101] However, UV absorbance (254 nm) was observed for the biopolymer and low M_r acid fractions in all extracts (Figure 2.8.5). An ON signal was measured for all biopolymer fractions (Figure 2.7.2B) but could not be assessed for the other fractions as the nitrogen signal from $NaNO_3$, which was detected at the same retention time as the remaining fractions, was too large. Areas of individual fractions were integrated as shown in (Figure 2.7.2A), quantified, and are presented as a percentage of chromatographable DOC (Figure 2.7.3).

As seen in (Figure 2.7.3), the biopolymer fraction represented 16–38 % of measured DOC, whereas the building block, low M_r acid, and neutral fractions corresponded to 16–25, 5–8, and 40–60 % DOC, respectively. Extract taken in July contained the least amount of biopolymers (16 % DOC) relative to the other OC fractions, whereas extracts from August and the beginning of November (6 November 2011) contained the largest amounts (38 and 37 % DOC, respectively). A decreasing trend was observed between November and December. From the quantification of OC and ON in the biopolymer fractions, an average C/N ratio of 4.3 ± 0.8 was calculated. The amount of building blocks varied less over the course of study, with the greatest amount found in the September extract. The low M_r acids

were consistent throughout all extracts. The neutral/amphiphilic fraction corresponded to the greatest percentage of measured DOC in the EPS extracts. Similar amounts were quantified in extracts from August through early November (37–40 % DOC) and greater amounts were measured in extracts from July (60 % DOC), November (19 November 2011; 49 % DOC) and December (53 % DOC) (Figure 2.7.3).

Calculated ranges of M_r for each fraction, using protein and polysaccharide-generated standard curves, are shown in Table 2.7.1. The M_r range of proteins in the biopolymer fraction was 12 to ≥80 kDa, whereas polysaccharides fell between 4 to ≥20 kDa. The low M_r acid fraction corresponded to a peptide range between 2 and 10 and 0.7 and 3 kDa for polysaccharides. Neutral/amphiphilic compounds corresponded to 0.5–3 kDa. The M_r of the building blocks fraction was not calculated because there were no distinct peaks corresponding to this fraction for which a M_r range could be calculated.

Differences between EPS extracts obtained in replicate, taken from the same set of biofilms harvested from one channel, was less than 20 % for biopolymers and building blocks and less than 10 % for low M_r acid and neutral / amphiphilic fractions (Figure 2.8.4). Variability between replicate measurements of the same sample using LC-OCD-OND was assessed by the manufacturer and reported the half confidence interval to be less than 10 % (12.4 % for the neutrals fraction) (DOC-Labor Dr. Huber, Germany).

2.4.3 Total polysaccharide and protein quantification

Polysaccharide and protein were present in similar amounts in EPS extracts and, in most cases, their summation accounted for the measured DOC (Figure 2.7.4). In the August extract, the sum of protein and polysaccharide was greater than measured DOC. Polysaccharide fluctuated between 0.3 and 1.3 mg C/g dry mass and protein between 0.7 and 2.5 mg C/g dry mass over the course of study. Additionally, total protein quantified was compared with the biopolymer fraction (Figure 2.7.5). Calculations of C/N ratios for the low M_r acid and neutrals fractions were not possible due to the interference of the NO_3 signal, and therefore these fractions were not included in the comparison with total protein. The biopolymer fraction ranged from 30 to 67 % of the total quantified protein.

2.5 Discussion

2.5.1 Extraction technique

As the focus of this work was to obtain an EPS extraction technique suitable for use in future metal-binding studies, a protocol was developed to extract DOC from EPS for subsequent metal analysis. Because introducing agitation, such as shaking and stirring, as well as longer periods of extraction time, did not increase the extraction efficiency of DOC (Figure 2.7.1), such steps were not included in the extraction protocol. No significant differences in the types of extracted OC compounds were observed between $NaNO_3$ and $NaHCO_3$ extraction solutions (Figure 2.8.3), and, therefore, $NaNO_3$ was chosen to avoid possible formation of metal-carbonate complexes.

It is important to note that the relative amounts of extracted compounds are dependent upon the method of extraction.[71,102,103] Extraction procedures can be physical methods, as used in this study, or chemical methods used to isolate specific types of compounds, whereby either easily extractable soluble compounds, or more tightly bound compounds are extracted, respectively. Soluble compounds include any soluble macromolecules or colloids, whereas the fraction more strongly bound to cell walls of embedded organisms or to other organic material is considered to contain the less easily extracted compounds of the EPS.[71] Characterization of the soluble compounds is more commonly reported in the literature; however, there have also been studies that characterized the more tightly bound fraction.[76,104,105] In this study, extracted DOC only reflects OC from soluble and loosely bound EPS. The extraction technique established in this work is suitable when metal speciation is an important consideration. Using sequential chemical extraction techniques can influence properties of the EPS, which can impact metal speciation and produce artifacts.[106] Additionally, using cation exchange resins or EDTA removes metal cations from the EPS,[104] allowing for the extraction of tightly bound compounds, but also making it difficult to identify specific EPS fractions involved in metal binding.

To assess differences in EPS composition between extracts taken in this study, it was important to determine the variability associated with replicate extractions, which takes into account both the variability associated with biological heterogeneity of the biofilms, as well as that associated with the extraction procedure. Comparison of replicates from extractions performed on two separate occasions showed that the

variability is low for DOC and OC compounds over the course of study (Figure 2.8.4). Percent differences between replicates taken in July was less than 10 % for DOC, building blocks, low M_r acids, and neutrals and less than 20 % for biopolymers. In November, percent differences for DOC and biopolymers was less than 5 % and less than 20 % for the remaining compounds. This analysis shows that differences between replicate extracts is low enough to compare differences between extracts over the period of study.

2.5.2 EPS composition

Biopolymers, building blocks of HS, low M_r acids, and neutral/amphiphilic compounds were identified in all EPS extracts and should only reflect either those compounds excreted from organisms, incorporated from the surrounding water, or released intracellular compounds coming from dying or dead organisms. The extraction procedure itself should not have caused the release of additional compounds, as no detectable amount of cell lysis occurred as a result of extraction (Table 2.8.1). To date, the majority of work analyzing M_r fractions of EPS comes from bacterial biofilms and there is little work done with EPS from phototrophic biofilms. However, as periphyton are not just comprised of algae, but also contain bacterial communities, the results obtained in this study were compared with the available work conducted with bacterial EPS.

The biopolymer fraction can correspond to high M_r polysaccharides, which are hydrophilic and non-UV absorbing. Al-Halbouni et al. reported the biopolymer fraction of EPS taken from a membrane bioreactor (MBR) to be mainly composed of polysaccharides[95] and Hong et al. reported <1 % of protein in the biopolymer fraction.[107] However, this fraction can also contain amino sugars and proteins. In the present study, the biopolymer fraction was UV absorbing and the C/N ratio was more similar to ratios calculated for protein calibration standards (C/N = 0.8 – 1:1) than for PEG standards (C/N = 30 – 40). Therefore, as the C/N ratio is influenced by the relative amounts of proteins and polysaccharides, it seems that the biopolymer fraction was largely composed of proteins. In another MBR study, Jiang et al. also indicated the presence of proteins in the biopolymer peak of soluble microbial products measured in sludge water (C/N = 17 – 18), although less than what was measured in the present study.[108]

The biopolymer fraction contained a range of different M_r proteins, as can be seen by the broad peaks corresponding to this fraction (Figure 2.7.2A). Part of the biopolymer peak contained proteins corresponding to the column separation range (Table 2.7.1), while many of these compounds fell within the void volume of the column, corresponding to M_r larger than 80 kDa. Resolution of individual proteins within the biopolymer fraction having similar M_r close to the void volume (i.e., BSA and Ovalbumin) was not possible using the OC signal (Figure 2.8.2). Therefore, a column with a higher separation range should be used with LC-OCD-OND for further characterization of the biopolymer fraction.

Studies assessing the M_r distribution of EPS from microbial biofilms have also reported high M_r fractions in similar ranges as found in this study. Simon et al. observed a fraction corresponding to 32–126 kDa in protein equivalent for anaerobic sludge.[93] Another study investigating the M_r distribution of EPS from activated sludge flocs found two high M_r fractions corresponding to 16–190 and 270–275 kDa.[109] Alasonati and Slaveykova reported specific proteins ranging from 29 to 90 kDa that were identified in EPS from the bacterium *Sinorhizobium meliloti* and, by using asymmetrical flow field-flow fractionation, concluded that a 140-kDa fraction was predominately protein-like substances.[110] In most extracts, the biopolymer fraction consistently accounted for 30–35 % of the total protein measured using the Bradford assay. This suggests that lower M_r proteins present in the other LC-OCD-OND fractions may contribute to 65–70 % of the total measured protein. It has been observed that peptides down to 3 kDa are detectable using the Bradford assay,[111] and therefore, peptides in the low M_r acid fraction should be detected. Assays of individual fractions would be needed to determine protein content in the low M_r acid fraction, as calculation of C/N ratios was not possible because of interference of the NO_3 signal.

No HS were measured in the EPS extracts, despite being continually measured in the Chriesbach stream water over the course of this 6-month study (data not shown). Liu and Fang reported humic acids to represent 8.4–30.6 % of extracted EPS from different sludge types,[102] whereas other studies investigating EPS from sludge and wastewater treatment sources cited lower values of 5 and 6.9 %.[112,113] A study conducted with periphyton taken from an acidic river showed humic acids to only compose up to 4 % of EPS.[76] The absence of HS in this study is probably because EPS were extracted from newly colonized biofilms after 25 days of growth,

and that no HS were incorporated into the EPS from the stream water used to colonize the biofilms. However, building blocks of HS were measured. This fraction, defined as lower M_r break down products of HS,[101] was most likely not HS degradation products, but rather small organics incorporated from river water or exudates from organisms. Contrary to what was observed in the biopolymer fraction, the more consistent amounts quantified in extracts (Figure 2.7.3) indicate that the compounds within the building block fraction reflected less the changes taking place within the periphyton community over the course of the 6-month study. The percent of building blocks relative to DOC corresponds well with values found by Hong et al. who reported values between 11.2 and 19.3 % DOC of foulants in a MBR.[107]

The low M_r acid peak, corresponding to final degradation products of organics and products from algal and bacterial excretion, is the sum of all free mono- and diprotic low M_r organic acids. As in the case of building blocks, a narrow M_r range for the low M_r acids was observed and did not display significant changes between July and December (Table 2.7.1). In agreement with this finding, Comte et al. reported that a significant portion of low M_r compounds in EPS extracted from activated sludge were between 0.7 and 2.7 kDa.[109] Hong et al. did not observe low M_r acids;[107] however, Al-Halbouni et al. presented LC-OCD-OND chromatograms with similar percentages of low M_r acid fractions as found in this study.[95]

The low M_r neutral/amphiphilic fraction corresponds to alcohols, aldehydes, ketones and amino acids. This fraction measured in our study was in a similar range as found by Hong et al., who reported slightly lower amounts (25.1–38.3 % DOC).[107] Interestingly, another group reported that the neutral fraction was only observed in the tightly bound EPS that had been extracted using Dowex cation exchange resin and was not present when only centrifugation was used for extraction.[95]

2.5.3 *Applications of LC-OCD-OND in EPS studies*

Information on the C/N ratio of the biopolymer fraction could be useful in studying changes in EPS as a result of shifts in species composition from seasonal succession, different stages of biofilm development, or changes in environmental conditions. Changes in extracellular monosaccharide composition of phototrophic biofilms were observed with seasonal changes[114] and with shifts in community structure.[88] A decrease in the total C/N ratio, indicating an increase in protein, of EPS extracted from marine biofilms was observed as a function of biofilm age,[114] and

specific proteins were identified necessary for bacterial biofilm formation and development.[115] To monitor such changes, LC-OCD-OND could be used as a comprehensive approach that provides more information than total C/N ratios and is not limited to the analysis of specific saccharides and proteins, as done using HPLC. The proteinaceous nature of the biopolymer fraction is also of particular interest with respect to metal binding. A study conducted by Guibaud et al. showed that proteins were an important contributor to the number of binding sites and overall complexation constants that were determined for Cd, Cu, and Pb.[80] Additionally, it was reported that certain M_r proteins in EPS extracted from periphyton were involved in the binding of Hg[116] and Cu.[117] The metal binding ability of EPS and its role in metal toxicity to periphyton is important to investigate, as many studies have measured total metal accumulation and toxicity to periphyton,[118-121] but less work has been done to understand how metal binding properties of EPS influence metal bioavailability to periphytic organisms. When coupled to metal analysis, LC-OCD-OND could aid in understanding which components of EPS are significant in metal binding.

2.6 Conclusions

The technique LC-OCD-OND is advantageous over other size based fractionation methods as it quantifies both OC and ON, thus providing additional information about relative amounts of proteins and polysaccharides in different fractions. We have developed both polysaccharide and protein calibrations for better M_r determination in LC-OCD-OND and this is the first study to use this technique for analysis of EPS originating from periphyton. We have shown that seasonal variation in EPS composition can be detected and quantified, and that LC-OCD-OND has applications beyond purely chemical characterization. Suggested applications include studies of biofilm community structure and metal-EPS binding. Therefore, we conclude that LC-OCD-OND can be used as a new tool for periphyton EPS characterization to simultaneously identify and quantify OC fractions with respect to protein and polysaccharide content as well as M_r distribution.

2.7 Figures

Table 2.7.1: M_r Distribution of EPS fractions identified with LC-OCD-OND. Both protein and polysaccharide equivalent M_r ranges calculated for each sample from calibrations generated from globular protein standards and PEG standards and using min. and max. elution times for each fraction (Figure 2.8.1).

	Biopolymers		Low M_r Acids		Neutrals	
	M_r (kDa)					
	Protein	Polysaccharide	Protein	Polysaccharide	Protein	Polysaccharide
12/5/11	≥ 80 - 25	≥ 20 - 9	9 - 3	3 - 0.7	3 - ≤ 0.5	0.7 - ≤ 0.5
19/11/11	≥ 80 - 19	≥ 20 - 7	9 - 3	3 - 0.7	3 - ≤ 0.5	0.7 - ≤ 0.5
6/11/11	≥ 80 - 25	≥ 20 - 9	8 - 3	3 - 0.7	3 - ≤ 0.5	0.7 - ≤ 0.5
24/9/11	≥ 80 - 12	≥ 20 - 4	7 - 2	2 - 0.7	2 - ≤ 0.5	0.7 - ≤ 0.5
24/8/11	≥ 80 - 14	≥ 20 - 4	7 - 3	2 - 0.8	2 - ≤ 0.5	0.8 - ≤ 0.5
26/7/11	≥ 80 - 42	≥ 20 - 15	10 - 3	3 - 0.9	3 - ≤ 0.5	0.9 - ≤ 0.5
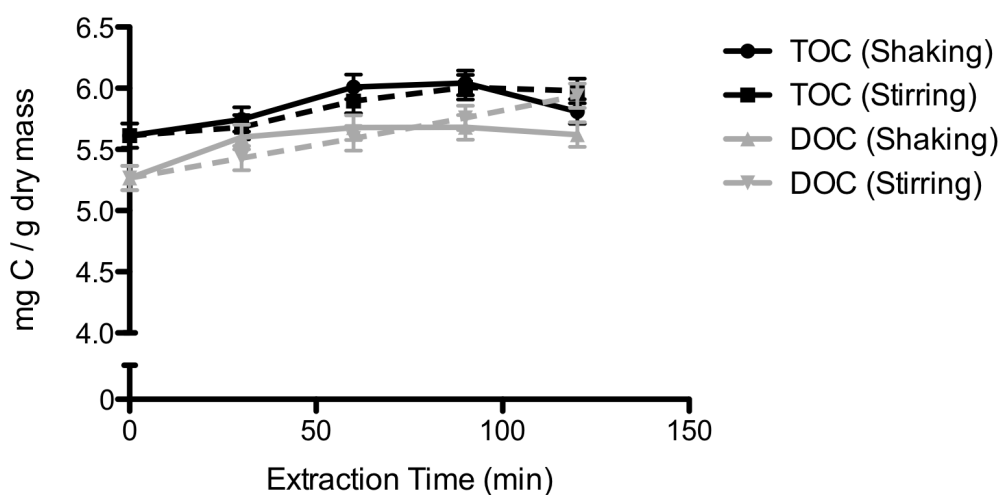
Figure 2.7.1: OC extraction efficiency of shaking and stirring extraction methods. Biomass slurry from harvested biofilms was split into separate aliquots and EPS was extracted either with shaking (—) or stirring (---) methods over 120 minutes in triplicate. Samples were taken at different time points for analysis with LC-OCD-OND. Error bars generated from standard deviation of triplicates.
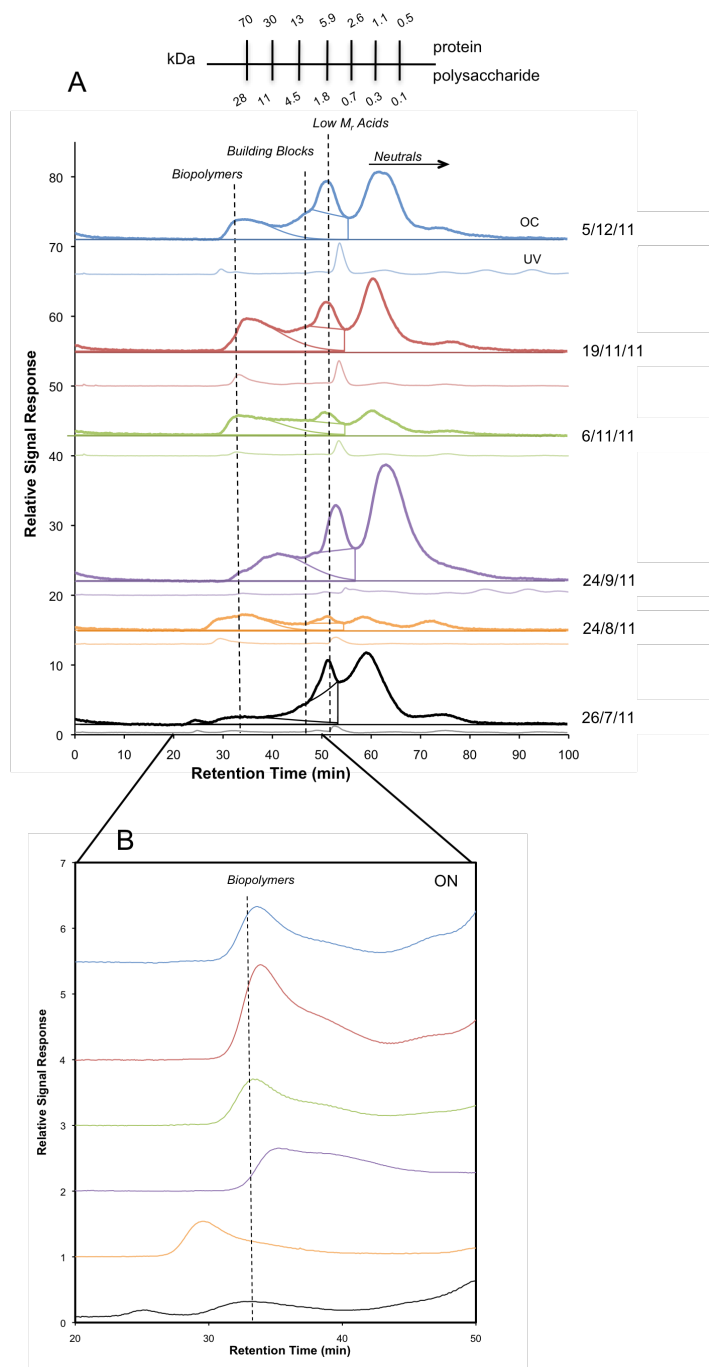
Figure 2.7.2: LC-OCD-OND chromatograms of periphyton EPS extracts taken between July and December 2001 from 25 day old biofilms. (A) For each sample set upper chromatograms correspond to OC signal and lower to UV absorbance detected at 254nm. Integration lines are shown within OC chromatograms. M_r for protein and polysaccharide equivalents generated from calibration curve. (B) ON signals correspond to biopolymer fractions.
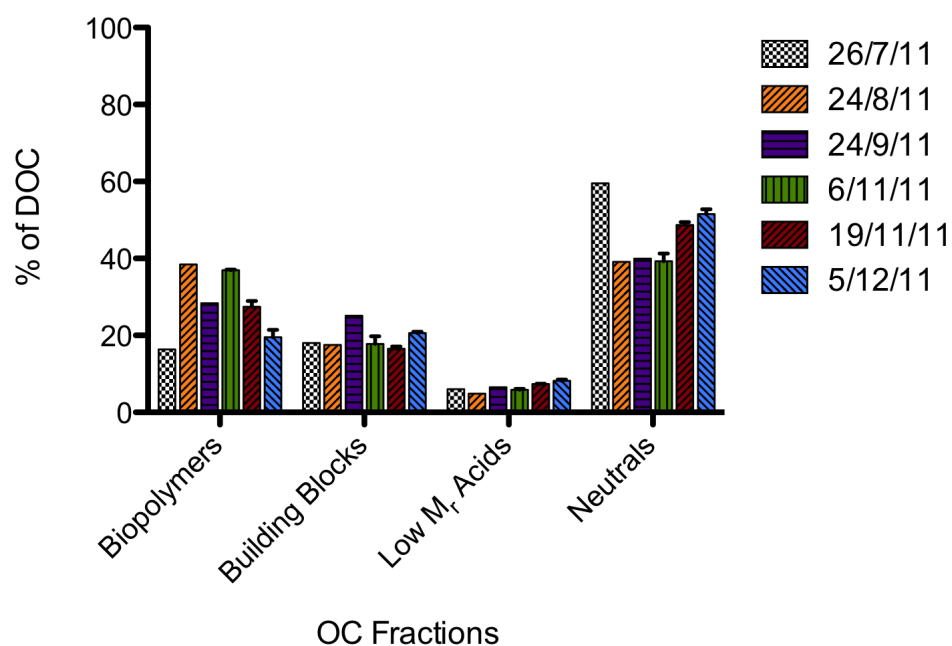
Figure 2.7.3: Quantification of OC fractions from periphyton EPS samples as determined by LC-OCD-OND using the software integration program FIFFIKUS. Values expressed as percent of chromatographable DOC. Standard deviation bars were generated from replicate extractions performed on the same set of biofilms.
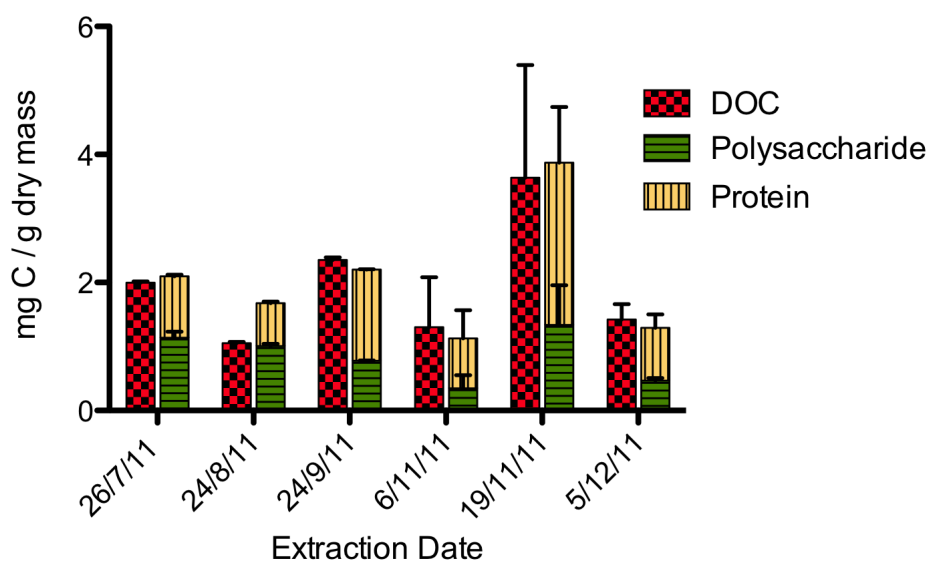
Figure 2.7.4: Comparison of DOC to total protein and polysaccharide from periphyton EPS extracts. Total protein and polysaccharide measured was converted to mg C and normalized to lyophilized dry biomass to compare with measured DOC. Standard deviation bars were generated from triplicate measurements.
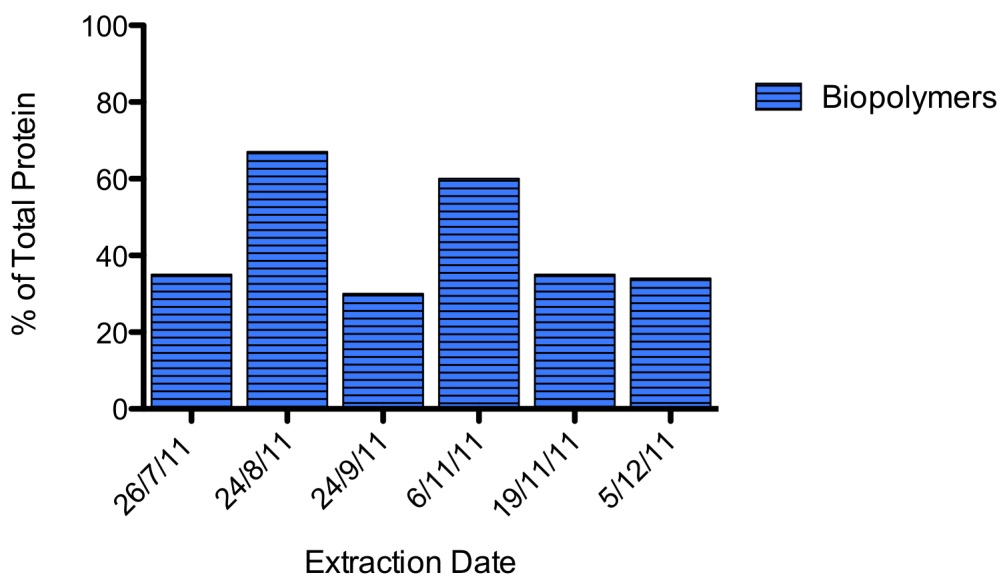
Figure 2.7.5: Comparison of biopolymer fractions to total protein from periphyton EPS. Total protein measured was converted to mg C to compare with the biopolymer fraction and biopolymer fraction presented as a percentage of total protein as determined by the Bradford method.

2.8 Supplementary Information
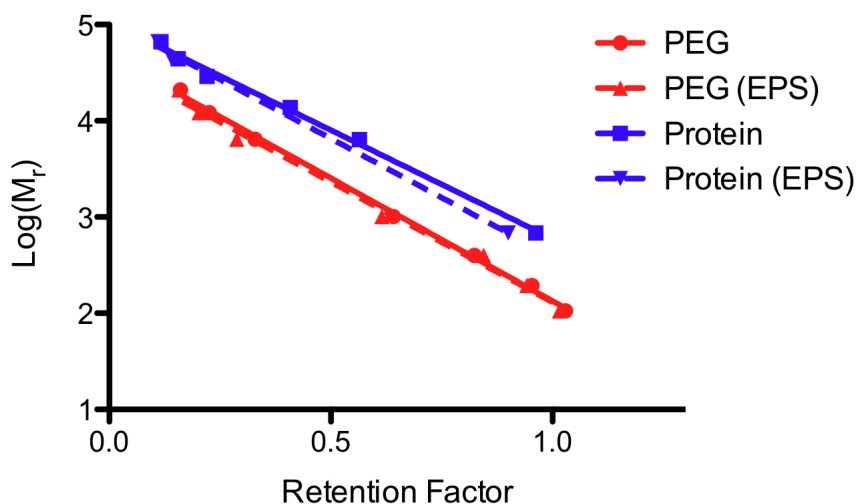
Figure 2.8.1: LC-OCD-OND calibration curve for polysaccharides and proteins. Polyethyleneglycol (PEG) standards (0.106-21.03 kDa) were diluted with nanopure water (MilliQ Ω 18.1) (——) or spiked into EPS extract (---). Protein standards were diluted with phosphate buffer (20mM, pH 6.6) and NaCl (150 mM)(——) or spiked into EPS extract (---).
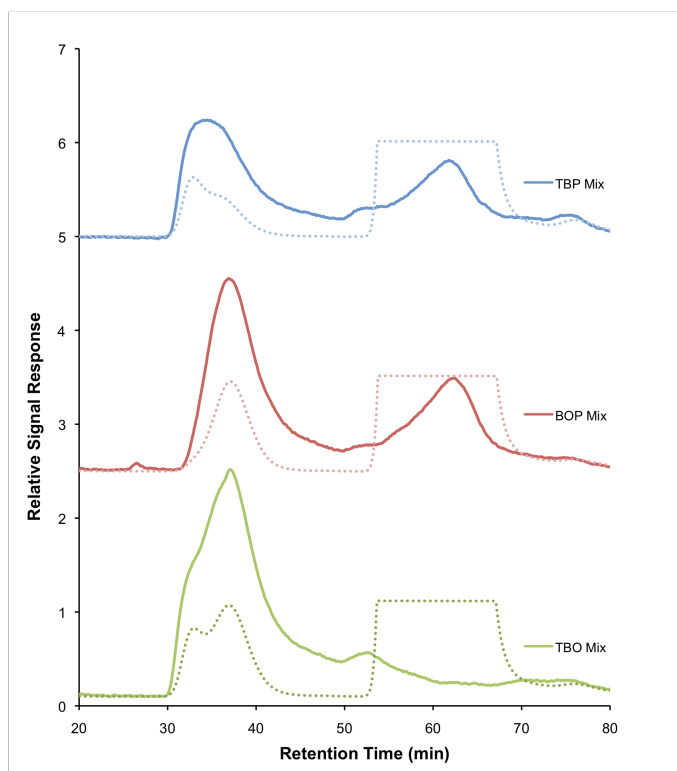
Figure 2.8.2: Thyroglobulin (T), BSA (B), Ovalbumin (O) and Pepstatin A (P) protein calibration standards combined in mixtures (TBP, BOP, and TBO) in 10 mM $NaNO_3$ and analyzed with LC-OCD-OND. Solid lines represent OC signal and dashed lines represent ON signal. Cutoff of ON signal from high NO_3 concentrations in solution.
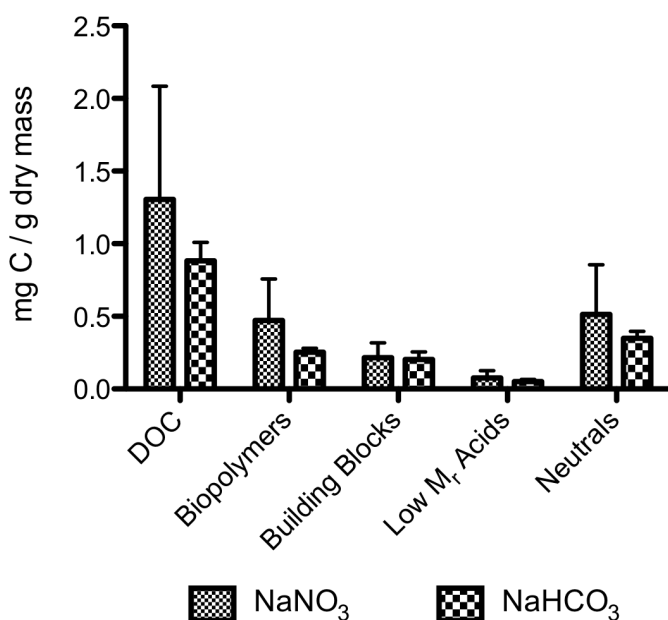
Figure 2.8.3 Comparison of different solutions on OC extraction. Biofilms were harvested and split for extractions in $NaNO_3$ (10 mM, pH 7.4) and $NaHCO_3$ (2mM, pH 7.6). Extracts were analyzed with LC-OCD-OND and OC fractions were quantified and normalized to dry biomass obtained from lyophilization.
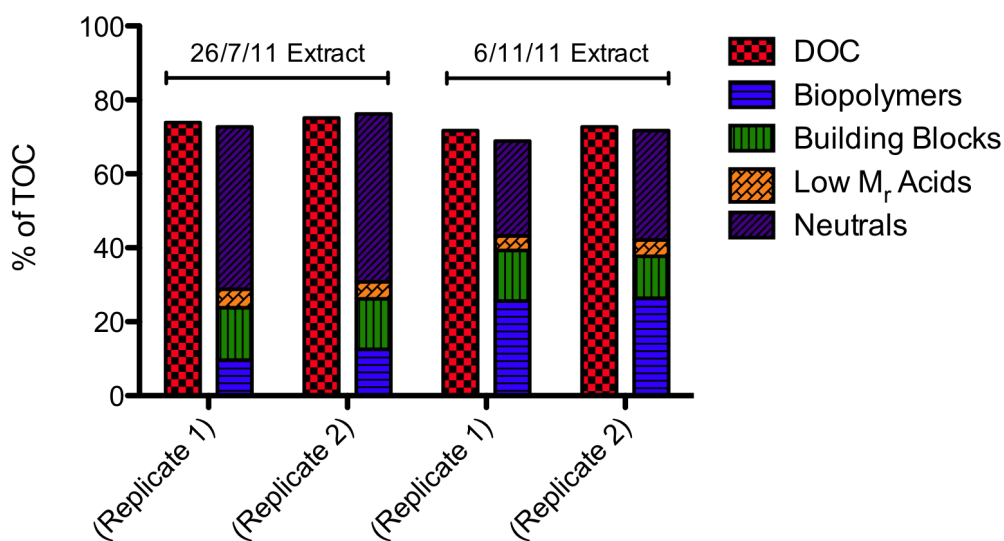
Figure 2.8.4 Variability of EPS composition. Two separate occasions are displayed when biofilms were collected from one channel and slides split into two groups (replicates 1 and 2). EPS was extracted according to the established protocol for each replicate and extracts were analyzed using LC-OCD-OND. OC fractions were quantified and expressed as % TOC.
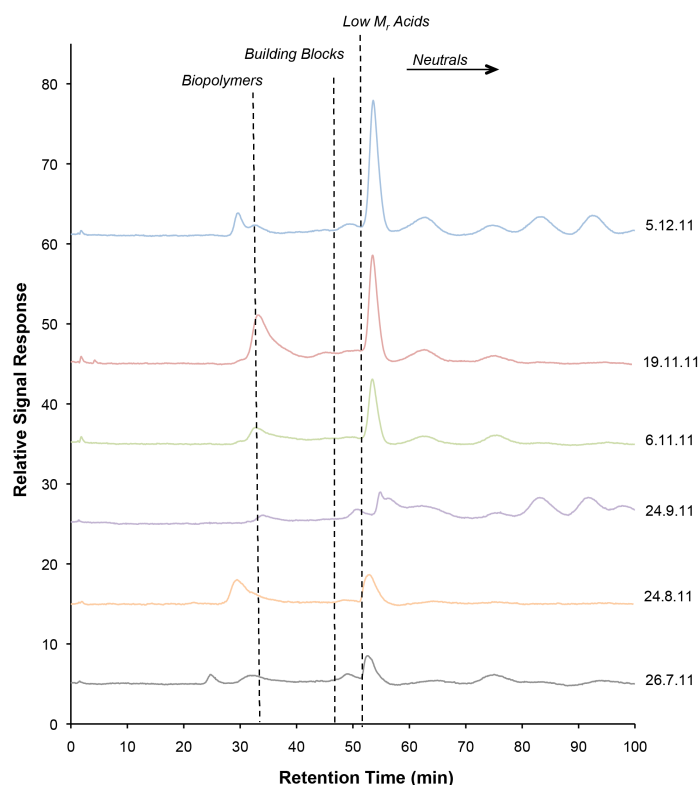
Figure 2.8.5: UV absorbance of EPS extracts taken between July and December 2011. UV absorbance was detected at 254 nm of OC fractions separated using LC-OCD-OND. Dotted lines represent elution times of corresponding OC fractions.

Table 2.8.1: G6P-DH assay results from subsequent extraction steps. Lysis of whole biomass with and without protease inhibitors (PI) was used as a representation of 100% of biomass activity.

Sample	Activity	% Total Activity
	U/mL	*%*
Cell lysis of biomass (− PI)	0.051 ± 0.002	100
Cell lysis of biomass (+ PI)	0.083 ± 0.002	100
Scraping		0
First sonication		0
Second sonication	Below LOD	0
Centrifugation		0
0.22 μm filtration		0

2.9 Supplementary Chapter: Pb-EPS Binding

2.9.1 Materials & Methods

The EPS was extracted according to Stewart et. al[122] from periphyton communities harvested on three separate occasions for each pH value tested, as not enough material was available to conduct binding experiments for all concentrations and pH values with the same EPS extract. Approximately 40 mg DOC/L of EPS were placed inside dialysis tubing (SpectraPor Biotech CE) with a defined M_r cutoff between 100-500 Da, which were previously washed with nanopure water. The dialysis tubes were placed in either 10 mM MES buffer (pH 6), MOPS buffer (pH 7), or HEPES buffer (pH 8) at 4 °C for 2 weeks in 500 mL polycarbonate Nalgene™ bottles, stirring at 300 rpm. The volume of EPS extract corresponded to 2.5% of the outer solution volume. Previous experiments indicated that equilibrium between inner and outer solutions was established after two weeks exposure to Pb. The outer solution was spiked with $Pb(NO_3)_2$ at concentrations ranging from 1 nM - 1 μM Pb^{2+}. Binding of Pb as a function of Pb^{2+} concentration at a given pH was conducted using the same EPS extract. Exposures were conducted in triplicate for each Pb concentration. To determine the amount of Pb bound to the EPS at equilibrium, a mass balance approach was taken according to Eq. 2.9.1. Total Pb of the inner solution ($Pb_{T\ inner}$), of the control EPS ($Pb_{EPSbackground}$), and of the outer solution (Pb_{outer}) were digested with 4 mL suprapure HNO_3 (65%) and 1 mL H_2O_2 (30%) in Teflon® tubes using an ultraCLAVE 4 digester (MLS GmbH) for 24 minutes at a maximum of 200 °C and 100 bar and quantified using HR-ICP-MS (Element 2 High Resolution Sector Field, Thermo Finnigan), using rhodium as an internal standard. The total unbound Pb species assumed to be in equilibrium with the outer solution ($Pb_{T\ innerPbspecies}$), was calculated according to Eq. 2.9.2 using the known volumes of the inner solution (V_{inner}) and outer solution (V_{outer}). The amount of Pb bound to the EPS was calculated according to Eq. 2.9.1 and normalized to DOC as determined by LC-OCD-OND.

$$Pb_{EPS} = Pb_{T_{inner}} - Pb_{T_{innerPbspecies}} - Pb_{EPSbackground}$$

(Eq. 2.9.1)

$$Pb_{T_{innerPbspecies}} = \frac{Pb_{T_{outer}} \times V_{inner}}{V_{outer}}$$

(Eq. 2.9.2)

Approximation of conditional stability constants at each pH were calculated according to Eq. 2.9.3 for each pH by assuming an average ligand concentration of 60 mmol ligand/g DOC obtained from a previous acid base titration.

$$K = \frac{[Pb-L]}{[Pb^{2+}][L]}$$
(Eq. 2.9.3)

2.9.2 Results & Discussion

Complexation of Pb with EPS showed a linear relationship with Pb^{2+} over a concentration rage spanning more than two orders of magnitude at all pH values tested (Figure 2.9.1). These results indicated an excess of binding sites present, as saturation of binding sites was not reached upon exposure to 1 μM Pb^{2+}. Lamelas et al. showed that only at concentrations higher than 1 μM Pb^{2+} was saturation of binding sites observed in alginic acid (50 mg/L).[123] To obtain Pb binding capacities of extracted EPS, exposure to higher Pb^{2+} concentrations are required.

In agreement with other EPS metal binding studies,[124,125] we did not observe a significant pH dependence of the Pb-EPS binding between pH 6 and pH 8, also observed in Pb binding to alginates.[123] Reported pKa values for extracted bacterial EPS ranged between 5.7 – 6.6 and 8.7 – 9.4, corresponding to carboxylic/phosphoric groups and phenolic and amino groups, respectively.[124,126] Reported pKa values were between 3 – 4 for carboxylic functional groups from alginic, mannuronic and guluronic acids commonly found in EPS.[127,128] Therefore, pH independence of Pb binding at pH 6 - 8 likely arises because within the pH range tested, carboxylic groups are expected to be deprotonated and phenolic and amino functional groups are likely still protonated.

Conditional stability constants ($logK_{Pb\text{-}EPS}$) for pH 6 – 8, calculated using concentrations in mol/L, were on average 2.8 ± 0.3 (Table 2.9.1) and did not significantly vary with pH. Values reported in the literature for Pb binding to bacterial EPS at pH 7 ranged from logK 3.1 to 4.9 depending upon the method of extraction[129] and did not show a significant pH dependence between pH 6 – 8.[124] Modeling of Pb binding to NOM at pH 7 predicted an average logK value of 4.48.[130] In contrast high logK values (9.4 ± 0.8) were reported for Pb binding to NOM sampled from Paul Lake (MI, USA),[131] and equally high values (9.44 ± 0.18) were reported for Pb sorbed to particulates in the river Glatt (Switzerland), which were attributed not only to

complexation with organic material, but also sorption to Fe and Mn oxides.[132] The conditional stability constants for EPS extracted from periphyton are relatively weak compared to those reported for bacteria EPS NOM, and inorganic particulates. This is a first indication that the EPS may not play a significant role in immobilization of Pb in periphyton, particularly in the presence of more strongly sorbing phases or complexing ligands. However, because an average ligand concentration was assumed for all calculations, acid base titrations must be performed for each EPS extract to more accurately determine $logK_{Pb-EPS}$ values.

2.9.3 Figures
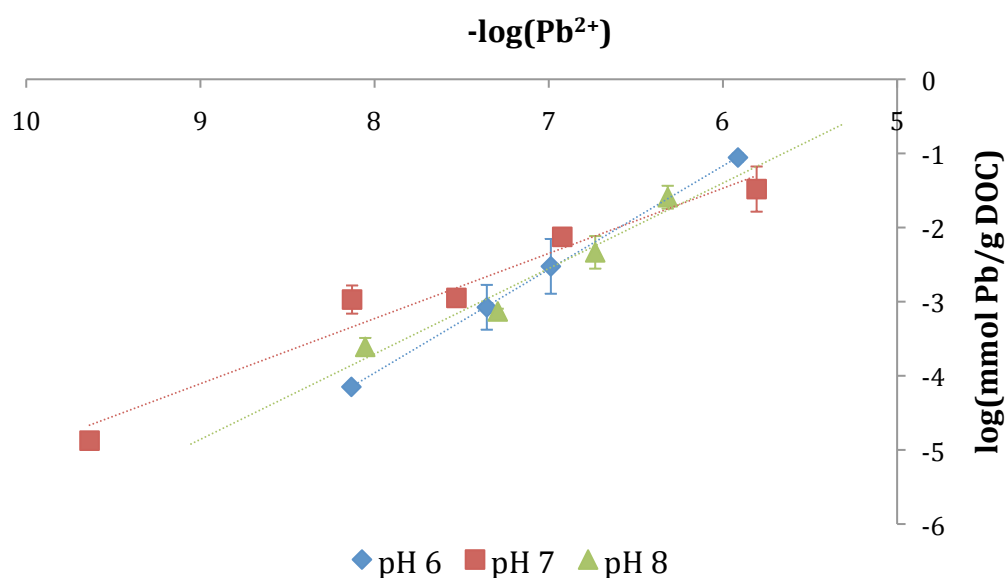
Figure 2.9.1: Pb binding to extracted EPS at pH 6-8 as function of Pb^{2+}

Table 2.9.1 Conditional stability constants for Pb-EPS binding

pH	logK (L/mol)
6	3.06 ± 0.05
7	2.50 ± 0.06
8	2.9 ± 0.3

Impact of chronic lead exposure on metal distribution and biological effects to periphyton

Stewart, T. J., Behra, R., Sigg, L. Submitted to *Environmental Science and Technology.*

3.1 Abstract

Chronic Pb exposure microcosm studies were carried out on two different periphyton communities over the course of three weeks to link Pb distribution to biological effects in periphyton. We show that three-week exposures of periphyton to 210 nM Pb^{2+} does not cause observable biological effects to photosynthesis, respiration, extracellular enzymatic activities or biomass accrual. Metal distribution studies showed that the majority of Pb is associated with the operationally defined sorbed and intracellular fractions, and relatively little with extracellular polymeric substances (EPS). No significant effects of Pb on Fe and Mn distributions were observed, whereas higher Cu accumulation occurred from increased Cu^{2+} in the exposure medium. High Fe:C and Mn:C ratios indicated the presence of inorganic Fe and Mn material associated with the biomass, which may sequester Pb and explain why no biological effects were observed. Toxic effects to periphytic organisms are likely mitigated through sorption to inorganic material, such as Fe and Mn oxides, and additionally through intracellular sequestration. Although no toxic effects of Pb were observed to the periphytic organisms themselves, periphyton can be a significant source of Pb to grazing organisms in aquatic ecosystems.

3.2 Introduction

Periphyton is an essential part of primary productivity and nutrient cycling[59] and is capable of influencing the fate and transport of both essential and non-essential metals in aquatic environments.[81,133] Metal-periphyton interactions can be highly dynamic, reflecting metal fluctuations in the overlying water column[13,134] and, depending upon the exposure conditions and kinetics of metal accumulation and release, metals concentrated in periphyton can lead to both toxic effects to periphyton structure and function[135] as well as to the trophic transfer of metals, resulting in adverse impacts to aquatic invertebrates and fish.[136,137]

Total metal accumulation in periphyton is highly dependent on metal speciation in the overlying water. Models like the Free Ion Activity Model (FIAM) and its derived Biotic Ligand Model (BLM), have been able in many cases to accurately predict and illustrate the importance of the free metal ion for metal uptake in organisms.[17] However, studies with periphyton have demonstrated that there are many cases in which labile metal complexes are more important for metal

accumulation in periphyton.[119,134] In the case of Pb, where the colloidal fraction is often significantly larger than the dissolved fraction, periphyton accumulation has been correlated to the colloidal rather than the dissolved fraction.[14]

Metal distribution within periphyton can occur via four main interactions: sorption to ionisable functional groups from extracellular polymeric substances (EPS), sorption to cellular surfaces of organisms embedded within the EPS, sorption to inorganic material, and intracellular uptake by periphytic organisms. Some studies have focused exclusively on the metal binding properties of EPS,[79,124] whereas others have measured total metal accumulation and subsequent toxic effects to periphyton.[82,138] However, a better understanding of the relationship between metal distribution in periphyton and biological effects to periphytic organisms is still lacking.

In our work, we examined this link by determining the distribution of Pb in two different communities after three-week chronic exposures. Metal distributions are reported in three operationally defined fractions: EPS, sorbed, and intracellular. The EPS fraction includes metals bound to water-soluble macromolecules or colloids. The sorbed fraction corresponds to EDTA-exchangeable metals that are either complexed with EPS that is strongly associated with the biomass (capsular EPS) or metals directly sorbed to cell surfaces of organisms. The intracellular fraction includes non-EDTA exchangeable metals that are either intracellular accumulated or sorbed to inorganic precipitates. Additionally, Cu, Mn and Fe distributions were measured to assess if Pb uptake caused a re-distribution of essential trace metals. Photosynthesis, respiration, extracellular enzymatic activities, and biomass accrual were compared between controls and Pb exposed communities, and we relate Pb distribution within periphyton to results from these biological endpoints.

3.3 Materials & Methods

3.3.1 Periphyton colonization & Pb exposure

All periphyton were colonized on glass microscope slides using a stream water flow through system as described by Stewart et al.[122] Slides were colonized for either two or four weeks and transferred to plastic boxes containing synthetic PERIQUIL medium (Table 3.8.1) representing natural freshwater, so that drying of the biofilms was avoided during transport and for the acclimatization to PERIQUIL medium prior to exposure. Three-week exposures were carried out, whereby 10 slides were placed in triplicate polystyrene microcosms (180 x 134 x 60 mm;

Semadeni AG) containing either 300 mL of PERIQUIL medium or PERIQUIL containing 20 μM Pb_T, corresponding to 210 nM Pb^{2+} (Table 3.8.2). The pH was buffered to 7.5, however, pH fluctuations between 7.5 and 8.1 were observed under the 12 hour light/dark regime used (BioSun fluorescent, MLT Moderne Light-Technik AG, ML-T8 36W/965/G13B). All solutions were refreshed every 3-4 days so that nutrient depletion did not occur and so that total Pb concentrations remained constant over the three-week exposure period. All microcosms were placed on a three-dimensional orbital shaker (Edmund Bühler GmbH, TL 10) rotating at 20 rpm with an angle of 5° at 15 °C.

3.3.2 *Metal distribution*

After the three week exposure, both control and Pb exposed periphyton were washed with fresh PERIQUIL medium and then scraped into 50 mL of PERIQUIL medium containing 1 μg/mL protease inhibitor cocktail, with equal amounts of Aprotinin, Leupeptin, and Pepstatin A (AppliChem AG) on ice. The biofilm suspensions were mixed by gentle pipetting and then further resuspended using a water sonication bath (VWR Ultrasonic Cleaner 45kHz 60 W) for 30 seconds. Suspensions corresponded to each individual microcosm (three controls and three Pb exposed). Aliquots (10 mL) were taken from each suspension for metal distribution analysis. The metal distribution analysis was performed as illustrated in Figure 3.8.1. Total metal was measured by directly digesting 1 mL of the suspension with 4 mL suprapure HNO_3 (65%) and 1 mL H_2O_2 (30%) in Teflon$^{®}$ tubes using an ultraCLAVE 4 digester (MLS GmbH) for 24 minutes at a maximum of 200 °C and 100 bar. The remaining suspensions were centrifuged at 1880 × g for 10 minutes and 1 mL of the supernatant containing EPS was directly digested. The remaining biomass was resuspended in EDTA (4 mM) to remove metals either directly bound to cells or metals bound with cell associated EPS. After centrifugation the supernatant containing sorbed EDTA exchangeable metals was digested. A subsequent biomass wash with 10 mM MOPS buffer was also conducted to remove any residual metal-EDTA complexes, analyzed for metal content and included in the sorbed fraction. The metal content in the remaining biomass corresponded to the operationally defined intracellular fraction. Biomass was lyophilized and weighed. Ash free dry weights (AFDWs) were taken by combusting at 480 °C for 1 hour in a muffle furnace

(LE 1/11, Nabertherm GmbH, Germany). The AFDW was calculated as the difference between the dry weight and the weight post combustion and expressed as mg/cm^2. Carbon and nitrogen content of the biomass fractions were determined using a CNS analyzer (HEKAtech GmbH, Germany). All fractions were digested, appropriately diluted, and metal content of the digests was analyzed using HR-ICP-MS (Element 2 High Resolution Sector Field, Thermo Finnigan), using rhodium as an internal standard. Measurements were checked using reference material M105A (IFA, errors: ^{208}Pb <20%, ^{65}Cu < 8%, ^{56}Fe < 3%, ^{55}Mn < 3%). Metal concentrations were normalized to either dry weight or to the total surface area of the colonized glass slides.

3.3.3 Biological endpoints

Photosynthetic yields of periphyton suspensions were measured using PHYTO-PAM (Heinz Walz GmbH, Germany). Both light and dark-adapted suspensions were measured to assess both the effective and maximum quantum yields, respectively. For each of the triplicate suspensions, four technical replicates were measured, each for the light and dark-adapted samples. Photosynthetic yields were measured at four different wavelengths: 470 nm, 520 nm, 645 nm and 665 nm. Although each wavelength does not correspond to a specific type of algae (i.e. green algae, diatoms, and cyanobacteria), the different wavelengths give a rough estimate of different algal populations by contributing in different extents to the excitation of Chl*a* in green algae, to fucoxanthin/peridinin in diatom and dinoflagellates, and to phycocyanin and allophycocyanin in cyanobacteria.[139]

Aliquots of periphyton suspension were taken and fixed in 0.01% paraformaldehyde and 0.1% glutaraldehyde and stored at 4 °C prior to algal species composition determination using light microscopy. Species were identified and assessed based on their relative abundance: 5 – dominant, 4 – frequent, 3 – periodic, 2 – rare, 1 – singular. Assessments were conducted individually for each triplicate microcosm and values were averaged (Figure 3.8.2).

Respiration measurements were conducted using the MicroResp™ system according to Tlili et al.,[140] based on a colorimetric method in which color changes of a pH indicator dye are related to the release of CO_2 by heterotrophic communities. Briefly, for each triplicate periphyton suspension (control and Pb exposed), aliquots

were added in technical triplicates to either nanopure water (NPW) (Ω 18, Milli-Q), to assess the basal respiration, or to a specific carbon substrate, to assess the substrate induced respiration, in 96-deepwell plates so that the final substrate concentration was 25 mM. A top plate containing a pH indicator gel was sealed to the bottom deep well plate and the system was incubated in the dark at 25 °C for 24 hours. Results were calculated relative to basal respiration in the presence of NPW.

Potential extracellular enzymatic activities of β-glucosidase (β-GLU), leucine aminopeptidase (LAP), and alkaline phosphatase (AP) were measured. Activities were measured using fluorescent substrate analogues containing either 4-methylumbelliferyl (MUF) (Sigma-Aldrich) for β-GLU and AP or 7-amido-4-methylcoumarin (AMC) (Sigma-Aldrich) for LAP. Each of the triplicate periphyton suspensions (1 mL) was incubated with each of the substrates (1 mM) under saturating conditions for 40 minutes in the dark at 25 °C, after which the reaction was stopped with glycine buffer (1 M, pH 10.55). Fluorescence of the converted substrate was measured at emission/excitation wavelengths of 366/442 nm for MUF-containing substrates and 340/436 nm for AMC-containing substrates. Fluorescence values were converted into mmol of converted substrate per unit time using a standard calibration (Figure 3.8.3) and normalized to the dry weight of biomass.

3.4 Results

3.4.1 Metal accumulation and distribution in periphyton

Total accumulation and distribution of Pb, Cu, Mn and Fe in both control and Pb exposed periphyton were quantified to identify the important fractions responsible for accumulation, and to determine if the accumulation of Pb caused re-distribution of Cu, Mn, and Fe. Figure 3.7.1A shows that background Pb in control periphyton was 60 ± 20 nmol Pb/g DW and, upon exposure, total Pb accumulation increased to 11 ± 4 μmol Pb/g DW. No significant differences in total Pb accumulation between the two Pb exposed communities were observed. The majority of accumulated Pb was present in the sorbed and intracellular fractions, whereas little (9 ± 3%) was present in the EPS fraction. In the control periphyton similar distributions were also observed, and Pb was below the detection limit for the EPS fraction. The ratios of Pb:C were similar in both communities in the Pb exposed biomass (100 ± 20 μmol/mol and 80 ±

20 μmol/mol) and in the controls (0.5 ± 0.2 μmol/mol and 0.16 ± 0.09 μmol/mol), calculated based upon the metal and carbon contents of the intracellular fraction (Table 3.7.1).

On average, greater total accumulation of Cu in Pb exposed periphyton communities (2.2 ± 0.8 μmol Pb/g DW) was observed relative to control communities (0.5 ± 0.2 μmol Pb/g DW) (Figure 3.7.1B). This greater accumulation likely reflects the increase in Cu^{2+} in the Pb exposure medium (Table 3.8.2). Although total Cu was similar in both control communities, Cu accumulation in the Pb exposed communities was significantly higher in the first community, relative to the second community. This increase was also reflected in the sorbed fraction. However, despite the increase in Cu accumulation in Pb exposed communities, intracellular Cu was similar in both control and Pb exposed periphyton. The Cu in the EPS fractions was below the detection limit. Similar to Pb, the majority of Cu was found in the sorbed and intracellular fractions. Exposure to Pb did not change Cu:C ratios (Table 3.7.1), however the first control community had smaller Cu:C ratios relative to the second, 1.7 ± 0.4 μmol/mol and 13 ± 2 μmol/mol, respectively.

Average total Mn content for all communities was 40 ± 10 μmol Mn/g DW. Total Mn was statistically similar for all periphyton measured with the exception of Pb exposed periphyton in the first community (57 ± 4 μmol Mn/g DW), which was higher relative to the control (35 ± 2 μmol Mn/g DW) (Figure 3.7.1C). Intracellular Mn content of controls and Pb exposed periphyton were statistically similar for both communities and Mn was predominately associated with the intracellular fraction, (Figure 3.7.1C). Significantly higher Mn:C ratios, relative to Pb:C and Cu:C, were calculated, which ranged between 590 ± 70 μmol/mol and 1100 ± 600 μmol/mol (Table 3.7.1). Total Fe was on average 90 ± 40 μmol Fe/g DW (Figure 3.7.1D). Exposure to Pb did not influence total accumulated Fe and was statistically similar in all periphyton measured. The majority of Fe was associated with the intracellular fraction and, similar to Mn:C ratios, Fe:C ratios were significantly higher than Pb:C and Cu:C and were on average 2000 ± 1000 μmol/mol (Table 3.7.1).

3.4.2 Biological effects to periphyton

A series of endpoints specific to autotrophs, heterotrophs or targeting the whole community were used to assess the effects of chronic Pb exposure to periphyton. Assessment of photosynthetic yield was used to target the autotrophic

population, and substrate induced respiration was measured to target the heterotrophic community, which is predominantly responsible for respiration in periphyton with a relatively minor contribution from autotrophs. Extracellular enzymatic activities and biomass were used as more general endpoints for effects to the whole community.

Effects specific to photosynthetic algae were measured by comparing both the effective and maximum photosynthetic yields between controls and Pb exposed periphyton at four different wavelengths targeting green, blue and brown algal species. Although effective and maximum photosynthetic yields for controls in the first community were significantly higher than in the second community ($p<0.0001$), no significant differences were observed between controls and Pb exposed for either community (Figure 3.7.2). Algal species composition analysis (Figure 3.8.2) did not reveal any significant shifts in composition of the algal community upon Pb exposure in either of the periphyton communities exposed, with the exception of a decrease in the cyanobacteria *Chameasiphon* in the second community upon Pb exposure.

To determine if Pb exposure caused an impact to the heterotrophic community, substrate induced respiration was measured in control and Pb exposed periphyton (Figure 3.7.3). Respiration in the absence of any substrate was used to determine basal respiration activity and relative changes in respiration activity in the presence of different carbon substrates were used as a fingerprint for the bacterial community, assuming that substrate specific respiration induction varies depending upon the composition of the heterotrophic community. Significant differences in the induction patterns were observed between the two different control periphyton communities tested (Figure 3.8.4), indicating that different communities were present. An increase in respiration induced by glucose -1- phosphate was observed in the Pb exposed periphyton of the first community, whereas increase in respiration induced by D L-α-Glycerol phosphate in the Pb exposed periphyton was observed in the second community. However, these substrate induced respiration patterns overall were not significantly different between the controls and the corresponding Pb exposed periphyton (Figure 3.7.3).

The extracellular enzymatic activity of β-GLU, LAP, and AP, which are representative enzymes for the degradation organic matter into assimilable nutrients, were quantified in both control and Pb exposed periphyton to determine how chronic Pb exposure might affect the important ecological function of nutrient acquisition and

cycling. As shown in Figure 3.7.4, significant differences between the two control communities for β-GLU and LAP were observed and activities for AP in controls were statistically similar. However, none of the enzymatic activities were significantly affected by chronic exposure to Pb. Ash free dry weights (AFDWs) were used to assess the impact of Pb exposure on overall biomass accrual during the exposure. As shown in Figure 3.7.5, AFDWs at the end of the three-week exposure did not significantly differ between the control and exposed periphyton, and were actually similar between the two periphyton communities.

3.5   Discussion

3.5.1   Metal accumulation

Total metal accumulation in periphyton is related not only to the total metal concentration, but also to the metal speciation during the exposure. Depending on the identity of the metal, its concentration, and water chemistry, the free ion, labile complexes and even the colloidal fraction, in the case of Pb, can be important in determining total accumulation in periphyton. In our study, periphyton was exposed to 20 μM Pb_T, which corresponded to 210 nM Pb^{2+} in the exposure medium. Total Pb accumulation in Pb exposed periphyton (11 ± 4 μmol Pb/g DW) corresponded well with a week long microcosm exposure study in which periphyton that were exposed to 100 μM Pb_T and 100 μM Cd_T, corresponding to 290 nM Pb^{2+}, accumulated 14 μmol Pb/g DW.[141] The free ion concentration was similar to our study and resulted in similar total Pb accumulation. Although the exposure time differed from our study, it appears that the free ion concentration was more related to Pb accumulation than total Pb and that total Pb accumulation seems to be independent from the community composition. In a study conducted by Ancion et al., approximately 24 μmol Pb/g DW accumulated in periphyton upon a three-week metal mixture microcosm exposure to 50 μM Pb_T, 50 μM Cu_T, and 500 μM Zn_T conducted in diluted stream water (metal speciation not reported),[118] also in a similar range as found in our study.

Accumulation of Pb in periphyton sampled from the field is often lower, in the nmol Pb/ g DW range, with exposure to nanomolar dissolved Pb concentrations. In a translocation study linking metal accumulation in periphyton with metal speciation in the overlying water, dissolved Pb ranging from 0.73 – 1.5 nM, of which 27-93% was

labile, resulted in a total Pb accumulation ranging from 34 to 114 nmol Pb/ g DW.[13] In another study monitoring metal accumulation in stream periphyton sampled from 23 different field sites, although dissolved Pb concentrations were not reported, Pb accumulation was on average less than approximately 100 nmol Pb/ g DW.[78] These results are in good agreement with the total background Pb measured in our control periphyton (60 ± 20 nmol Pb/g DW). Biofilms collected in the Boulder River watershed, with areas affected by acid mine drainage and, therefore, high metal inputs, contained dissolved Pb ranging from 0.5 – 10 nM and colloidal Pb ranging from 0.5 – 40 nM Pb, which corresponded to total accumulated Pb from 58 nmol Pb/ g DW up to 5.3 μmol Pb/ g DW, the latter corresponding to the range of total Pb accumulation measured in our microcosm studies.[14] Interestingly, it was the colloidal fraction of Pb that seemed to dictate the total accumulation in periphyton, rather than the dissolved. This correlation indicates that periphyton can serve as an important Pb sink, as it is appears to retain deposited colloidal Pb.

In our study, exposure of Pb had an indirect impact on total Cu accumulation by outcompeting Cu for binding to EDTA, leading to an increase in Cu^{2+} in the exposure solution from 1.5×10^{-14} M to 3.1×10^{-10} M. The resulting increase in total Cu accumulation in periphyton was due to an increase in the sorbed fraction. As intracellular Cu was similar between control and Pb exposed periphyton, we observed no indication of competition for intracellular uptake in periphytic organisms, despite a recent study demonstrating competition effects between Pb^{2+} and Cu^{2+} in the green algae *C. reinhardtii* for the same transporter.[142] In contrast to this study, Meylan et al. observed increasing intracellular Cu in periphytic organisms with increasing Cu^{2+} concentrations, which may indicate that the higher amounts of Cu in the sorbed fraction upon Pb exposure was sequestered and not available to be taken up by organisms.[143]

Content of Cu in both the control and Pb exposed periphyton communities corresponded well with values reported in periphyton collected from the Birs and Thur rivers in Switzerland, where measured dissolved Cu (3 – 150 nM) was in the range of total Cu in our medium (125 nM).[144] Accumulated Cu in periphyton taken from uncontaminated sites along these rivers ranged from 0.07 – 0.71 μmol Cu / g DW, corresponding to Cu in our control periphyton (0.4 – 0.6 μmol Cu / g DW), and Cu accumulation as high as 3.93 ± 1.56 μmol Cu / g DW was measured in the Birs

River and corresponded to Cu accumulated in our Pb exposed periphyton (1.5 – 3.0 μmol Cu / g DW).[144] In a study linking metal speciation to Cu and Zn accumulation in periphyton sampled from a Swiss stream, background total Cu accumulation was between 0.3-1.4 μmol Cu / g DW, similar to our control periphyton, and during rain events increased to between 1.4 – 9.0 μmol Cu / g DW, similar to total Cu in the Pb exposed periphyton.[134]

Values for total accumulated Mn and Fe reported in several freshwater periphyton studies ranged from 21.5 μmol Mn/m^2 [145] - 42.5 μmol Mn/m^2 [146] and 162 μmol Fe/m^2 [147] - 496 μmol Fe/m^2.[146] Values for Mn were slightly higher in our periphyton (40 ± 7 to 96 ± 20 μmol Mn/m^2) and similar in the case of Fe (50 ± 10 to 270 ± 70 μmol Fe/m^2). In these studies, Fe and Mn oxides were responsible for the majority of Pb binding relative to the organic fraction, in some cases responsible for more than 90% of sorbed Pb, where Mn oxides had up to an order of magnitude higher binding capacity relative to Fe oxides.[148] Reported binding capacities for Fe oxides in periphyton were between 0.4 mmol Pb/mol Fe[147] and 36.3 mmol Pb/mol Fe,[145] whereas binding capacities for Mn oxides were generally higher between 7 mmol Pb/mol Mn[147] and 833 mmol Pb/mol Mn.[145] In our study, ratios of Pb:Fe and Pb:Mn ranged between 125 – 162 mmol Pb/mol Fe and 234 – 279 mmol Pb/mol Mn. These results indicate that if Fe and Mn originate from oxides rather than intracellular content, enough would be present to sequester Pb in the periphyton measured in our study.

Just as metal speciation in the overlying water is important for metal accumulation in periphyton, the metal speciation within periphyton is critical for determining metal bioavailability and subsequent biological effects. Metal distribution results are discussed based upon the assumption than no metal redistribution occurred during the fractionation process. However, it is possible that disruption of the three-dimensional structure of periphyton caused a redistribution of weakly complexed metals to stronger ligands.

The EPS are generally proposed in the literature as having protective function by limiting metal diffusion and intracellular uptake of metals that may pose toxic effects to organisms. Increased EPS production in phytoplankton has been observed as a result of metal exposure,[69] and another study reported that heavy metal concentrations were, on average, four times greater in the EPS fraction than in the

bound fraction of periphyton, but that Pb was in greater amounts in the bound fraction relative to the EPS.[76] Our result are in agreement with this observation, as only 9 ± 3 % of total Pb was associated with the EPS fraction, and suggest that easily extractable EPS do not play an important role in immobilizing Pb in periphyton.

In our study, the majority of total Pb was associated with the sorbed and intracellular fractions. The intracellular fraction, which corresponded to 30% ± 6 % of the total accumulated Pb, is often used as a measure of intracellular uptake and is the fraction of interest with respect to biological effects. As Mn and Fe were also predominantly associated with the intracellular fractions (Figure 3.7.1C,D), and ratios of Fe:C and Mn:C (Table 3.7.1) are one to two orders of magnitude higher than those values reported in the literature for phytoplankton,[149,150] it seems that the Fe and Mn associated with this fraction originate from inorganic material such as Fe and Mn oxides. Previous studies have shown that Fe and Mn oxides present in biofilms are important phases for the sequestration of Pb and contribute more to the binding capacity of the biofilm than the organic fraction.[146] Therefore, it is possible that, in addition to being intracellularly accumulated, Pb is also sequestered by extracellular Fe and Mn oxides.

3.5.2 Biological effects

Despite the majority of Pb associated with the sorbed and intracellular fractions, chronic Pb exposure did not cause any significant effects to photosynthesis, bacterial community compositions, extracellular enzymatic activities, or to biomass accrual. These results indicate that Pb sequestration mechanisms are present, which mitigate Pb toxicity to periphytic organisms. The EPS are a first protective barrier against the uptake and potential toxicity of metals. In addition to providing functional groups for metal binding, the EPS also contain extracellular enzymes, which play a key role in nutrient cycling by breaking down organic matter into assimilable nutrients. Accumulation of metals in the EPS can potentially interfere with activities of extracellular enzymes from direct inhibition of the enzyme. Additionally, effects can also result from the inhibition of enzyme production, or be a combination of these two modes of action. We initially hypothesized that if the EPS served a protective role in sequestering Pb, β-GLU activity could be a likely target, as this enzyme was shown to be exclusively located in the EPS fraction, and with addition of 1 μM AgNO$_3$ a complete inhibition was reported.[151] However, although

differences in control communities were observed, which can arise from differences in substrate availability,[152] Pb exposed communities showed similar activities as the controls, likely due to the low amounts of Pb associated with the EPS fraction.

We also hypothesized that LAP, a cell surface bound metalloenzyme, for which Zn^{2+} in addition to Mg^{2+} and Mn^{2+} are functionally important, would be a likely target, as Pb has shown inhibitory effects through competition with Zn, Mg and Mn.[153] However, as with β-GLU activity, no effects of Pb were observed to LAP activity. The absence of effects to extracellular enzymatic activities is interesting with respect to the sorbed fraction of Pb, because this EDTA-exchangeable fraction, depending upon the Pb binding stability of other natural ligands present, would be more available to interact with surface bound enzymes like LAP and AP, relative to the intracellular fraction. However, it appears that Pb within the sorbed fraction is not bioavailable to cause inhibition of enzymes. These results further indicate that Pb^{2+} concentrations in periphyton are low, either resulting from intracellular Pb sequestration or Pb sorption to Fe and Mn inorganic material embedded in the EPS.

Effects to photosynthesis and respiration would both require the disruption of intracellular processes in algal and bacterial communities. Decrease in photosynthesis was reported in the green algae *C. reinhartdii* upon long-term exposure to 1 - 10 nM Pb^{2+}, where intracellular Pb (approximately 6 µmol Pb / g DW) was in the same range as our intracellular fraction (2 – 3 µmol Pb / g DW).[15] Although no known studies have been conducted specifically on the effects of Pb uptake on bacterial respiration in periphyton, EC_{50} values ranging between 0.58 and 5.55 nM Pb_T in pore water of soils was reported with respect to shifts in bacterial community composition.[154] We observed no effects to photosynthesis and did not measure significant changes in the bacterial communities, which indicates a low degree of bioavailability in the intracellular fraction as a result of intracellular sequestration or from possible sequestration by extracellular Fe and Mn inorganic precipitates.

In the case of intracellular accumulation, sequestration of Pb, either through binding to phytochelatins (PCs) or intracellular precipitation, may explain the lack of toxicity observed. Induction of PCs in periphyton have been measured in response to elevated Zn concentrations[155] and induction of PCs was measured in the green algae *C. reinhardtii* upon Pb exposure down to 1 nM Pb^{2+}.[15] Intracellular speciation measurements in *C. reinhardtii* upon exposure to 0.1 nM Pb^{2+} revealed that Pb is

initially sequestered as $PbO_{(s)}$ and $Pb_3(PO_4)_{2(s)}$ and shifts to thiol complexation upon longer exposure times (Stewart et al., Chapter 4), indicating importance of precipitation and thiol complexation in the intracellular sequestration of metals.

3.6 Conclusions

We have seen that despite significantly higher total Pb accumulation relative to what is measured in control periphyton, and that the majority of Pb is associated with the biomass, Pb does not seem to present a direct threat to periphytic organisms. Sequestration of Pb through intracellular precipitation and thiol complexation as well as Pb sorption to Fe and Mn inorganic material associated with the biomass are possible explanations for the absence of toxic effects. Therefore, as Pb content in periphyton has been reported to positively correspond to Pb concentrations in macroinvertebrates,[14] what is of more ecological concern is the role of periphyton as a sink and potentially toxic source of Pb to grazing organisms higher in the tropic chain.

3.7 Figures
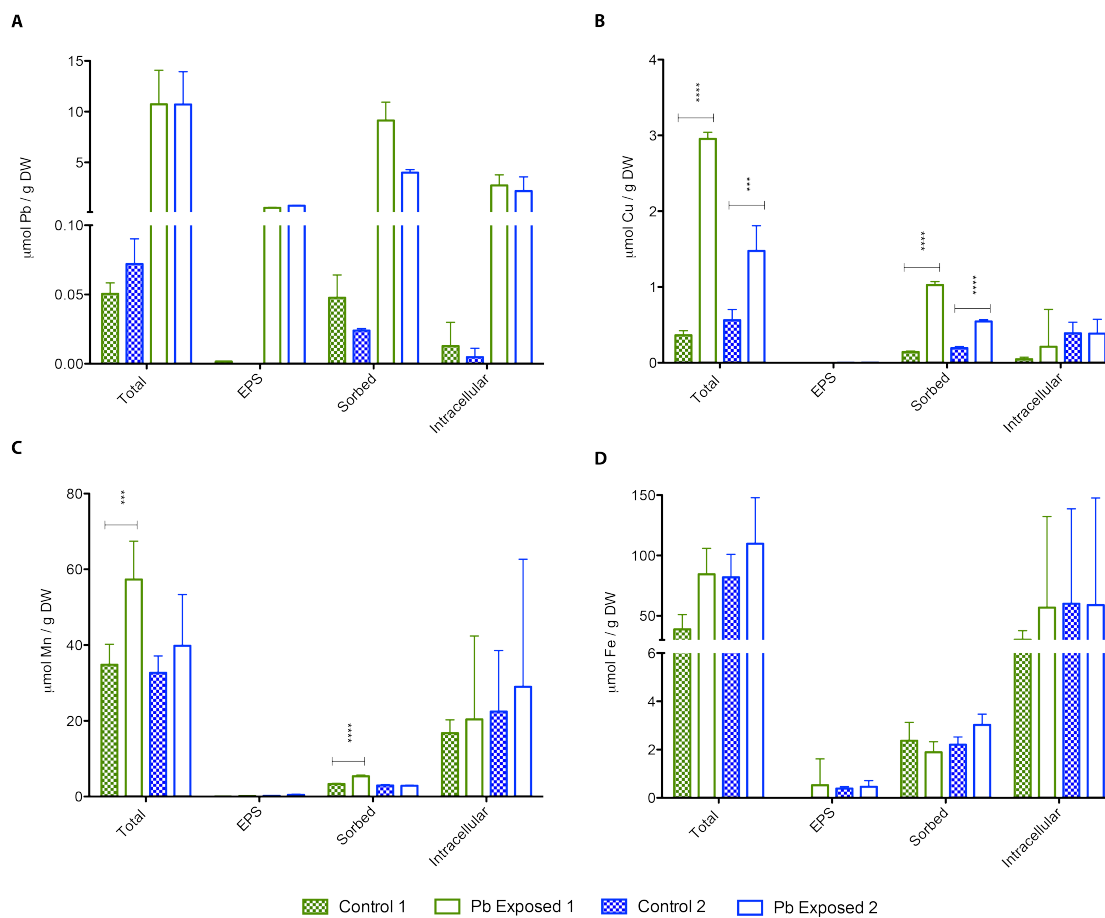
Figure 3.7.1: Distribution of metal in periphyton upon chronic Pb exposure. Two different communities of periphyton were exposed for three weeks to 210 nM Pb^{2+}. Metal distributions of Pb (A), Cu (B), Mn (C) and Fe (D) were measured after the chronic Pb exposure from both control and Pb exposed periphyton. Error bars represent the 95 % CI associated with the average of three replicate microcosm exposures. Asterix indicate degree of significance between Pb exposed periphyton within a specific fraction: *** $p < 0.001$, **** $p < 0.0001$

A

B
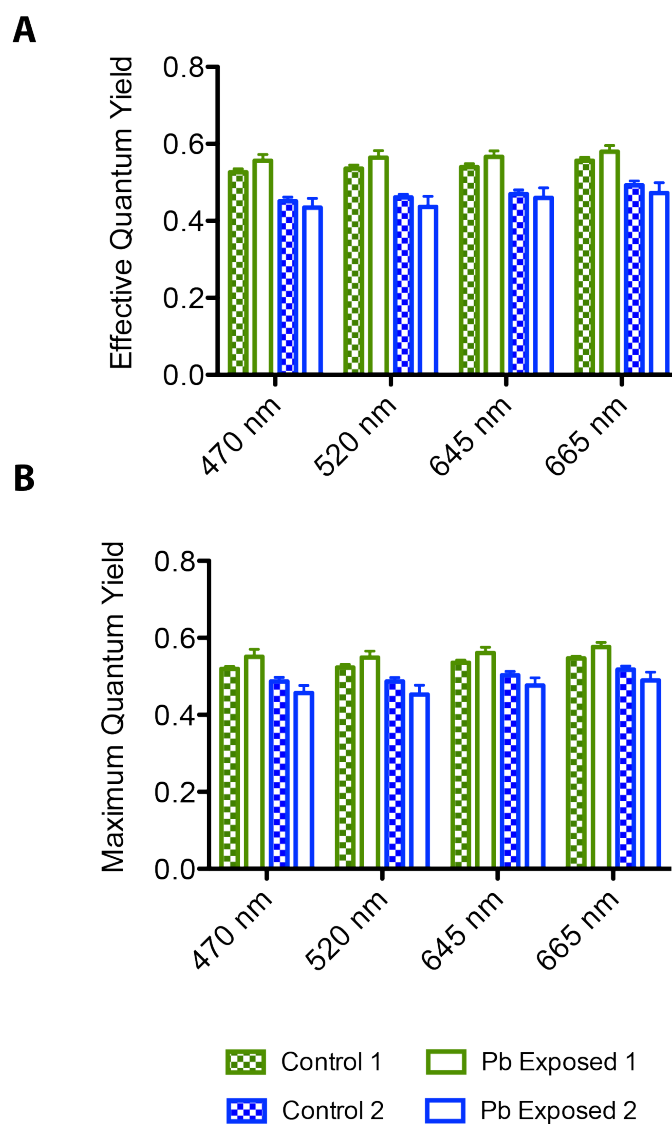
Figure 3.7.2: Impact of chronic Pb exposure on effective quantum yield (A) and maximum quantum yield (B) of two different periphyton communities. Error bars (95% CI) were generated from triplicate microcosm exposures.

A

B
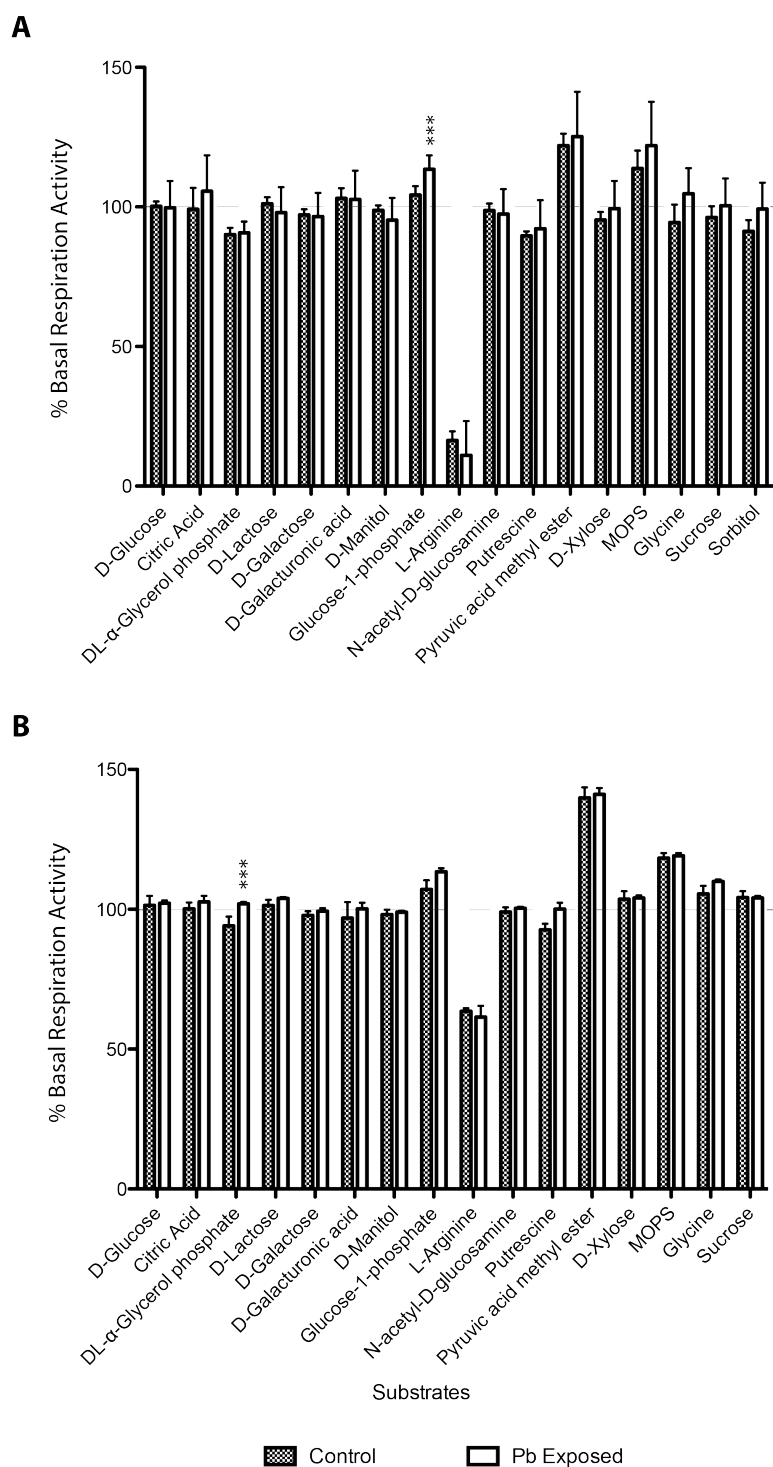
Figure 3.7.3: Effects of chronic Pb exposure on carbon substrate induced respiration of periphyton. Respiration of non-exposed and exposed periphyton was measured in periphyton community 1 (A) and community 2 (B) using MicroResp^{TM} in the presence of 16 different carbon substrates and expressed as percent of basal respiration, measured without addition of substrate. Error bars correspond to 95% CI associated with triplicate microcosm exposures. Asterix indicate degree of significance between Pb exposed periphyton for a specific substrate: *** p < 0.001.
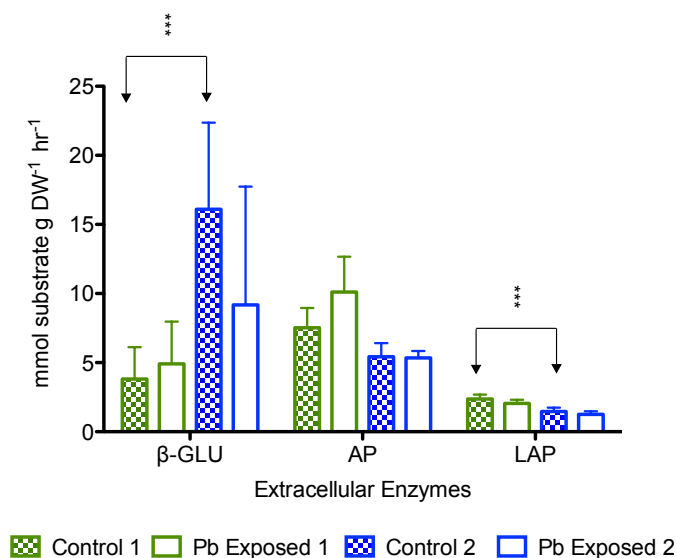
Figure 3.7.4: Impact of chronic Pb exposure on extracellular activities of β-Glucosidase (β-GLU), leucine aminopeptidase (LAP), and alkaline phosphatase (AP) in two different periphyton communities. Results are in mmol of converted substrate as calculated from standard curves (Figure 3.7.3) and normalized to DW of biomass. Error bars (95% CI) were generated from triplicate microcosm exposures.
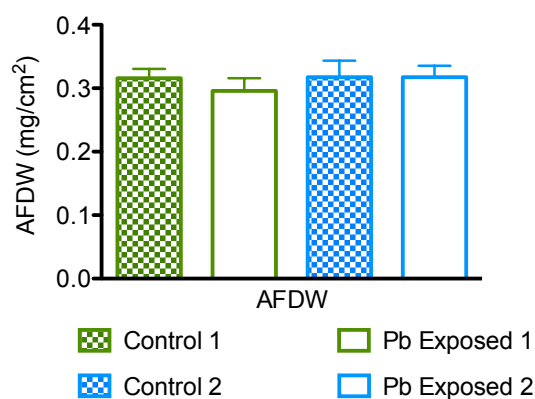
Figure 3.7.5: Comparison of ash free dry weights (AFDWs) of control and Pb exposed periphyton in two different communities.

Table 3.7.1: Carbon to nitrogen and metal to carbon ratios of periphyton biomass.

	Community 1		Community 2	
	Control	Pb Exposed	Control	Pb Exposed
C:N (mol/mol)	8.4 ± 0.4	9.1 ± 0.4	8.30 ± 0.09	8.08 ±0.03
Fe:C (µmol/mol)	1100 ± 100	2000 ± 1000	2000 ± 1000	2000 ± 1000
Mn:C (µmol/mol)	590 ± 70	1100 ± 600	800 ± 200	1000 ± 500
Cu:C (µmol/mol)	1.7 ± 0.4	8 ± 7	13 ± 2	13 ± 3
Pb:C (µmol/mol)	0.5 ± 0.2	100 ± 20	0.16 ± 0.09	80 ± 20

3.8 Supplementary Information

Table 3.8.1: PERIQUIL growth medium for periphyton

	Concentration (M)
Salts	
$CaCl_2$	2×10^{-4}
$Ca(NO_3)_2$	1×10^{-4}
$MgSO_4$	1.5×10^{-4}
$NaHCO_3$	1.2×10^{-3}
KNO_3	1×10^{-4}
Nutrients	
K_2HPO_4	5×10^{-6}
NH_4NO_3	1×10^{-4}
Na_2SiO_3	5×10^{-5}
Trace Elements	
$CoCl_2$	5×10^{-8}
H_3BO_3	5×10^{-5}
Na_2MoO_4	8×10^{-8}
$CuSO_4$	1.25×10^{-7}
$MnCl_2$	1×10^{-6}
$ZnSO_4$	1×10^{-7}
$FeCl_3$	9×10^{-7}
Metal Ligand	
Na_2EDTA	2×10^{-5}
Buffer	
MOPS, pH 7.5	1×10^{-2}

Table 3.8.2: Calculated trace metal speciation in PERIQUIL (-Pb) and PERIQUIL (+Pb) in mol/L

	(-Pb)	(+Pb)
Co^{+2}	1.6×10^{-12}	2.0×10^{-8}
Cu^{+2}	1.5×10^{-14}	3.1×10^{-10}
Fe^{+3}	1.5×10^{-20}	2.7×10^{-16}
Mn^{+2}	1.1×10^{-8}	9.3×10^{-7}
Zn^{+2}	4.5×10^{-12}	4.7×10^{-8}
Pb^{+2}		2.1×10^{-7}
$PbCO_{3 \, (aq)}$		5.6×10^{-7}
$PbOH^{+}$		9.0×10^{-8}
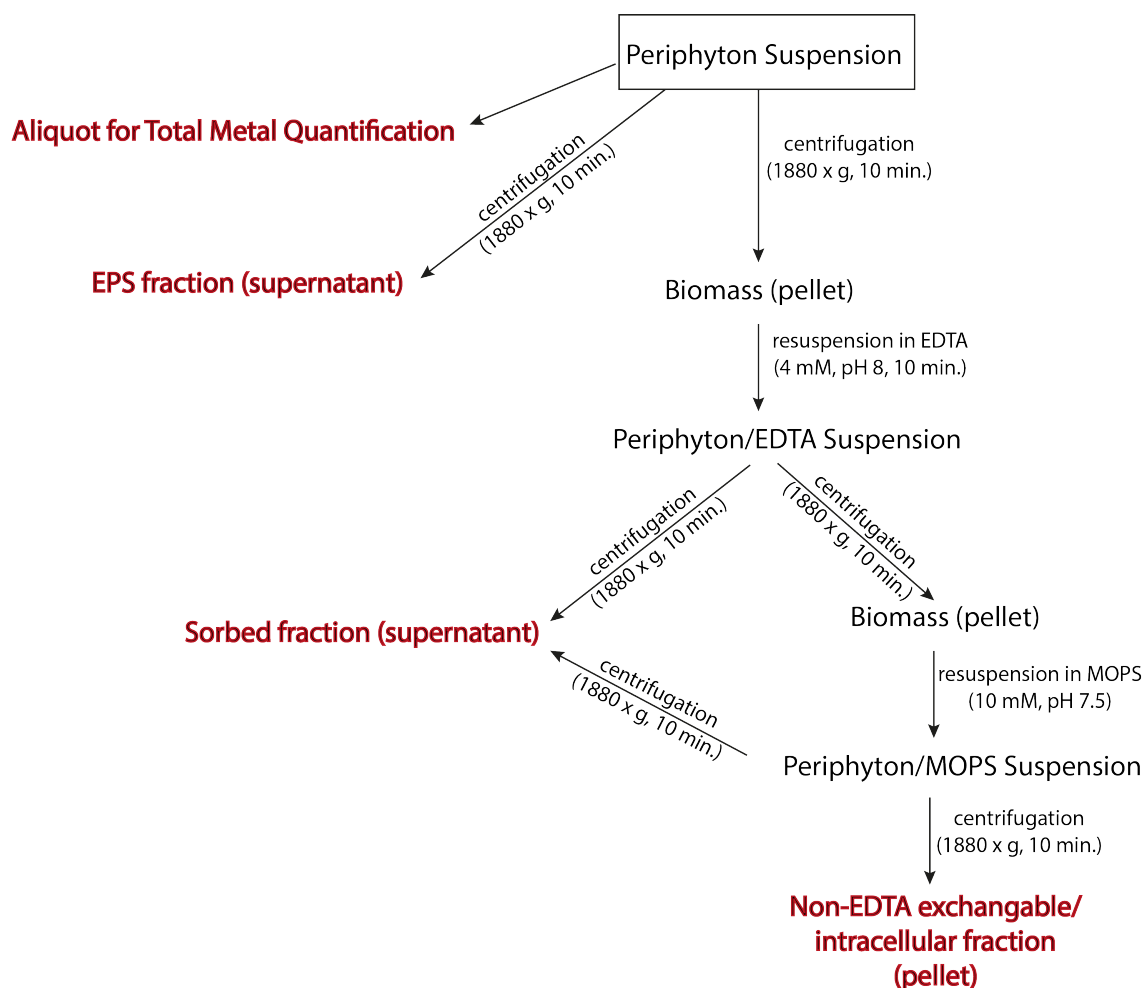
Figure 3.8.1: Metal distribution quantification scheme
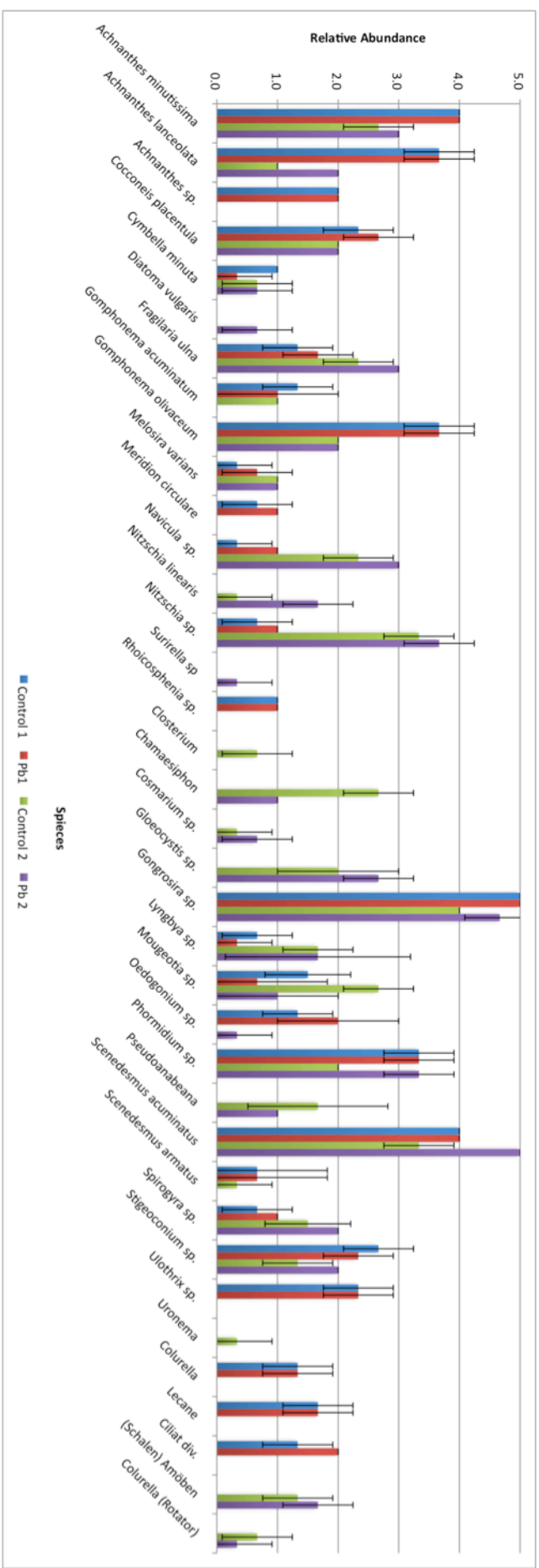
Figure 3.8.2: Comparison of algal composition in control and Pb exposed periphyton. Species were identified and assessed based on their relative abundance: 5 – dominant, 4 – frequent, 3 – periodic, 2 – rare, 1 – singular. Assessments were conducted individually for each triplicate microcosm and values were averaged.
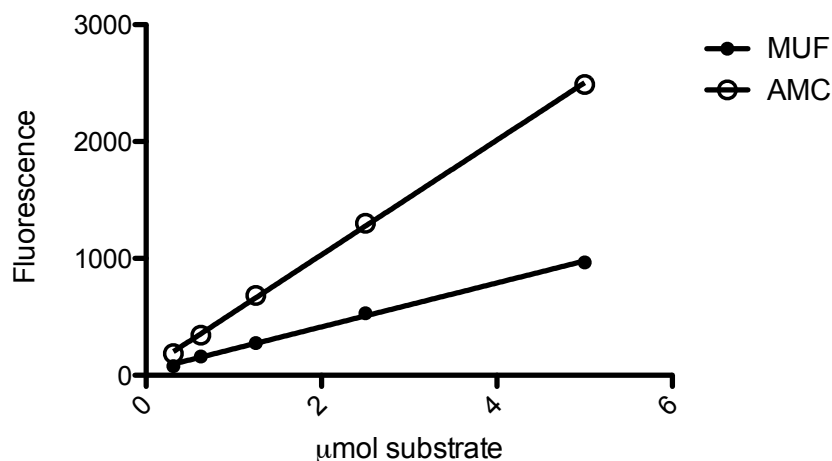
Figure 3.8.3: Calibration curves for conversion of fluorescence to μmol converted substrate. Fluorescence plotted as a function μmol of MUF or AMC fluorophores. Linear regression equation for MUF was calculated to be y = 505.18x and for AMC was calculated to be AMC y = 199.24x. The 1:1 molar ratio of substrate – fluorophore complex allows for the conversion to mole of converted substrate.
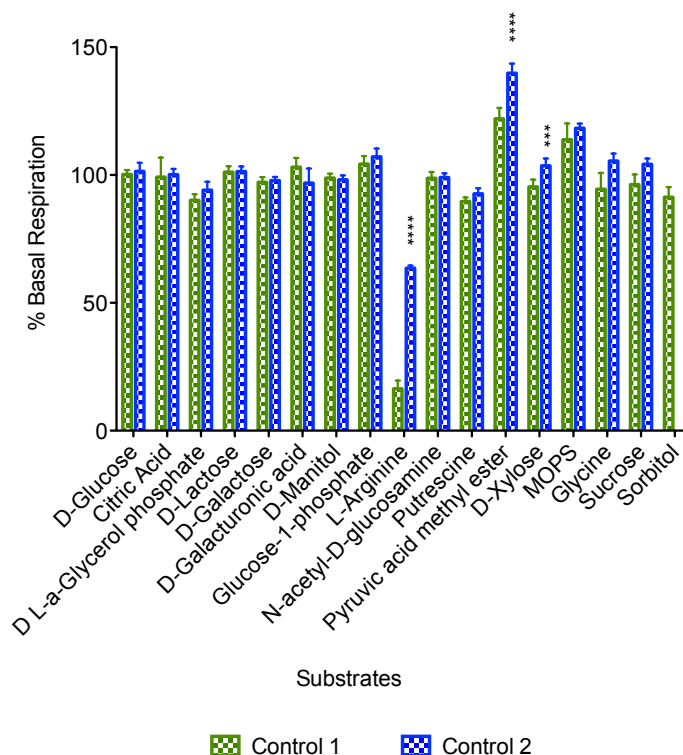
Figure 3.8.4: Comparison of carbon substrate induced respiration of two different periphyton communities tested. Respiration was measured in periphyton using MicroResp™ in the presence of 16 different carbon substrates and expressed as percent of basal respiration, measured without addition of substrate. Error bars correspond to 95% CI associated with triplicate microcosm exposures. Asterix indicate degree of significance between Pb exposed periphyton for a specific substrate: *** $p < 0.001$, **** $p < 0.0001$.

Tracking the temporal dynamics of intracellular metal speciation

4.1 Abstract

Algae, an integral part of the aquatic food web, have developed metal regulatory mechanisms in response to changes in the bioavailability of trace metals. Just as metal bioavailability dictates cellular uptake, intracellular metal speciation determines the availability of metals to exert biological effects. Furthermore, metal uptake by organisms has a profound effect on biogeochemical cycles and intracellular metal complexation is poorly understood. Therefore, the missing link in understanding the relationship between metal uptake and biological responses is the ability to accurately measure intracellular metal speciation. Here we identified temporal changes in intracellular Pb speciation in a model green alga under conditions relevant for fresh water ecosystems using resonant X-ray emission spectroscopy (RXES). With its enhanced sensitivity to functional group chemistry, relative to X-ray absorption spectroscopy (XAS), 2D-RXES maps containing detailed information on the electronic structure of Pb complexes were generated. We show that despite proposed detoxification responses involving peptide complexation, only a small fraction of total intracellular Pb is complexed by thiol groups. Under low exposure concentrations (0.1 nM Pb^{2+}), initial sequestration of Pb in oxides and inorganic phosphate was followed by binding of Pb to organic phosphate, which may indicate that Pb starts to interfere in vital cellular functions. Under conditions of higher Pb^{2+} exposure (25 nM Pb^{2+}), Pb complexation with organic phosphate was observed later in the exposure and the formation of $PbS_{(s)}$ was observed, indicating that exposure conditions influence both the temporal dynamics as well as the types of intracellular Pb species formed.

4.2 Introduction

Over the centuries human activity has led to a large redistribution of metals in the environment, overwhelming biogeochemical cycles and placing pressure on organisms to cope with fluctuating concentrations of potentially toxic metals.[5] In response, organisms have developed highly regulated metal homeostasis mechanisms, optimizing uptake and utilization of nutrient trace metals[1] while employing various defense mechanisms, such as intracellular chelation, against toxicity from elevated metal concentrations.[2] The importance of metal solution

chemistry in accurately assessing metal bioavailability and uptake in organisms has long been established.[17] However, the missing link in understanding the relationship between metal uptake and biological responses is the ability to accurately measure intracellular metal speciation.

A fundamental necessity for understanding biological responses to metal toxicity is the determination of intracellular metal speciation, which identifies specific cellular metal-ligand interactions. Techniques to determine metal speciation within the cell are needed to link metal uptake to cellular responses so that a more complete understanding of metal – organism interactions in the aquatic environment is achieved. Synchrotron based X-ray absorption spectroscopy (XAS) has been used for probing metal speciation on the atomic scale in biological samples, as it is an elementally specific technique that can speciate metals within intact hydrated samples at environmentally relevant concentrations.[50,51] Speciation of Pb using XAS has been conducted in a range of biological samples, from fungal cell walls[52] and bacterial biofilms[53] to metal hyper accumulating plants.[54] However, distinguishing between different types of organic ligands that scatter only lightly is virtually impossible with XAS. Furthermore, distorted geometries of Pb complexes, due to a lone electron pair, lead to poorer resolution and make it challenging to go beyond identification of the direct coordination and thus ligand identification.[55]

With synchrotron-based resonant X-ray emission spectroscopy (RXES), highly resolved 2D spectra of metal complexes are obtained. As we will show here for the first time, these RXES planes are analogous to a metal-ligand fingerprint, and allow for discernment between different types of oxygen and sulfur ligand bound Pb complexes. Obtaining this degree of detailed metal speciation is not possible with XAS.[56] The ability to identify and track temporal changes in intracellular metal-ligand complexes with high resolution has significant biological implications in understanding cellular metal regulation. Therefore, the goal of our work was to measure the changes of intracellular Pb speciation in a model green alga as a function of exposure time under conditions relevant for freshwater ecosystems.

4.3 Methods

4.3.1 Chemicals and materials

3-morpholinopropanesulfonic acid (MOPS), nitrilotriacetic acid (NTA), $Pb(NO_3)_2$, $PbSO_4$, PbO, PbS, $Pb(CH_3CO_2)_2$, Na_2HPO_4, adenosine 5′-triphosphate disodium salt hydrate (ATP), L-Glutathione reduced (GSH), glycine, and other metal salts used as trace metals in culture medium were obtained from Sigma-Aldrich. Nitric acid suprapure (HNO_3; 65%) was ordered from Merck. Glass and plasticware were presoaked in 0.01M HNO_3 and rinsed with deionized water (18 MΩ-cm, Q-H2O grade; Barnstead Nanopure) before use. All solutions and media for cell culturing and Pb exposure were prepared in deionized water in autoclaved containers.

4.3.2 Cell cultivation and Pb exposure

Chlamydomonas reinhardtii (CC125) was obtained from the Chlamydomonas Genetics Center (Durham, NC, USA). Prior to exposure, cells were subcultured twice in Talaquil medium in glass Erlenmeyers at 25°C under continuous illumination (120 $\mu Em^{-2}s^{-1}$ provided by cool white fluorescent lamps) and shaking at 90 rpm (Infors HT) according to Scheidegger et al.[15] For the exposure, $[Pb^{2+}]$ in growth medium was buffered over the course of the experiment with 20 µM NTA. Other trace metals were excluded from the exposure medium to avoid possible metal competition. Media were allowed equilibrate with respect to $[Pb^{2+}]$ after the addition of $Pb(NO_3)_2$ stock solution prior to the addition of cells. Exponentially growing algae were first washed with 10 mM MOPS buffer (pH 7) before being transferred to the exposure media. Cells were exposed to either 0.1 nM Pb^{2+} in Talaquil medium or to 25 nM Pb^{2+} in a modified Talaquil medium (Table 4.7.1) over the course of 24 hours at an initial cell density of 2×10^5 cells/ml. For each time point (3, 5, 10 and 24 hours) triplicate cultures, each containing 1 L, were sampled for cell number, cell volume, and intracellular Pb content, and average values are reported. Cell numbers were measured using a cell counter and analyzer (Roche CASY Model TT, 60 µm capillary). Metal speciation calculations for the exposure media were calculated using the speciation software Visual MINTEQ.[156]

4.3.3 Pb quantification and sample preparation

After exposure, intracellular Pb was quantified by first removing cell surface bound Pb by washing with EDTA (4 mM) to ensure that the speciation measured only corresponded to that of intracellularly bound, non-EDTA exchangeable Pb. Aliquots of cells were filtered and digested with 4 mL suprapure HNO_3 (65%) and 1 mL H_2O_2 (30%) in Teflon® tubes using an ultraCLAVE 4 digester (MLS GmbH) for 24 minutes at a maximum of 200 °C and 100 bar. Metal content of the digests was analyzed using HR-ICP-MS (Element 2 High Resolution Sector Field, Thermo Finnigan) for the determination of intracellular Pb accumulation at each time point. All sample preparation for metal analysis was conducted in a clean room to avoid contamination. Remaining EDTA-washed cells for 3, 5, 10, 24 hour time points were collected using centrifugation at 1880 × g, subsequently washed with MOPS buffer to remove residual Pb-EDTA complexes (10 mM, pH 7), lyophilized, and stored under anoxic conditions at -80 °C prior to analysis at the SuperXAS beamline (Swiss Light Source, Paul Scherrer Institute, Switzerland).

4.3.4 Standard references

Standards of $PbO_{(s)}$, $PbAcetate_{(s)}$, $PbS_{(s)}$ and $PbSO_{4(s)}$ were purchased from Sigma Aldrich. The $Pb(OH)_{2(s)}$ was made by titration of $Pb(NO_3)_2$ solution with NaOH (1 M) up to pH 8.6 and the formed solid was collected via centrifugation, subsequently washed three times with deionized water, and lyophilized. The $Pb_3(PO_4)_{2(s)}$ was made by adding equimolar amounts of $Pb(CH_3CO_2)_2$ and Na_2HPO_4. Solutions were heated to 80 °C and Na_2HPO_4 was added dropwise into the $Pb(CH_3CO_2)_2$ solution while stirring.[157] The mixture was allowed to cool to room temperature, the resulting precipitate was collected using centrifugation, the solid was washed three times with deionized water, and lyophilized. Solid standards were pressed into pellets without further preparation. A 50 mM Pb^{2+} standard in solution was made from dissolution of $Pb(NO_3)_2$ in deionized water and measured in solution. PbATP (40 mM) was made by titrating $Pb(NO_3)_2$ (80 mM) into an ATP solution (80 mM) at pH 7.[158] $Pb(GSH)_3$ (26 mM) was made according to Mah and Jalilehvand[159] with a 1:5 ratio of Pb:GSH so that $Pb(GSH)_3$ was the dominant species in solution. During complex formation, all solutions were continually purged with $Ar_{(g)}$, filtered through 0.22 μm PES filters, and stored at 4 °C under anoxic conditions until

measurement to prevent oxidation. Liquid standards were measured using a liquid cell with kapton windows.

4.3.5 RXES measurements

RXES measurements were conducted at the SuperXAS – X10DA beamline at the Swiss Light Source (SLS) located at the Paul Scherrer Institute, Villigen Switzerland. The ring energy at the SLS was 2.4 GeV and operated in top up mode at 400 mA. The X-rays, delivered from a superbend magnet (2.9 Tesla), were collimated with a Rh mirror and monochromatized with a channel cut Si(311) crystal. The channel cut crystal provides ultimate beam position stability over the course experiment. Downstream from the monochromator, the X-ray beam was focused by means of a toroidal Rh mirror. The beam size on the sample was approximately 100 x 100 μm^2 with a photon flux of approximately 10^{11} photons/second. The incident X-ray energy was tuned around the Pb L_3 edge (13035 eV) and the $L_{\alpha1}$ X-ray fluorescence from the sample was recorded by means of a von Hamos type spectrometer.[160] The spectrometer was equipped with a cylindrically bent Si(555) crystal and operated at a Bragg angle of approximately 69°. The diffracted X-rays were recorded by means of strip-type detector with spatial resolution of 50 μm^2. Full 2D RXES planes were generated for each standard and algae samples. Incident energy ranged from 13000 – 13100 eV. Fluorescence emission, spanning the $L_{\alpha1}$ and $L_{\alpha2}$ emission energies, was detected between 10350 – 10635 eV in steps sizes of 0.5 eV. Samples were measured with a liquid nitrogen cryojet to mitigate radiation damage of the samples during measurements. A series of scans for each sample was conducted to both improve the resolution and monitor possible radiation damage of the organic samples. Algae samples taken after 3, 5, and 10 hours exposure to 0.1 nM Pb^{2+} and after 10 and 24 hours exposure to 25 nM Pb^{2+} were measured. The 2D RXES data were fitted by means of a least square fitting procedure, employing the RXES planes of measured reference compounds. The error bars correspond to standard errors for parameter of each value.

4.4 Results & Discussion

To examine both the influence of exposure time and Pb bioavailability on intracellular Pb speciation, we exposed *C. reinhardtii* to the same total Pb

concentration but to two different free ion concentrations (0.1 nM and 25 nM Pb^{2+}) over the course of 24 hours in medium representative of natural freshwater buffered for pH and metal concentrations (table 4.7.1). A maximum exposure time of 24 hours ensured that exponentially growing cells were subjected to Pb and that nutrient limitation did not occur, which can influence metal uptake.[161] Relatively constant intracellular Pb concentrations (1.2 ± 0.7 mmol Pb / L_{cell}) (Figure 4.6.1a) were measured over time during the 0.1 nM Pb^{2+} exposure, whereas intracellular Pb concentrations increased with time upon exposure to 25 nM Pb^{2+} (3.0 ± 0.4 mmol Pb / L_{cell}) (Figure 4.6.1b), both in a similar range as reported for intracellular Pb content of *C. reinhardtii* upon short term Pb exposure.[15,31] Despite these millimolar internal Pb concentrations and previous work with *C. reinhardtii* that indicated strong Pb induced reactive oxygen species (ROS) formation,[3] the effects to growth and photosynthesis have only been reported after 45 hours of exposure to 1 nM Pb^{2+}.[15] In agreement, we observed no adverse effects on growth up to 24 hours of exposure to 0.1 nM Pb^{2+}, however a decrease in the growth rate upon exposure to 25 nM Pb^{2+} was observed (Figure 4.6.2) Findings reported in the literature in conjunction with our results indicate that *C. reinhardtii* is able to maintain normal growth and photosynthetic activity upon short term Pb exposure, but when exposed to high enough concentrations for long enough exposure periods, effects to growth and photosynthesis do occur. It seems that the presence of cellular responses minimize Pb availability to sensitive sub-cellular targets and mitigate toxicity to a certain extent, but that Pb does interfere with essential processes affecting growth and photosynthesis.

To identify and quantify the major intracellular ligands associated with Pb sequestration, we measured algal samples after 3, 5, and 10 hours of Pb exposure to 0.1 nM Pb^{2+} and after 10 and 24 hours exposure to 25 nM Pb^{2+} using RXES. By scanning the incident energy around the Pb L_3 absorption edge (probing $2p_{3/2} \rightarrow nd$, $n \geq 6$ transitions), while simultaneously acquiring around the Pb Lα emission line (nd $\rightarrow 2p_{3/2}$) at each incident energy point, both with high-energy resolution, we obtained 2D RXES planes from the X-ray absorption near edge region (Figure 4.6.3). By additionally measuring RXES planes of biologically important Pb complexes (Figure 4.6.4), we used these references to identify and quantify the relative amounts of the dominant intracellular ligands involved in Pb binding in *C. reinhardtii* using a linear combination fitting approach. The best fits (Table 4.7.2), together with standard

errors for contribution estimates, are presented in Figure 4.6.5. Algae RXES planes were reconstructed based upon the relative percent contributions of the references (Figure 4.6.6f-h). 2D RXES planes of the pre-edge region increases the sensitivity to weakly scattering organic ligands.[162] This increased sensitivity can be seen when comparing spectra of O ligand Pb complexes generated from both cuts along the incident energy axis and diagonal cuts as a function of the energy transfer of the system, which is the difference in energy between initial and final states (Figure 4.7.1). Greater differences are seen from the energy transfer spectra (Figure 4.7.1c), and these differences are lost when doing conventional XAS analysis.

Pronounced differences between algal RXES planes were observed for different time points as illustrated in Figure 4.6.6d,e for the 0.1 nM Pb^{2+} exposure and were also observed for algae under the 25 nM Pb^{2+} exposure condition (data not shown), indicating changes in intracellular Pb speciation as a function of exposure time. Upon 0.1 nM Pb^{2+} exposure, $PbO_{(s)}$ and $Pb_3(PO_4)_{2(s)}$ were the dominant species after 3h and 5h exposure. A decrease in $Pb_3(PO_4)_{2(s)}$ and increase in organic phosphorus and tri dentate thiol complexation was observed after 10h of exposure (Figure 4.6.5a). Upon 25 nM Pb^{2+} exposure at 10h, tridentate thiol binding and formation of $PbS_{(s)}$ were measured and only after 24h of exposure was binding to organic phosphorus measured (Figure 4.6.5b).

Upon initial exposure to 0.1 nM Pb^{2+}, solid phase $PbO_{(s)}$ precipitate was the predominant species and decreased over time, initially representing 79 ± 2% of Pb after 3 hours and 47 ± 3% after 10 hours (Figure 4.6.5a). Formation of $PbO_{(s)}$ can occur from local oversaturation of Pb under slightly basic conditions. In the alga *Micrasterias denticulate*, $ZnO_{(s)}$ and $CuO_{(s)}$ was reported to precipitate within the cell wall.[163] The cell wall serves as a protective barrier by slowing the kinetics of metal uptake, illustrated by *C. reinhardtii* cell wall free mutants that exhibit higher sensitivity to metal exposure.[164] Thus, precipitation of Pb within the wall can act to slow internalization and may explain why no effects to growth and photosynthesis have been observed upon short term Pb exposure. The decrease of $PbO_{(s)}$ in conjunction with stable intracellular Pb concentrations (Figure 4.6.1a) is consistent with Pb redistribution from $PbO_{(s)}$ to other ligands. The solid phase precipitate $Pb_3(PO_4)_{2(s)}$ accounted for the remaining Pb after 3 hours (21 ± 3%) and increased to 44 ± 1% after 5 hours before decreasing to low levels (9 ± 9%) after 10 hours (Figure 4.6.5a). Discernment between $PbO_{(s)}$ and $Pb_3(PO_4)_{2(s)}$ was readily possible (Figure 4.7.2e),

and these experimental spectral differences were reproduced using calculated RXES planes from theoretical structures (Figure 4.7.2f). We interpret the decrease of $PbO_{(s)}$ and corresponding proportionate increase of $Pb_3(PO_4)_{2(s)}$ between 3 and 5 hours as a partial redistribution of Pb to more thermodynamically stable $Pb_3(PO_4)_{2(s)}$. The presence of $Pb_3(PO_4)_{2(s)}$ likely originates from precipitation with phosphate released from polyphosphatase mediated hydrolysis of inorganic polyphosphate,[165] present in elevated concentrations within vacuoles of *C. reinhardtii*.[166] Several studies have shown metals to be sequestered through intracellular precipitation with inorganic phosphate,[165,167,168] however, the temporal dynamics of these intracellular metal phosphates have not been measured. Reports of natural ligand mediated dissolution of inorganic lead phosphate precipitates for both thiol ligands and humic acid[169] suggest that the observed decrease of $Pb_3(PO_4)_{2(s)}$ and increase in organic complexation at 10 hours is from further redistribution of Pb from inorganic precipitates to organic complexes.

An increase in organic phosphorus complexes as represented by PbATP (30 ± 10%) was measured after 10 hours of exposure to 0.1 nM Pb^{2+} (Figure 4.6.5a). The observed binding to organic phosphate represents binding to ATP, nucleic acids, and sugar phosphates. Binding of Pb directly to ATP has been reported *in vitro*[170] and strong binding of Pb to organic phosphate ligands has been observed, indicating that Pb can outcompete both Ca and Zn for binding to phosphate monoesters and phosphonates.[171] In addition, we previously found that 70% of intracellular Pb recovered from *C. reinhardtii* after 14 hours exposure to 0.1 μM Pb^{2+} was bound to macromolecules in the high M_r range (>10 kDa) and proposed this finding was due to the high affinity of Pb to oxygen, nitrogen, and sulfur containing functional groups of proteins.[42] Therefore, the shift towards organic phosphorus complexation may be a first indication of Pb association with larger macromolecules and interference in vital cellular functions.

Tri-dentate thiol complexation, represented by $Pb(GSH)_3$, was also measured after 10 hours of Pb exposure (10 ± 4%). In previous work, 10% of intracellular Pb recovered from *C. reinhardtii* was associated with an unidentified thiol peptide between 450-700 Da, corresponding to the M_r of γ-Glu-Cys,[42] a precursor of glutathione (GSH), important in the antioxidative response to ROS, and phytochelatins (PCs), widely reported to play an important role in detoxification of certain metals, including Pb[15,37,38] by chelation and proposed transport to vacuoles.

Formation of the measured tridentate thiol-Pb complexes may indicate such a defense response. Our previous work on Pb detoxification in *C. reinhardtii* indicated that PCs are induced above basal levels upon Pb exposure and do bind to Pb under similar conditions as in this study, but that the total amount of quantified thiols from PCs is not sufficient to bind all intracellularly accumulated Pb.[15] Although millimolar concentrations of GSH in *C. reinhardtii* would provide enough thiols to bind and sequester intracellular Pb, and the direct involvement of GSH in metal detoxification in algae has been proposed,[172] based upon our speciation results, only a relatively small fraction of Pb is thiol bound and, in the case of the 0.1 nM Pb^{2+} exposure, the majority of Pb is complexed with organic phosphate and sequestered in the solid oxide phase.

Upon exposure to 25 nM Pb^{2+} a similar contribution of $Pb(GSH)_3$ was observed (30 ± 20%) at 10 hours, relative to the 0.1 nM Pb^{2+} exposure, which did not change after 24 hours of exposure. However, $PbS_{(s)}$ precipitation (50 ± 30 %) was also measured after 10 and 24 hours of exposure (Figure 4.6.5b). Only after 24 hours of exposure was Pb complexation to organic phosphate measured (35 ± 9 %), which was statistically similar to the amount of organic phosphate complexation measured at 10 hours upon exposure to 0.1 nM Pb^{2+}. These results show that although increasing the bioavailability of Pb did not significantly increase intracellular concentrations after 10h of exposure, increased Pb^{2+} in the exposure medium led to the formation of different intracellular Pb species.

The free metal ion is often the species that dictates the concentration of metal-cell surface complexes, which in turn can influence uptake kinetics, the amount of accumulated metal, and toxicity.[22] A positive correlation between Pb^{2+} concentration and the internalization flux in the green alga *Chlorella vulgaris* in both the presence and absence of labile Pb complexes was observed.[24] With 250 times more Pb^{2+} present in the exposure medium, a faster internalization of Pb is expected, which may have caused an initially higher internal Pb concentration resulting in the measured precipitation of $PbS_{(s)}$. Intracellular precipitation of PbS has been observed in both bacteria[173] and yeast,[174] and formation of PC coated CdS nanocrystals has been reported in *C. reinhardtii*.[175] Differences in Pb uptake kinetics, resulting from different free ion concentrations, can be on the time scale of minutes[24] and may not be reflected in intracellular concentrations measured after 3 hours of Pb exposure, as seen in the similar internal Pb concentrations under both exposure conditions (Figure

4.6.1). These observations indicate that it is not only the internal concentration of a metal, but also the metal uptake kinetics that can dictate biological responses and intracellular metal speciation.

4.5 Conclusions

We have shown that intracellular Pb speciation in *C. reinhardtii* is temporally dynamic and dependent on the extracellular metal speciation in the exposure solution. These Pb species shift from inorganic precipitates towards organic complexes after longer exposure times, and proposed detoxification responses through thiol coordination represent only a small fraction of total intracellular Pb complexation. By using RXES for the first time on biological samples, intracellular organic ligands involved in metal complexation can now be identified and quantified, providing information on the dynamic nature of biological responses to metal uptake under low, environmentally relevant, exposure concentrations. The application of RXES for the determination of metal speciation in biological samples can increase our understanding of metal homeostatic mechanisms at the cellular level, as it improves upon the spectral resolution of organic ligands obtained using XAS, providing more information on the local chemical environment of intracellular metal-ligand interactions.

4.6 Figures
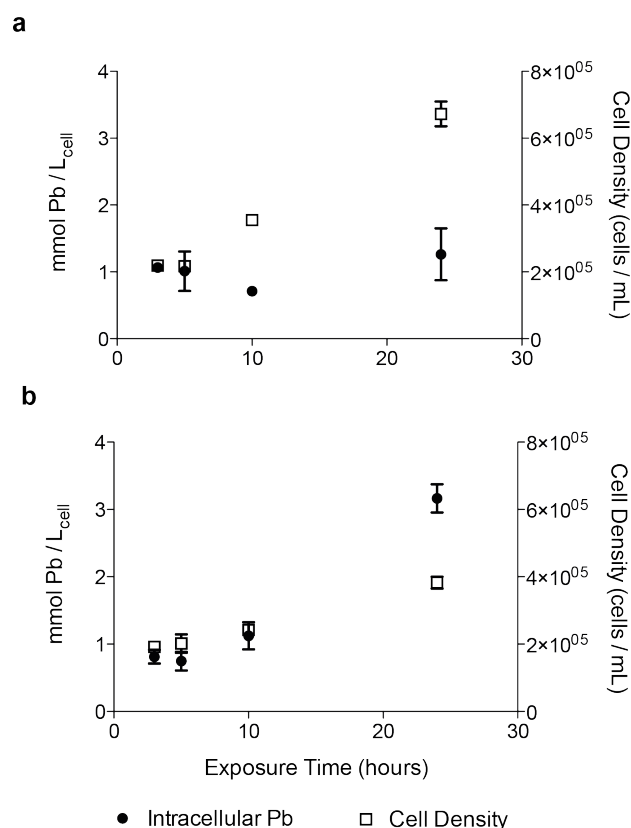
Figure 4.6.1: Intracellular Pb content and cell density as a function of exposure time to (a) 0.1 nM Pb^{2+} and (b) 25 nM Pb^2. Error bars generated from standard deviation of triplicate experiments.
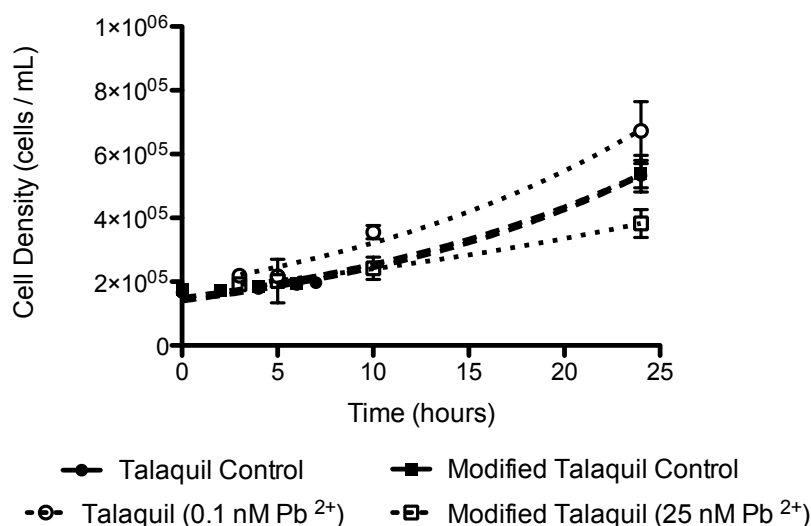
Figure 4.6.2: Comparison of cell growth in Talaquil and Modified Talaquil media with and without Pb. Calculated growth rates (95% CIs reported in brackets) were 0.056 hr^{-1} [0.053-0.059] (Talaquil control), 0.053 hr^{-1}[0.050-0.056] (Modified Talaquil control), 0.053 hr^{-1} [0.047-0.059] (Talaquil, 0.1 nM Pb^{2+}), and 0.033 hr^{-1}[0.029-0.038] (Modified Talaquil, 25 nM Pb^{2+}). Rates were determined using a non-linear regression least squares fit, where the rate constant k (hr^{-1}) = $1/X(lnY-lnY_0)$. For control cultures, growth rates were calculated from technical replicates (n=3). For Pb exposed cultures growth rates were calculated from biological replicates (n=3). Error bars were generated from 95% CIs.
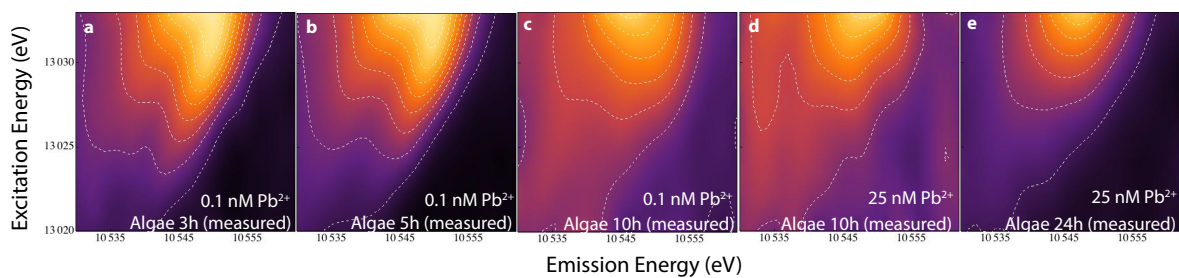
Figure 4.6.3: 2D RXES planes of algae after 3, 5, and 10 hours exposed to 0.1 nM Pb^{2+} (a-c) and 10 and 24 hour exposures to 25 nM Pb^{2+}(d,e).
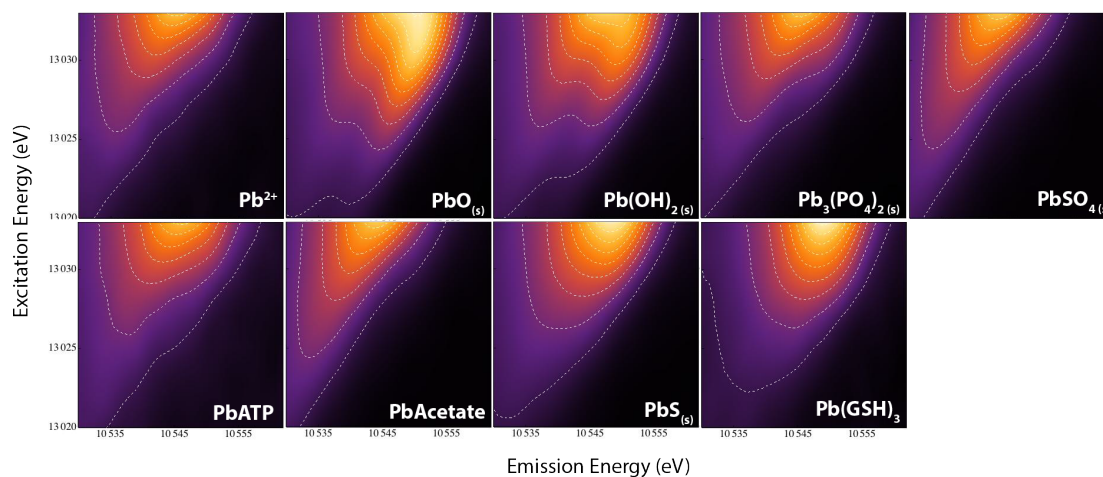
Figure 4.6.4: 2D RXES planes of Pb references employed for the determination of intracellular Pb speciation in algae.
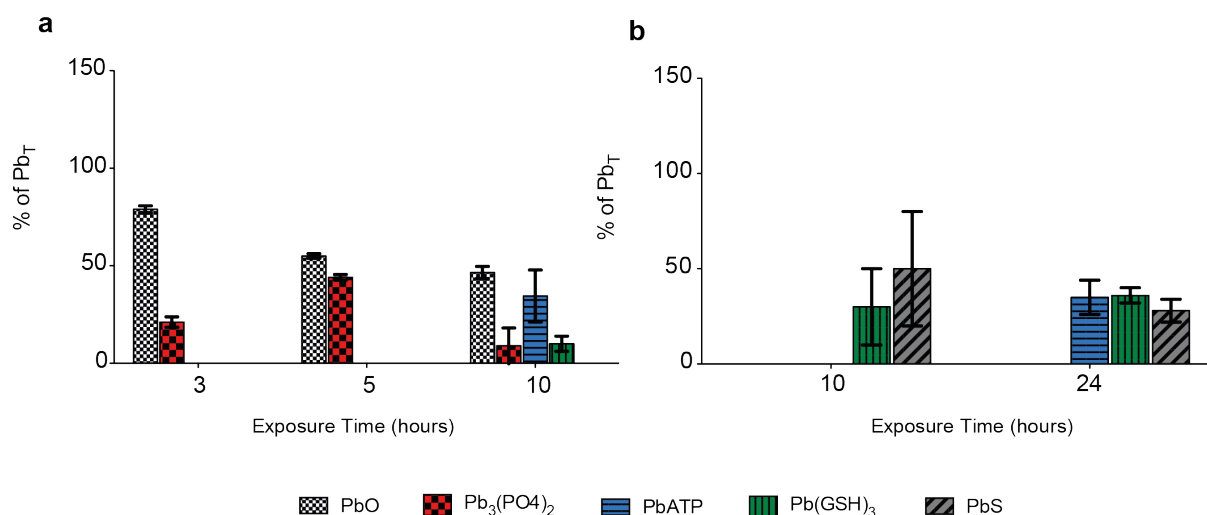
Figure 4.6.5: Intracellular Pb speciation in *C. reinhardtii* as a function of exposure time to (a) 0.1 nM Pb^{2+} and (b) 25 nM Pb^{2+}. Percent of Pb species and standard deviations were obtained from linear combination fitting of 2D RXES planes of references (solid phase $PbO_{(s)}$, $Pb_3(PO_4)_{2(s)}$, and $PbS_{(s)}$, and PbATP and $Pb(GSH)_3$ complexes).
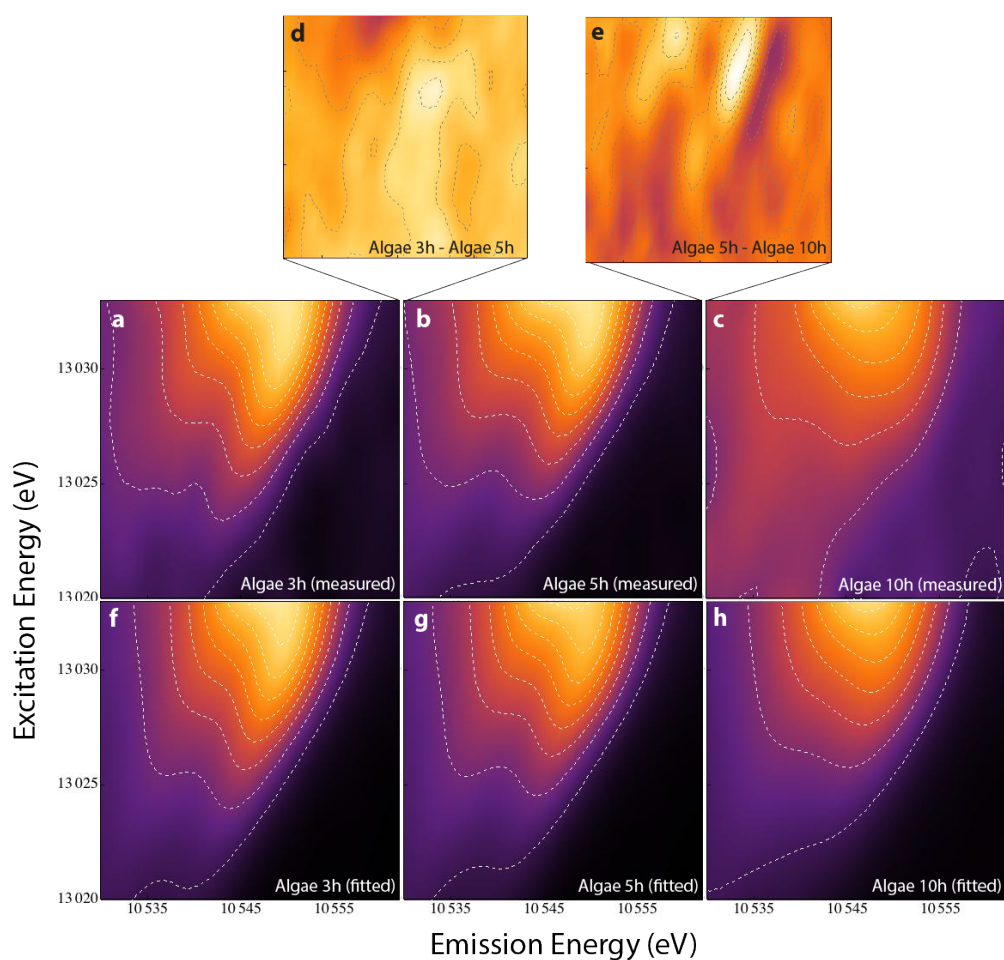
Figure 4.6.6: 2D RXES planes of algae after 3, 5, and 10 hours exposed to 0.1 nM Pb^{2+} (a-c). Differences in the RXES planes were calculated to compare spectral differences between time points (d,e). RXES planes were fitted using measured reference spectra for each time point (f-h). R^2 values of fits are reported in Table 4.7.2.

4.7 Supplementary Information

Table 4.7.1: Chemical composition of exposure media. Calculations were performed using the equilibrium software program Vminteq (citation) with consideration of $Pb_5(PO_4)_3Cl_{(s)}$ ($logK_s$ = -84.43) and $Pb_5(PO_4)_3OH_{(s)}$ ($logK_s$ = -62.79) as possible solid phases. Total Pb concentrations were obtained from ICP-MS measurements of aliquots taken from each exposure flask prior algal cell exposure. Pb_T in Talaquil medium was $2.8 \pm 0.2 \times 10^{-5}$ M and $2.3 \pm 0.1 \times 10^{-5}$ M in Modified Talaquil medium.

Talaquil Medium		Modified Talaquil (-Cl) Medium	
Salts	**Concentration (M)**	**Salts**	**Concentration (M)**
$CaCl_2 \cdot 2H_2O$	5.0×10^{-4}	$Ca(NO_3)_2 \cdot 2H_2O$	5.0×10^{-4}
$MgSO_4 \cdot 7H_2O$	1.5×10^{-4}	$MgSO_4 \cdot 7H_2O$	1.5×10^{-4}
$NaHCO_3$	1.2×10^{-3}	$NaHCO_3$	1.2×10^{-3}
Nutrients		**Nutrients**	
$K_2HPO_4 \cdot 3H_2O$	5.0×10^{-5}	$K_2HPO_4 \cdot 3H_2O$	5.0×10^{-5}
NH_4Cl	1.0×10^{-3}	NH_4NO_3	1.0×10^{-3}
Metal Ligand		**Metal Ligand**	
Na_3NTA	2.0×10^{-5}	Na_3NTA	2.0×10^{-5}
Major Pb Species		**Major Pb Species**	
$Pb_5(PO_4)_3Cl_{(s)}$	5.508×10^{-6}	$Pb_5(PO_4)_3OH_{(s)}$	1.306×10^{-6}
$PbNTA^-$	4.609×10^{-7}	$PbNTA^-$	1.640×10^{-5}
Pb^{2+}	1.269×10^{-10}	Pb^{2+}	2.507×10^{-8}
$PbCO_{3\ (aq)}$	1.155×10^{-10}	$PbCO_{3\ (aq)}$	2.278×10^{-8}
$PbHCO_3^+$	6.471×10^{-10}	$PbHCO_3^+$	1.277×10^{-8}
$PbOH^+$	2.314×10^{-10}	$PbOH^+$	4.566×10^{-9}
Buffer		**Buffer**	
MOPS, pH 7.0	1.0×10^{-2}	MOPS, pH 7.0	1.0×10^{-2}

Table 4.7.2: R^2 values for linear combination fitting of algae 2D RXES planes using Pb references $PbO_{(s)}$, $Pb_3(PO_4)_{2(s)}$, $PbS_{(s)}$, PbATP, and $Pb(GSH)_3$.

Algae Sample	R^2
3 hour exposure (0.1 nM Pb^{2+})	0.98
5 hour exposure (0.1 nM Pb^{2+})	0.99
10 hour exposure (0.1 nM Pb^{2+})	0.92
10 hour exposure (25nM Pb^{2+})	0.70
24 hour exposure (25 nM Pb^{2+})	0.97
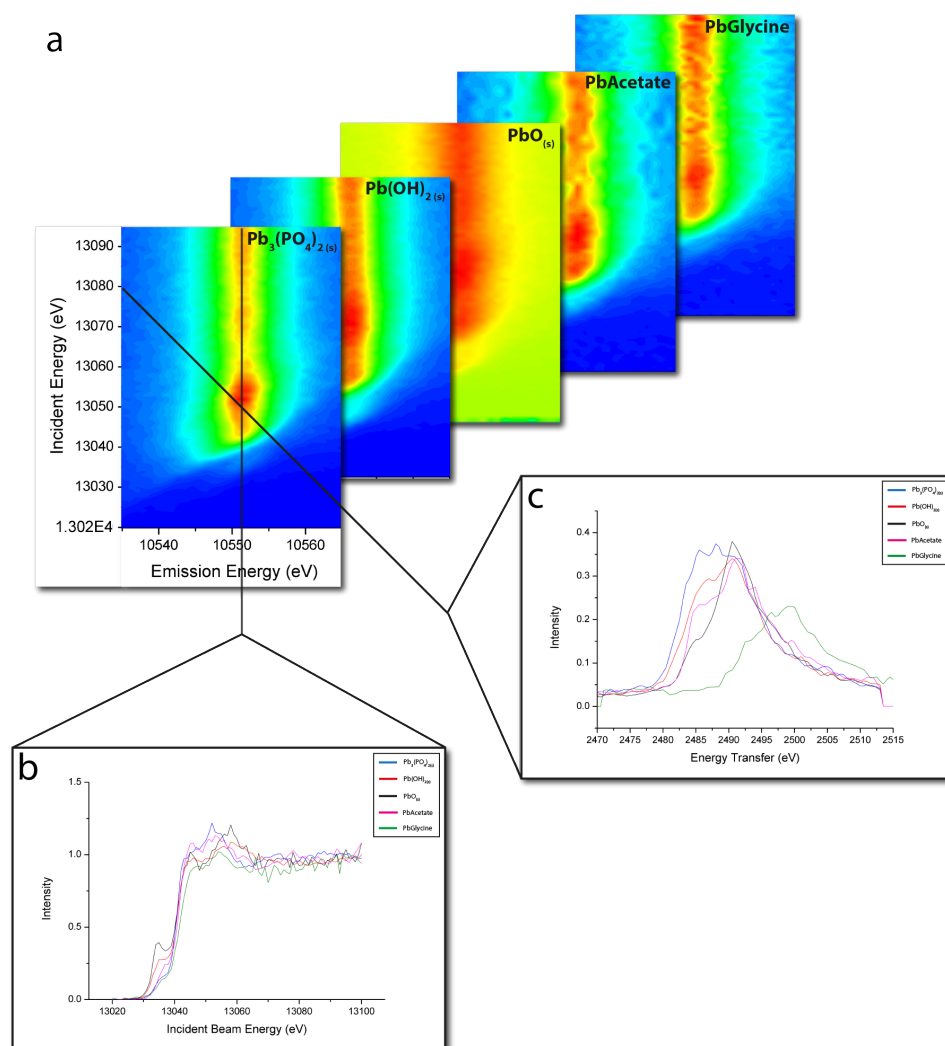
Figure 4.7.1: Results of test-experiment on different Pb samples for the determination of best excitation energy ranges for RXES Pb chemical speciation. (a) 2D RXES planes of oxygen bound Pb complexes (b) HERFD-XANES spectra generated from the linear cut of the RXES plane as a function of the incident energy (c) Spectra generated from the energy transfer cut at 13038 eV. Spectra of $Pb_3(PO_4)_{2\,(s)}$ are shown in blue, $Pb(OH)_{2\,(s)}$ shown in red, $PbO_{(s)}$ shown in black, PbAcetate shown in magenta, and PbGlycine shown in green.
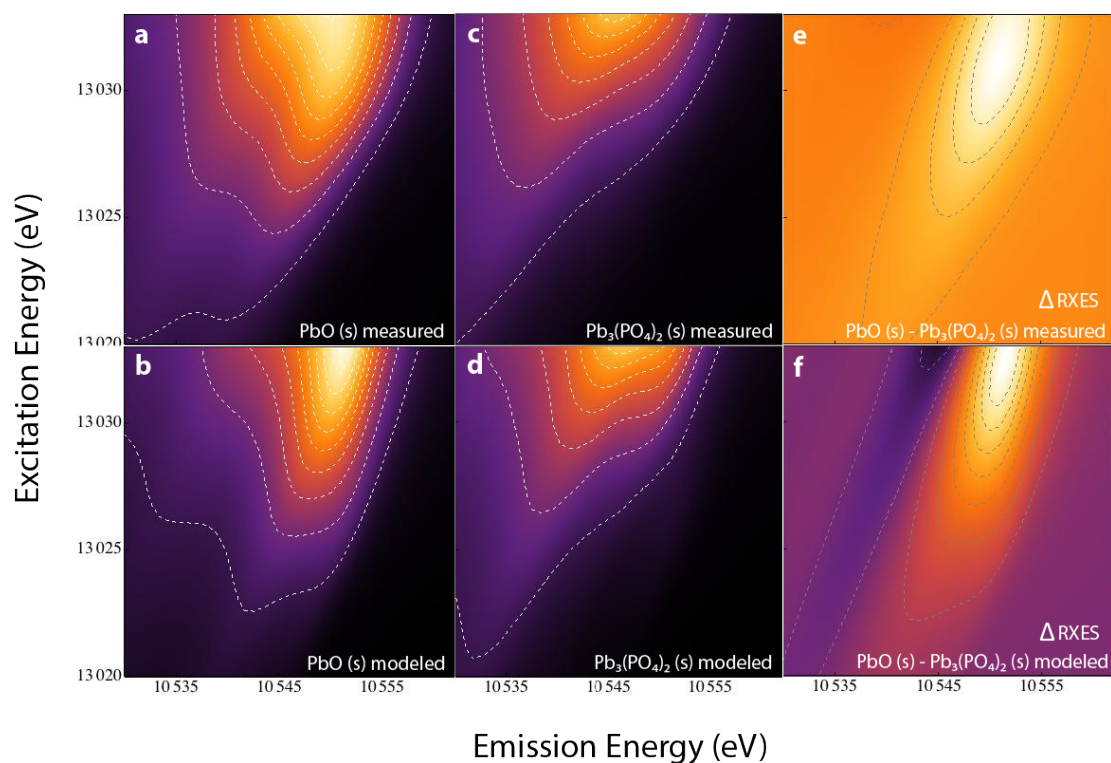
Figure 4.7.2: Comparison and modeling of $PbO_{(s)}$ and $Pb_3(PO_4)_{2\ (s)}$ RXES planes. Measured 2D RXES planes of $PbO_{(s)}$ (a) and $Pb_3(PO_4)_{2\ (s)}$ (c) and the difference between these two standards (e) were modeled (b, d, f) using Kramers-Heisenberg relation[176] and using density of states calculated with FEFF code.[177] For energies and lifetimes of initial and final states, tabulated values were used.[178,179]

Outlook

This doctoral work has demonstrated that, despite significant Pb accumulation in periphyton over the course of three-week Pb exposures, Pb does not adversely impact the overall structure and function of periphyton. The mitigation of toxicity to periphytic organisms is likely due to Pb sequestration, both at the cellular level through intracellular precipitation and chelation, as well as at the community scale via sorption to inorganic material in periphyton. Therefore, what is of ecological significance is the potential trophic transfer of Pb from periphyton to grazing organisms. Several important points that arise from this work include:

1. Distribution of Pb in periphyton should be assessed without the disruption of its three-dimensional structure so that an accurate determination can be made with respect to the relative contributions of intracellular and extracellular sequestration.

2. Further work must be conducted to better understand which intracellular Pb species result from detoxification mechanisms and which arise from toxic modes of action to more strongly link intracellular speciation with biological effects.

3. The implications of trophic transfer of Pb to grazers should be further studied by understanding how Pb speciation in periphyton influences Pb uptake and to determine if adverse biological effects occur upon long-term dietary exposure.

Periphyton is not simply a sum of its individual components, and its three-dimensional structure cannot be ignored with respect to the chemistry and biological interactions occurring within the community. A fractionation approach was taken to determine Pb distribution in periphyton. However, with this approach comes the risk of causing a redistribution of Pb to stronger binding sites when this three-dimensional structure is disrupted. Therefore, non-disruptive techniques would be required to more accurately assess Pb distribution within intact periphyton. Micro-XAS presents a unique possibility to both spatially localize and speciate metals in biological samples with micrometer spatial resolution,[180] and has provided insight into the accumulation, transport and immobilization of metals within biofilms.[181] Although

quantitative information on Pb distribution in the whole periphyton community would not be possible, micro-XAS could be a powerful complimentary technique to distinguish intracellular Pb uptake in periphytic organisms versus Pb sorption to extracellular material within intact periphyton and be able to elucidate if Pb is, in fact, bound to metal oxides. To quantify Pb binding to Fe and Mn oxides, a simpler sequential extraction approach could also be used, where reductive dissolution of oxides could allow for the estimation of Pb associated with these phases.[182]

This work showed that intracellular Pb speciation in *C. reinhardtii* is temporally dynamic and is comprised of both inorganic precipitates as well as organic complexes. However, the underlying biological processes responsible for these speciation dynamics are not yet clear. Hypotheses were presented in Chapter 4, however, further experiments using complementary techniques that probe Pb speciation at the atomic level, identify biomolecules involved in complexation at the molecular level, and provide information on spatial localization at the cellular level are still required to distinguish between detoxification mechanisms and modes of toxicity.

Scheidegger et al. showed that Pb toxicity to growth and photosynthesis did occur under low exposure concentrations (1 nM Pb^{2+}), but only after 24 hours upon subsequent sub-culturing of *C. reinhardtii* in the presence of Pb.[15] Comparing intracellular speciation in such sub-cultures with algae where no toxic effects were observed could explain if the observed trend towards organic complexation, discussed in Chapter 4, is an indication of toxicity. Although determination of the local chemical environment at the atomic level provides useful speciation information, identification of biomolecules involved in Pb complexation is needed to better understand the biological processes influencing Pb speciation. Characterization of PC – Pb complexes revealed that a significant percentage of Pb was associated with a higher M_r fraction.[42] It would be important to further characterize these biomolecules to determine if Pb is binding to high M_r proteins, thus gaining more information on the origin of the tridentate Pb - thiol complexation we measured in *C. reinhardtii*. Finally, using nano-XAS for single cell analysis, would provide additional spatial and chemical information at the nanometer scale, which would be useful in understanding where certain Pb species are sequestered within the cell in the case of detoxification responses, or if Pb is concentrated in sensitive sub-cellular organelles, which could be responsible for toxic effects observed.

Because periphyton is able to accumulate and sequester Pb, it is conceivable that Pb could be transferred to grazing organisms, including benthic invertebrates and fish. Studies on the trophic transfer of Pb in marine[183] and freshwater[184] ecosystems focusing on phytoplankton as a primary source of Pb did not evidence biomagnification of Pb, likely because of the efficient excretion of Pb that has been reported for a wide range of marine organisms,[185] which may also hold true for freshwater organisms. However, these studies did not address the effects of long-term dietary Pb exposure in grazers. Studies have shown that the intracellular metal speciation of prey can influence trophic transfer to predators, whereby metals complexed to soluble organic biomolecules appear to be the most bioavailable.[186,187] Therefore, it would be of ecological interest to quantify the transfer of Pb from periphyton to grazing organisms, relating this transfer to Pb speciation in periphyton, and to determine if any biological effects are observed over long periods of dietary exposure.

Bibliography

(1)   Morel, F. M. M. The Biogeochemical Cycles of Trace Metals in the Oceans. *Science* **2003**, *300*, 944–947.

(2)   Mason, A. Z.; Jenkins, K. D. Metal detoxification in aquatic organisms. In *Metal speciation and bioavailability in aquatic systems*; Tessier, A.; Turner, D. R., Eds.; John Wiley & Sons, Inc, 1995; pp. 479–608.

(3)   Szivák, I.; Behra, R.; Sigg, L. Metal-induced reactive oxygen species production in *chlamydomonas reinhardtii* (chlorophyceae). *J. Phycol.* **2009**, *45*, 427–435.

(4)   Nriagu, J. O.; Pacyna, J. M. Quantitative assessment of worldwide contamination of air, water and soils by trace metals. *Nature* **1988**, *333*, 134–139.

(5)   Nriagu, J. O. History of global metal pollution. *Science* **1996**, *272*, 223–223.

(6)   Nriagu, J. O. The rise and fall of leaded gasoline. *Sci. Total Environ.* **1990**, *92*, 13–28.

(7)   Nriagu, J. O. A global assessment of natural sources of atmospheric trace metals. *Nature* **1989**, *338*, 47–49.

(8)   Hettelingh, J. P.; van het Bolcher, M.; Denier van der Gon, H.; Groenenberg, B. J.; Ilyin, I.; Reinds, G. J.; Slootweg, J.; Travnikov, O.; Visschedijk, A.; de Vries, W. Heavy Metal Emissions, Depositions, Critical Loads and Exceedances in Europe. *UNECE Report* **2006**, 1–99.

(9)   Dunlap, C. E.; Bouse, R.; Flegal, A. R. Past Leaded Gasoline Emissions as a Nonpoint Source Tracer in Riparian Systems: A Study of River Inputs to San Francisco Bay. *Environ. Sci. Technol.* **2000**, *34*, 1211–1215.

(10)   Powell, K. J.; Brown, P. L.; Byrne, R. H.; Gajda, T.; Hefter, G.; Leuz, A.-K.; Sjöberg, S.; Wanner, H. Chemical speciation of environmentally significant metals with inorganic ligands. Part 3: The Pb^{2+} + OH^-, Cl^-, CO_3^{2-}, SO_4^{2-}, and PO_4^{3-} systems (IUPAC Technical Report). *Pure Appl. Chem.* **2009**, *81*, 2425–2476.

(11)   Pearson, R. G. The HSAB Principle — more quantitative aspects. *Inorg. Chim. Acta* **1995**, *240*, 93–98.

(12)   Coale, K. H.; Flegal, A. R. Copper, zinc, cadmium and lead in surface waters of Lakes Erie and Ontario. *Sci. Total Environ.* **1989**, *87/88*, 297–304.

(13)   Bradac, P.; Wagner, B.; Kistler, D.; Traber, J.; Behra, R.; Sigg, L. Cadmium speciation and accumulation in periphyton in a small stream with dynamic concentration variations. *Environ. Pollut.* **2010**, *158*, 641–648.

(14)   Farag, A. M.; Nimick, D. A.; Kimball, B. A.; Church, S. E.; Harper, D. D.; Brumbaugh, W. G. Concentrations of metals in water, sediment, biofilm, benthic macroinvertebrates, and fish in the Boulder River watershed, Montana, and the role of colloids in metal uptake. *Arch. Environ. Contam. Toxicol.* **2007**, *52*, 397–409.

(15)   Scheidegger, C.; Behra, R.; Sigg, L. Phytochelatin formation kinetics and toxic effects in the freshwater alga *Chlamydomonas reinhardtii* upon short- and long-term exposure to lead(II). *Aquat. Toxicol.* **2010**, *101*, 423–429.

(16)   Grosell, M.; Gerdes, R. M.; Brix, K. V. Chronic toxicity of lead to three freshwater invertebrates— *brachionus calyciflorus*, *chironomus tentans*, and *lymnaea stagnalis*. *Environ. Toxicol. Chem.* **2006**, *25*, 97–104.

(17)   Campbell, P. G. C. Interactions between trace metals and aquatic

organisms: A critique of the free-ion activity model. In *Metal speciation and bioavailabilty in aquatic systems*; Tessier, A.; Turner, D. R., Eds.; John Wiley & Sons, Inc: New York, 1995; Vol. 3, pp. 45–102.

(18)   Sigg, L.; Behra, R. Speciation and bioavailability of trace metals in freshwater environments. *Met. Ions Biol. Syst.* **2005**, *44*, 47–73.

(19)   Tipping, E. Cation Binding by Humic Substances; Cambridge University Press, 2002; Vol. 12.

(20)   Wei, L.; Ahner, B. A. Sources and sinks of dissolved phytochelatin in natural seawater. *Limnol. Oceanogr.* **2005**, *50*, 13–22.

(21)   Lead, J. R.; Wilkinson, K. J. Aquatic Colloids and Nanoparticles: Current Knowledge and Future Trends. *Environ. Chem.* **2006**, *3*, 159–171.

(22)   Campbell, P. G. C.; Errécalde, O.; Fortin, C.; Hiriart-Baer, V. P.; Vigneault, B. Metal bioavailability to phytoplankton-applicability of the biotic ligand model. *Comp. Biochem. Phys. C* **2002**, *133*, 189–206.

(23)   Knauer, K.; Behra, R.; Sigg, L. Effects of free Cu^{2+} and Zn^{2+} ions on growth and metal accumulation in freshwater algae. *Environ. Toxicol. Chem.* **1997**, *16*, 220–229.

(24)   Slaveykova, V. I.; Wilkinson, K. J. Physicochemical aspects of lead bioaccumulation by *Chlorella vulgaris*. *Environ. Sci. Technol.* **2002**, *36*, 969–975.

(25)   Slaveykova, V. I.; Wilkinson, K. J.; Ceresa, A.; Pretsch, E. Role of Fulvic Acid on Lead Bioaccumulation by *Chlorella kesslerii*. *Environ. Sci. Technol.* **2003**, *37*, 1114–1121.

(26)   Mylon, S. E.; Twining, B. S.; Fisher, N. S.; Benoit, G. Relating the speciation of Cd, Cu, and Pb in two Connecticut rivers with their uptake in algae. *Environ. Sci. Technol.* **2003**, *37*, 1261–1267.

(27)   Slaveykova, V. I.; Wilkinson, K. J. Predicting the Bioavailability of Metals and Metal Complexes: Critical Review of the Biotic Ligand Model. *Environ. Chem.* **2005**, *2*, 9–24.

(28)   Fortin, C.; Campbell, P. G. C. Thiosulfate Enhances Silver Uptake by a Green Alga: Role of Anion Transporters in Metal Uptake. *Environ. Sci. Technol.* **2001**, *35*, 2214–2218.

(29)   Phinney, J. T.; Bruland, K. W. Uptake of Lipophilic Organic Cu, Cd, and Pb Complexes in the Coastal Diatom *Thalassiosira weissflogii*. *Environ. Sci. Technol.* **1994**, *28*, 1781–1790.

(30)   Lamelas, C.; Wilkinson, K. J.; Slaveykova, V. I. Influence of the Composition of Natural Organic Matter on Pb Bioavailability to Microalgae. *Environ. Sci. Technol.* **2005**, *39*, 6109–6116.

(31)   Sánchez-Marín, P.; Fortin, C.; Campbell, P. G. C. Copper and lead internalisation by freshwater microalgae at different carbonate concentrations. *Environ. Chem.* **2013**, *10*, 80–90.

(32)   Clemens, S. Molecular mechanisms of plant metal tolerance and homeostasis. *Planta* **2001**, *212*, 475–486.

(33)   Godwin, H. A. The biological chemistry of lead. *Curr. Opin. Chem. Biol.* **2001**, *5*, 223–227.

(34)   Bittell, J. E.; Koeppe, D. E.; Miller, R. J. Sorption of Heavy Metal Cations by Corn Mitochondria and the Effects on Electron and Energy Transfer Reactions. *Physiol. Plant* **1974**, *30*, 226–230.

(35)   Miles, C. D.; Brandle, J. R.; Daniel, D. J.; Chu-Der, O.; Schnare, P. D.; Uhlik, D. J. Inhibition of Photosystem II in Isolated Chloroplasts by Lead.

Plant Physiol. **1972**, *49*, 820–825.

(36)   Vymazal, J. Toxicity and Accumulation of Lead with Respect to Algae and Cyanobacteria: A Review. *Acta Hydrochim. Hydrobiol.* **1990**, *18*, 513–535.

(37)   Le Faucheur, S.; Schildknecht, F.; Behra, R.; Sigg, L. Thiols in Scenedesmus vacuolatus upon exposure to metals and metalloids. *Aquat. Toxicol.* **2006**, *80*, 355–361.

(38)   Abboud, P.; Wilkinson, K. J. Role of metal mixtures (Ca, Cu and Pb) on Cd bioaccumulation and phytochelatin production by *Chlamydomonas reinhardtii. Environ. Pollut.* **2013**, *179*, 33–38.

(39)   Komine, Y.; Eggink, L. L.; Park, H.; Hoober, J. K. Vacuolar granules in *Chlamydomonas reinhardtii*: polyphosphate and a 70-kDa polypeptide as major components. *Planta* **2000**, *210*, 897–905.

(40)   Siderius, M.; Musgrave, A.; Ende, H.; Koerten, H.; Cambier, P.; Meer, P. *Chlamydomonas eugametos* (chlorophyta) stores phosphate in polyphosphate bodies together with calcium. *J. Phycol.* **1996**, *32*, 402–409.

(41)   Ahner, B. A.; Morel, F. Phytochelatin production in marine algae. 2. Induction by various metals. *Limnol. Oceanogr.* **1995**, *40*, 658–665.

(42)   Scheidegger, C.; Sigg, L.; Behra, R. Characterization of lead induced metal-phytochelatin complexes in *Chlamydomonas reinhardtii. Environ. Toxicol. Chem.* **2011**, *30*, 2546–2552.

(43)   Noctor, G.; Mhamdi, A.; Chaouch, S.; Han, Y.; Neukermans, J.; Marquez-Garcia, B.; Queval, G.; Foyer, C. H. Glutathione in plants: an integrated overview. *Plant Cell Environ.* **2012**, *35*, 454–484.

(44)   Foyer, C. H.; Noctor, G. Ascorbate and glutathione: the heart of the redox hub. *Plant Physiol.* **2011**, *155*, 2–18.

(45)   Szpunar, J. Bio-inorganic speciation analysis by hyphenated techniques. *Analyst* **2000**, *125*, 963–988.

(46)   Scheidegger, C.; Suter, M. J. F.; Behra, R.; Sigg, L. Characterization of Lead–Phytochelatin Complexes by Nano-Electrospray Ionization Mass Spectrometry. *Front. Microbiol.* **2012**, *3*, 1–7.

(47)   Gómez-Ariza, J. L.; Giráldez, I.; Sánchez-Rodas, D. Metal readsorption and redistribution during the analytical fractionation of trace elements in oxic estuarine sediments. *Anal. Chim. Acta* **1999**, *399*, 295–307.

(48)   Minkel, D. T.; Poulsen, K.; Wielgus, S.; Shaw, C. F.; Petering, D. H. On the sensitivity of metallothioneins to oxidation during isolation. *Biochem. J.* **1980**, *191*, 475–485.

(49)   Ortega, R.; Carmona, A.; Llorens, I.; Solari, P. L. X-ray absorption spectroscopy of biological samples. A tutorial. *J. Anal. At. Spectrom.* **2012**, *27*, 2054–2065.

(50)   Pokrovsky, O. S.; Pokrovski, G. S.; Feurtet-Mazel, A. A Structural Study of Cadmium Interaction with Aquatic Microorganisms. *Environ. Sci. Technol.* **2008**, *42*, 5527–5533.

(51)   Miot, J.; Morin, G.; Skouri-Panet, F.; Férard, C.; Aubry, E.; Briand, J.; Wang, Y.; Ona-Nguema, G.; Guyot, F.; Brown, G. E. XAS study of arsenic coordination in *Euglena gracilis* exposed to arsenite. *Environ. Sci. Technol.* **2008**, *42*, 5342–5347.

(52)   Sarret, G.; Manceau, A.; Spadini, L.; Roux, J. C.; Hazemann, J. L.; Soldo, Y.; Eybert-Bérard, L.; Menthonnex, J. J. Structural determination of Pb binding sites in *Penicillium chrysogenum* cell walls by EXAFS spectroscopy and solution chemistry. *J. Synchrotron. Radiat.* **1999**, *6*, 414–416.

(53)   Templeton, A. S.; Spormann, A. M.; Brown, G. E. Speciation of Pb(II) Sorbed by *Burkholderia cepacia*/Goethite Composites. *Environ. Sci. Technol.* **2003**, *37*, 2166–2172.

(54)   Tian, S.-K.; Lu, L.-L.; Yang, X.-E.; Huang, H.-G.; Brown, P.; Labavitch, J.; Liao, H.-B.; He, Z.-L. The impact of EDTA on lead distribution and speciation in the accumulator *Sedum alfredii* by synchrotron X-ray investigation. *Environ. Pollut.* **2011**, *159*, 782–788.

(55)   Manceau, A.; Boisset, M.; Sarret, G.; Hazemann, R.; Mench, M.; Cambier, P.; Prost, R. Direct determination of lead speciation in contaminated soils by EXAFS spectroscopy. *Environ. Sci. Technol.* **1996**, *30*, 1540–1552.

(56)   Swarbrick, J. C.; Skyllberg, U.; Karlsson, T.; Glatzel, P. High Energy Resolution X-ray Absorption Spectroscopy of Environmentally Relevant Lead(II) Compounds. *Inorg. Chem.* **2009**, *48*, 10748–10756.

(57)   Stevenson, J. An Introduction to Algal Ecology in Freshwater Benthic Habitats. In *Algal Ecology: Freshwater Benthic Ecosystems*; Stevenson, J.; Bothwell, M.; Lowe, R., Eds.; Academic Press: San Diego, 1996.

(58)   Pusch, M.; Fiebig, D.; Brettar, I.; Eisenmann, H. The role of micro-organisms in the ecological connectivity of running waters. *Freshwater Biol.* **1998**, *40*, 453–495.

(59)   Battin, T. J.; Kaplan, L. A.; Denis Newbold, J.; Hansen, C. M. E. Contributions of microbial biofilms to ecosystem processes in stream mesocosms. *Nature* **2003**, *426*, 439–442.

(60)   Tate, C. M.; Broshears, R. E.; Mcknight, D. M. Phosphate Dynamics in an Acidic Mountain Stream - Interactions Involving Algal Uptake, Sorption by Iron-Oxide, and Photoreduction. *Limnol. Oceanogr.* **1995**, *40*, 938–946.

(61)   Stoodley, P.; Sauer, K.; Davies, D. G.; Costerton, J. W. Biofilms as complex differentiated communities. *Annu. Rev. Microbiol.* **2002**, *56*, 187–209.

(62)   Chiovitti, A.; Bacic, A.; Burke, J.; Wetherbee, R. Heterogeneous xylose-rich glycans are associated with extracellular glycoproteins from the biofouling diatom *Craspedosauros australis* (Bacillariophyceae). *Eur. J. Phycol.* **2003**, *39*, 543–554.

(63)   Cogan, N.; Keener, J. The role of the biofilm matrix in structural development. *Math. Med. Biol.* **2004**, *21*, 147–166.

(64)   Lawrence, J.; Swerhone, G.; Kuhlicke, U.; Neu, T. In situ evidence for microdomains in the polymer matrix of bacterial microcolonies. *Can. J. Microbiol.* **2007**, *53*, 450–458.

(65)   Neu, T. R.; Lawrence, J. R. Extracellular polymeric substances in microbial biofilms. In *Microbial Glycobiology: Structures, Relevance and Applications*; Moran, A. P., Ed.; Elsevier, 2009; pp. 735–758.

(66)   Mayer, C.; Moritz, R.; Kirschner, C.; Borchard, W.; Maibaum, R.; Wingender, J.; Flemming, H. The role of intermolecular interactions: studies on model systems for bacterial biofilms. *Int. J. Biol. Macromol.* **1999**, *26*, 3–16.

(67)   Flemming, H.; Neu, T.; Wozniak, D. The EPS matrix: the 'house of biofilm cells'. *J. Bacteriol.* **2007**, *189*, 7945–7947.

(68)   Di Pippo, F.; Bohn, A.; Congestri, R.; De Philippis, R.; Albertano, P. Capsular polysaccharides of cultured phototrophic biofilms. *Biofouling* **2009**, *25*, 495–504.

(69)   Pistocchi, R.; Mormile, M. A.; Guerrini, F.; Isani, G. Increased production of extra- and intracellular metal-ligands in phytoplankton exposed to copper

and cadmium. *J. Appl. Phycol.* **2000**, *12*, 469–477.

(70)   Wingender, J.; Jaeger, K. Extracellular Enzymes in Biofilms; Bitton, G., Ed.; John Wiley & Sons, Inc, 2003.

(71)   Nielsen, H.; Jahn, A. Extraction of EPS. In *Microbial Extracellular Polymeric Substances: Characterization, Structures and Function*; Wingender, J.; Neu, T.; Flemming, H., Eds.; Springer-Verlag: Berlin Heidelberg, 1999.

(72)   Philippis, R.; Vincenzini, M. Exocellular polysaccharides from cyanobacteria and their possible applications. *FEMS Microbiol. Rev.* **1998**, *22*, 151–175.

(73)   Parker, D. L.; Schram, B. R.; Plude, J. L.; Moore, R. E. Effect of Metal Cations on the Viscosity of a Pectin-Like Capsular Polysaccharide from the Cyanobacterium Microcystis flos-aquae C3-40. *Appl. Environ. Microb.* **1996**, *62*, 1208–1213.

(74)   Beech, I. B.; Cheung, C. W. S. Interactions of Exopolymers Produced by Sulphate- reducing Bacteria with Metal Ions. *International Biodeterior. Biodegr.* **1995**, 59–72.

(75)   Decho, A. Microbial exopolymer secretions in ocean environments: their role(s) in food webs and marine processes. *Oceanogr. Mar. Biol. Ann. Rev.* **1990**, *28*, 73–153.

(76)   Aguilera, A.; Souza-Egipsy, V.; San Martín-Úriz, P.; Amils, R. Extracellular matrix assembly in extreme acidic eukaryotic biofilms and their possible implications in heavy metal adsorption. *Aquat. Toxicol.* **2008**, *88*, 257–266.

(77)   Lavoie, I.; Lavoie, M.; Fortin, C. A mine of information: Benthic algal communities as biomonitors of metal contamination from abandoned tailings. *Sci.Total Environ.* **2012**, *425*, 231–241.

(78)   Ancion, P.-Y.; Lear, G.; Dopheide, A.; Lewis, G. D. Metal concentrations in stream biofilm and sediments and their potential to explain biofilm microbial community structure. *Environ. Pollut.* **2013**, *173*, 117–124.

(79)   Guibaud, G.; Vanhullebusch, E.; Bordas, F. Lead and cadmium biosorption by extracellular polymeric substances (EPS) extracted from activated sludges: pH-sorption edge tests and mathematical equilibrium modelling. *Chemosphere* **2006**, *64*, 1955–1962.

(80)   Guibaud, G. Relation between extracellular polymers' composition and its ability to complex Cd, Cu and Pb. *Chemosphere* **2003**, *52*, 1701–1710.

(81)   Holding, K.; Gill, R.; Carter, J. The Relationship between Epilithic Periphyton (Biofilm) Bound Metals and Metals Bound to Sediments in Freshwater Systems. *Environ. Geochem. Health* **2001**, *25*, 87–93.

(82)   Guasch, H.; Admiraal, W.; Sabater, S. Contrasting effects of organic and inorganic toxicants on freshwater periphyton. *Aquat. Toxicol.* **2003**, *64*, 165–175.

(83)   Mehta, S. K.; Gaur, J. P. Use of Algae for Removing Heavy Metal Ions From Wastewater: Progress and Prospects. CRC *Cr. Rev. Biotechn.* **2005**, *25*, 113–152.

(84)   Morin, S.; Duong, T. T.; Dabrin, A.; Coynel, A.; Herlory, O.; Baudrimont, M.; Delmas, F.; Durrieu, G.; Sch fer, J.; Winterton, P.; et al. Long-term survey of heavy-metal pollution, biofilm contamination and diatom community structure in the Riou Mort watershed, South-West France. *Environ. Pollut.* **2008**, *151*, 532–542.

(85)   Bradford, M. M. A rapid and sensitive method for the quantitation of microgram quantities of protein utilizing the principle of protein-dye binding. *Anal. Biochem.* **1976**, *72*, 248–254.

(86)   DuBois, M.; Gilles, K. A.; Hamilton, J. K.; Rebers, P.; Smith, F. Colorimetric method for determination of sugars and related substances. *Anal. Chem.* **1956**, *28*, 350–356.

(87)   Celik, G. Y.; Aslim, B.; Beyatli, Y. Characterization and production of the exopolysaccharide (EPS) from *Pseudomonas aeruginosa* G1 and Pseudomonas putida G12 strains. *Carbohyd. Polym.* **2008**, *73*, 178–182.

(88)   Congestri, R. Seasonal succession of phototrophic biofilms in an Italian wastewater treatment plant: biovolume, spatial structure and exopolysaccharides. *Aquat. Microb. Ecol.* **2006,** *45*, 301–312.

(89)   Meisen, S.; Wingender, J.; Telgheder, U. Analysis of microbial extracellular polysaccharides in biofilms by HPLC. Part I: Development of the analytical method using two complementary stationary phases. *Anal. Bioanal. Chem.* **2008**, *391*, 993–1002.

(90)   Cao, B.; Shi, L.; Brown, R. N.; Xiong, Y.; Fredrickson, J. K.; Romine, M. F.; Marshall, M. J.; Lipton, M. S.; Beyenal, H. Extracellular polymeric substances from *Shewanella sp.* HRCR-1 biofilms: characterization by infrared spectroscopy and proteomics. *Environ. Microbiol.* **2011**, *13*, 1018–1031.

(91)   Zippel, B.; Neu, T. R. Characterization of glycoconjugates of extracellular polymeric substances in tufa-associated biofilms by using fluorescence lectin-binding analysis. *Appl. Environ. Microb.* **2011**, *77*, 505–516.

(92)   Ras, M.; Lefebvre, D.; Derlon, N.; Paul, E.; Girbal-Neuhauser, E. Extracellular Polymeric Substances diversity of biofilms grown under contrasted environmental conditions. *Water Res.* **2011**, *45*, 1529–1538.

(93)   Simon, S.; Païro, B.; Villain, M.; Abzac, P. D.; Van Hullebusch, E.; Lens, P.; Guibaud, G. Evaluation of size exclusion chromatography (SEC) for the characterization of extracellular polymeric substances (EPS) in anaerobic granular sludges. *Bioresource Technol.* **2009**, *100*, 6258–6268.

(94)   Villain, M.; Simon, S.; Bourven, I. The use of a new mobile phase, with no multivalent cation binding properties, to differentiate extracellular polymeric substances (EPS), by size exclusion chromatography (SEC), from biomass used for wastewater treatment. *Process Biochem.* **2010**, *45*, 1415–1421.

(95)   Al-Halbouni, D.; Traber, J.; Lyko, S.; Wintgens, T.; Melin, T.; Tacke, D.; Janot, A.; Dott, W.; Hollender, J. Correlation of EPS content in activated sludge at different sludge retention times with membrane fouling phenomena. *Water Res.* **2008**, *42*, 1475–1488.

(96)   Meng, F.; Drews, A.; Mehrez, R.; Iversen, V.; Ernst, M.; Yang, F.; Jekel, M.; Kraume, M. Occurrence, source, and fate of dissolved organic matter (DOM) in a pilot-scale membrane bioreactor. *Environ. Sci. Technol.* **2009**, *43*, 8821–8826.

(97)   Zheng, X.; Ernst, M.; Jekel, M. Identification and quantification of major organic foulants in treated domestic wastewater affecting filterability in dead-end ultrafiltration. *Water Res.* **2009**, *43*, 238–244.

(98)   Navarro, E.; Robinson, C.; Behra, R. Increased tolerance to ultraviolet radiation (UVR) and cotolerance to cadmium in UVR-acclimatized freshwater periphyton. *Limnol. Oceanogr.* **2008**, *53*, 1149–1158.

(99)   Esposito, S.; Guerriero, G.; Vona, V.; Di Martino Rigano, V.; Carfagna, S.; Rigano, C. Glucose-6P dehydrogenase in *Chlorella sorokiniana* (211/8k): an enzyme with unusual characteristics. *Planta* **2006**, *223*, 796–804.

(100)   Rouwenhorst, R. J.; Frank Jzn, J.; Scheffers, W. A.; van Dijken, J. P.

Determination of protein concentration by total organic carbon analysis. *J. Biochem. Biophys. Methods* **1991**, *22*, 119–128.

(101)   Huber, S. A.; Balz, A.; Abert, M.; Pronk, W. Characterisation of aquatic humic and non-humic matter with size-exclusion chromatography – organic carbon detection – organic nitrogen detection (LC-OCD-OND). *Water Res.* **2011**, *45*, 879–885.

(102)   Liu, H.; Fang, H. H. P. Extraction of extracellular polymeric substances (EPS) of sludges. *J. Biotechnol.* **2002**, *95*, 249–256.

(103)   Takahashi, E.; Ledauphin, J.; Goux, D.; Orvain, F. Optimising extraction of extracellular polymeric substances (EPS) from benthic diatoms: comparison of the efficiency of six EPS extraction methods. *Mar. Freshwater Res.* **2009**, *60*, 1201–1210.

(104)   Liang, Z.; Li, W.; Yang, S.; Du, P. Extraction and structural characteristics of extracellular polymeric substances (EPS), pellets in autotrophic nitrifying biofilm and activated sludge. *Chemosphere* **2010**, *81*, 626–632.

(105)   Sheng, G.-P.; Yu, H.-Q.; Li, X.-Y. Extracellular polymeric substances (EPS) of microbial aggregates in biological wastewater treatment systems: A review. *Biotechnol. Adv.* **2010**, *28*, 882–894.

(106)   van Hullebusch, E. D.; Zandvoort, M. H.; Lens, P. N. L. Metal immobilisation by biofilms: Mechanisms and analytical tools. *Rev. Environ. Sci. Biotechnol.* **2003**, *2*, 9–33.

(107)   Hong, S.; Aryal, R.; Vigneswaran, S.; Johir, M. A. H.; Kandasamy, J. Influence of hydraulic retention time on the nature of foulant organics in a high rate membrane bioreactor. *Desalination* **2012**, *287*, 116–122.

(108)   Jiang, T.; Kennedy, M. D.; Schepper, V. D.; Nam, S.-N.; Nopens, I.; Vanrolleghem, P. A.; Amy, G. Characterization of Soluble Microbial Products and Their Fouling Impacts in Membrane Bioreactors. *Environ. Sci. Technol.* **2010**, *44*, 6642–6648.

(109)   Comte, S.; Guibaud, G.; Baudu, M. Effect of extraction method on EPS from activated sludge: an HPSEC investigation. *J. Hazard. Mater.* **2007**, *140*, 129–137.

(110)   Alasonati, E.; Slaveykova, V. I. Composition and molar mass characterisation of bacterial extracellular polymeric substances by using chemical, spectroscopic and fractionation techniques. *Environ. Chem.* **2011**, *8*, 155–162.

(111)   Kruger, N. J. The Bradford method for protein quantitation. *The protein protocols handbook* **2002**, 15–21.

(112)   Frølund, B.; Palmgren, R.; Keiding, K. Extraction of extracellular polymers from activated sludge using a cation exchange resin. *Water Res.* **1996**, *30*, 1749–1758.

(113)   Nielsen, P.; Jahn, A. Conceptual model for production and composition of exopolymers in biofilms. *Water Sci.Technol.* **1997**, *36*, 11–19.

(114)   D'Souza, F.; Anita, G.; Bhosle, N. B. Seasonal variation in the chemical composition and carbohydrate signature compounds of biofilm. *Aquat. Sci.* **2005**, *41*, 199–207.

(115)   Southey-Pillig, C. J.; Davies, D. G.; Sauer, K. Characterization of Temporal Protein Production in *Pseudomonas aeruginosa* Biofilms. *J. Bacteriol.* **2005**, *187*, 8114–8126.

(116)   Zhang, D.; Pan, X.; Mostofa, K. M. G.; Chen, X.; Mu, G.; Wu, F.; Liu, J.; Song, W.; Yang, J.; Liu, Y.; et al. Complexation between Hg(II) and biofilm

extracellular polymeric substances: An application of fluorescence spectroscopy. *J. Hazard. Mater.* **2010**, *175*, 359–365.

(117)   Zhang, D.; Lee, D.-J.; Pan, X. Fluorescent quenching for biofilm extracellular polymeric substances (EPS) bound with Cu (II). *J. Taiwan Inst. Chem. E.* **2012**, *43*, 450–454.

(118)   Ancion, P.-Y.; Lear, G.; Lewis, G. D. Three common metal contaminants of urban runoff (Zn, Cu & Pb) accumulate in freshwater biofilm and modify embedded bacterial communities. *Environ. Pollut.* **2010**, *158*, 2738–2745.

(119)   Bradac, P.; Behra, R.; Sigg, L. Accumulation of cadmium in periphyton under various freshwater speciation conditions. *Environ. Sci. Technol.* **2009**, *43*, 7291–7296.

(120)   Bradac, P.; Navarro, E.; Odzak, N.; Behra, R.; Sigg, L. Kinetics of cadmium accumulation in periphyton under freshwater conditions. *Environ. Toxicol.* **2009**, *28*, 2108–2116.

(121)   Le Faucheur, S.; Behra, R.; Sigg, L. Phytochelatin induction, cadmium accumulation, and algal sensitivity to free cadmium ion in *Scenedesmus vacuolatus*. *Environ. Toxicol. Chem.* **2005**, *24*, 1731–1737.

(122)   Stewart, T. J.; Traber, J.; Kroll, A.; Behra, R.; Sigg, L. Characterization of extracellular polymeric substances (EPS) from periphyton using liquid chromatography-organic carbon detection-organic nitrogen detection (LC-OCD-OND). *Environ. Sci. Pollut. Res.* **2013**, *20*, 3214–3223.

(123)   Lamelas, C.; Avaltroni, F.; Benedetti, M.; Wilkinson, K. J.; Slaveykova, V. I. Quantifying Pb and Cd complexation by alginates and the role of metal binding on macromolecular aggregation. *Biomacromolecules* **2005**, *6*, 2756–2764.

(124)   Comte, S.; Guibaud, G.; Baudu, M. Biosorption properties of extracellular polymeric substances (EPS) towards Cd, Cu and Pb for different pH values. *J. Hazard. Mater.* **2008**, *151*, 185–193.

(125)   Ha, J.; Gélabert, A.; Spormann, A. M.; Brown, G. E., Jr. Role of extracellular polymeric substances in metal ion complexation on Shewanella oneidensis: Batch uptake, thermodynamic modeling, ATR-FTIR, and EXAFS study. *Geochim. Cosmochim. Ac.* **2010**, *74*, 1–15.

(126)   Comte, S.; Guibaud, G.; Baudu, M. Relations between extraction protocols for activated sludge extracellular polymeric substances (EPS) and complexation properties of Pb and Cd with EPS: Part II. Consequences of EPS extraction methods on Pb^{2+} and Cd^{2+} complexation. *Enzyme Microb. Tech.* **2006**, *38*, 246–252.

(127)   Cordero, B.; Herrero, R.; Lodeiro, P.; de Vicente, M. E. S. Biosorption of Cadmium by *Fucus spiralis*. *Environ. Chem.* **2004**, *1*, 180–187.

(128)   Haug, A. Dissociation of alginic acid. *Acta. Chem. Scand.* **1961**, *15*, 950–952.

(129)   Comte, S.; Guibaud, G.; Baudu, M. Relations between extraction protocols for activated sludge extracellular polymeric substances (EPS) and EPS complexation properties. *Enzyme Microb. Technol.* **2006**, *38*, 237–245.

(130)   Cabaniss, S. E. Forward Modeling of Metal Complexation by NOM: I. A priori Prediction of Conditional Constants and Speciation. *Environ. Sci. Technol.* **2009**, *43*, 2838–2844.

(131)   Taillefert, M.; Lienemann, C.; Gaillard, J.; Perret, D. Speciation, reactivity, and cycling of Fe and Pb in a meromictic lake. *Geochim. Cosmochim. Ac.* **2000**, *64*, 169–183.

(132) Müller, B.; Sigg, L. Interaction of trace metals with natural particle surfaces: Comparison between adsorption experiments and field measurements. *Aquat. Sci.* **1990**, *52*, 75–92.

(133) Beck, A. J.; Janssen, F.; Polerecky, L.; Herlory, O.; de Beer, D. Phototrophic Biofilm Activity and Dynamics of Diurnal Cd Cycling in a Freshwater Stream. *Environ. Sci. Technol.* **2009**, *43*, 7245–7251.

(134) Meylan, S.; Behra, R.; Sigg, L. Accumulation of Copper and Zinc in Periphyton in Response to Dynamic Variations of Metal Speciation in Freshwater. *Environ. Sci. Technol.* **2003**, *37*, 5204–5212.

(135) Guasch, H.; Serra, A.; Corcoll, N.; Bonet, B.; Leira, M. Metal Ecotoxicology in Fluvial Biofilms: Potential Influence of Water Scarcity. In *The Handbook of Environmental Chemistry*; Sabater, S.; Barceló, D., Eds.; Springer Berlin Heidelberg: Berlin, Heidelberg, 2009; Vol. 8, pp. 41–53.

(136) Fisher, N. S.; Reinfelder, J. R. The trophic transfer of metals in marine systems. In *Metal Speciation and Bioavailability in Aquatic Systems*; Tessier, A.; Turner, D. R., Eds.; Wiley, 1995; pp. 363–406.

(137) Clearwater, S. J.; Farag, A. M.; Meyer, J. S. Bioavailability and toxicity of dietborne copper and zinc to fish. *Comp. Biochem. Phys. C* **2002**, *132*, 269–313.

(138) Morin, S.; Duong, T. T.; Herlory, O.; Feurtet-Mazel, A.; Coste, M. Cadmium Toxicity and Bioaccumulation in Freshwater Biofilms. *Arch. Environ. Contam. Toxicol.* **2007**, *54*, 173–186.

(139) Jakob, T.; Schreiber, U.; Kirchesch, V.; Langner, U.; Wilhelm, C. Estimation of chlorophyll content and daily primary production of the major algal groups by means of multiwavelength-excitation PAM chlorophyll fluorometry: performance and methodological limits. *Photosyn. Res.* **2005**, *83*, 343–361.

(140) Tlili, A.; Maréchal, M.; Montuelle, B.; Volat, B.; Dorigo, U.; Berard, A. Use of the MicroResp™ method to assess pollution-induced community tolerance to metals for lotic biofilms. *Environ. Pollut.* **2011**, *159*, 18–24.

(141) Bere, T.; Tundisi, J. G. Cadmium and lead toxicity on tropical freshwater periphyton communities under laboratory-based mesocosm experiments. *Hydrobiologia* **2012**, *680*, 187–197.

(142) Sánchez-Marín, P.; Fortin, C.; Campbell, P. G. C. Lead (Pb) and copper (Cu) share a common uptake transporter in the unicellular alga *Chlamydomonas reinhardtii. Biometals* **2014**, *27*, 173–181.

(143) Meylan, S.; Behra, R.; Sigg, L. Influence of Metal Speciation in Natural Freshwater on Bioaccumulation of Copper and Zinc in Periphyton: A Microcosm Study. *Environ. Sci. Technol.* **2004**, *38*, 3104–3111.

(144) Behra, R.; Landwehrjohann, R.; Vogel, W.; Wagner, B.; Sigg, L. Copper and zinc content of periphyton from two rivers as a function of dissolved metal concentration. *Aquat. Sci.* **2002**, *64*, 300–306.

(145) Dong, D.; Nelson, Y. M.; Lion, L. W.; Shuler, M. L.; Ghiorse, W. C. Adsorption of Pb and Cd onto metal oxides and organic material in natural surface coatings as determined by selective extractions: new evidence for the importance of Mn and Fe oxides. *Water Res.* **2000**, *34*, 427–436.

(146) Wilson, A. R.; Lion, L. W.; Nelson, Y. M.; Shuler, M. L.; Ghiorse, W. C. The Effects of pH and Surface Composition on Pb Adsorption to Natural Freshwater Biofilms. *Environ. Sci. Technol.* **2001**, *35*, 3182–3189.

(147) Dong, D.; Derry, L. A.; Lion, L. W. Pb scavenging from a freshwater lake by Mn oxides in heterogeneous surface coating materials. *Water Res.* **2003**,

37, 1662–1666.

(148) Nelson, Y. M.; Lion, L. W.; Shuler, M. L.; Ghiorse, W. C. Effect of Oxide Formation Mechanisms on Lead Adsorption by Biogenic Manganese (Hydr)oxides, Iron (Hydr)oxides, and Their Mixtures. *Environ. Sci. Technol.* **2002**, *36*, 421–425.

(149) Finkel, Z. V.; Quigg, A.; Raven, J. A.; Reinfelder, J. R. Irradiance and the elemental stoichiometry of marine phytoplankton. *Limnol. Oceanogr.* **2006**, *51*, 2690–2701.

(150) Twining, B. S.; Baines, S. B.; Bozard, J. B.; Vogt, S.; Walker, E. A.; Nelson, D. M. Metal quotas of plankton in the equatorial Pacific Ocean. *Deep-Sea Res. Pt. II* **2011**, *58*, 325–341.

(151) Gil-Allué, C.; Schirmer, K.; Tlili, A.; Gessner, M. O.; Behra, R. Short-term effects of silver nanoparticles on stream periphyton. *Environ. Sci. Technol. in submission*.

(152) Lin, H.-Y.; Shih, C.-Y.; Liu, H.-C.; Chang, J.; Chen, Y.-L.; Chen, Y.-R.; Lin, H.-T.; Chang, Y.-Y.; Hsu, C.-H.; Lin, H.-J. Identification and characterization of an extracellular alkaline phosphatase in the marine diatom *Phaeodactylum tricornutum*. *Mar. Biotechnol.* **2013**, *15*, 425–436.

(153) Chrost, R. J. Microbial Enzymes in Aquatic Environments; Springer Verlag, 1991.

(154) Lazzaro, A.; Schulin, R.; Widmer, F.; Frey, B. Changes in lead availability affect bacterial community structure but not basal respiration in a microcosm study with forest soils. *Sci. Total Environ.* **2006**, *371*, 110–124.

(155) Le Faucheur, S.; Behra, R.; Sigg, L. Thiol and Metal Contents in Periphyton Exposed to Elevated Copper and Zinc Concentrations: A Field and Microcosm Study. *Environ. Sci. Technol.* **2005**, *39*, 8099–8107.

(156) Gustafsson, J. P. Visual MINTEQ. http://vminteq.lwr.kth.se/

(157) Millet, H.; Jowett, M. The solubilities of lead phosphates. *J. Am. Chem. Soc.* **1929**, 51, 997–1004.

(158) Bock, J. L. The binding of metal ions to ATP: a proton and phosphorus nmr investigation of diamagnetic metal-ATP complexes. *J. Inorg. Biochem.* **1980**, *12*, 119–130.

(159) Mah, V.; Jalilehvand, F. Lead(II) Complex Formation with Glutathione. *Inorg. Chem.* **2012**, *51*, 6285–6298.

(160) Szlachetko, J.; Nachtegaal, M.; de Boni, E.; Willimann, M.; Safonova, O.; Sa, J.; Smolentsev, G.; Szlachetko, M.; van Bokhoven, J. A.; Dousse, J. C.; et al. A von Hamos x-ray spectrometer based on a segmented-type diffraction crystal for single-shot x-ray emission spectroscopy and time-resolved resonant inelastic x-ray scattering studies. *Rev. Sci. Instrum.* **2012**, *83*, 103105.

(161) Webster, R. E.; Dean, A. P.; Pittman, J. K. Cadmium Exposure and Phosphorus Limitation Increases Metal Content in the Freshwater Alga *Chlamydomonas reinhardtii*. *Environ. Sci. Technol.* **2011**, *45*, 7489–7496.

(162) Simon, M.; Schmitt, T. Progress in resonant inelastic X-ray scattering. *J. Electron Spectrosc.* **2013**, *188*.

(163) Volland, S.; Andosch, A.; Milla, M.; Stöger, B.; Lütz, C.; Lütz-Meindl, U. Intracellular metal compartmentalization in the green algal model system *micrasterias denticulata* (streptophyta) measured by transmission electron microscopy-coupled electron energy loss spectroscopy. *J. Phycol.* **2011**, *47*, 565–579.

(164)   Piccapietra, F.; Allue, C. G.; Sigg, L.; Behra, R. Intracellular Silver Accumulation in *Chlamydomonas reinhardtii* upon Exposure to Carbonate Coated Silver Nanoparticles and Silver Nitrate. *Environ. Sci. Technol.* **2012**, *46*, 7390–7397.

(165)   Keasling, J. D. Regulation of intracellular toxic metals and other cations by hydrolysis of polyphosphate. *Ann. N. Y. Acad. Sci.* **1997**, *829*, 242–249.

(166)   Ruiz, F. A.; Marchesini, N.; Seufferheld, M.; Govindjee; Docampo, R. The polyphosphate bodies of *Chlamydomonas reinhardtii* possess a proton-pumping pyrophosphatase and are similar to acidocalcisomes. *J. Biol. Chem.* **2001**, *276*, 46196–46203.

(167)   Lavoie, M.; Le Faucheur, S.; Fortin, C.; Campbell, P. G. C. Cadmium detoxification strategies in two phytoplankton species: Metal binding by newly synthesized thiolated peptides and metal sequestration in granules. *Aquat. Toxicol.* **2009**, *92*, 65–75.

(168)   Nishikawa, K.; Yamakoshi, Y.; Uemura, I.; Tominaga, N. Ultrastructural changes in *Chlamydomonas acidophila* (Chlorophyta) induced by heavy metals and polyphosphate metabolism. *FEMS Microbiol. Ecol.* **2003**, *44*, 253–259.

(169)   Martínez, C. E.; Jacobson, A. R.; McBride, M. B. Lead Phosphate Minerals: Solubility and Dissolution by Model and Natural Ligands. *Environ. Sci. Technol.* **2004**, *38*, 5584–5590.

(170)   Harrison, P. G.; Healy, M. A. The reaction of lead (II) acetate with dimethylphosphite. A model for the interaction with ATP. *Inorg. Chim. Acta* **1983**, *80*, 279–285.

(171)   Sigel, H.; Da Costa, C.; Martin, R. Interactions of lead(II) with nucleotides and their constituents. *Coordin. Chem. Rev.* **2001**, *219*, 435–461.

(172)   Howe, G.; Merchant, S. Heavy Metal-Activated Synthesis of Peptides in *Chlamydomonas reinhardtii*. *Plant Physiol.* **1992**, *98*, 127–136.

(173)   Kowshik, M.; Vogel, W.; Urban, J.; Kulkarni, S.; Paknikar, K. Microbial synthesis of semiconductor PbS nanocrystallites. *Adv. Mater.* **2002**, *14*, 815–818.

(174)   Seshadri, S.; Saranya, K.; Kowshik, M. Green synthesis of lead sulfide nanoparticles by the lead resistant marine yeast, *Rhodosporidium diobovatum*. *Biotechnol. Progress* **2011**, *27*, 1464–1469.

(175)   Hu, S.; Lau, K. W. K.; Wu, M. Cadmium sequestration in *Chlamydomonas reinhardtii*. *Plant Sci* **2001**, *161*, 987–996.

(176)   Tulkki, J.; Aberg, T. Behavior of Raman Resonance Scattering Across the K-X-Ray Absorption-Edge. *J. Phys. B At. Mol. Opt.* **1982**, *15*, L435–L440.

(177)   Rehr, J. J.; Kas, J. J.; Vila, F. D.; Prange, M. P.; Jorissen, K. Parameter-free calculations of X-ray spectra with FEFF9. *Phys. Chem. Chem. Phys.* **2010**, *12*, 5503–5513.

(178)   Campbell, J. L.; Papp, T. Widths of the atomic k–n7 levels. *Atomic Data Nucl. Data* **2001**, *77*, 1–56.

(179)   Deslattes, R.; Kessler, E.; Indelicato, P.; de Billy, L.; Lindroth, E.; Anton, J. X-ray transition energies: new approach to a comprehensive evaluation. *Rev. Mod. Phys.* **2003**, *75*, 35–99.

(180)   Ortega, R. Direct speciation analysis of inorganic elements in single cells using X-ray absorption spectroscopy. *J. Anal. At. Spectrom.* **2010**, *26*, 23–29.

(181)   Chen, G.; Chen, X.; Yang, Y.; Hay, A. G.; Yu, X.; Chen, Y. Sorption and

distribution of copper in unsaturated *Pseudomonas putida* CZ1 biofilms as determined by X-ray fluorescence microscopy. *Appl. Environ. Microb.* **2011**, *77*, 4719–4727.

(182) Nelson, Y. M.; Lion, L. W.; Shuler, M. L.; Ghiorse, W. C. Lead binding to metal oxide and organic phases of natural aquatic biofilms. *Limnol. Oceanogr.* **1999**, *44*, 1715–1729.

(183) Soto-Jiménez, M. F.; Arellano-Fiore, C.; Rocha-Velarde, R.; Jara-Marini, M. E.; Ruelas-Inzunza, J.; Páez-Osuna, F. Trophic transfer of lead through a model marine four-level food chain: *Tetraselmis suecica*, *Artemia franciscana*, *Litopenaeus vannamei*, and *Haemulon scudderi*. *Arch. Environ. Contam. Toxicol.* **2011**, *61*, 280–291.

(184) Suedel, B. C.; Boraczek, J. A.; Peddicord, R. K.; Clifford, P. A.; Dillon, T. M. Trophic transfer and biomagnification potential of contaminants in aquatic ecosystems. *Rev. Environ. Contam. Toxicol.* **1994**, *136*, 21–89.

(185) Weis, J. S. Bioaccumulation/Storage/Detoxification. In *Physiological, Developmental and Behavioral Effects of Marine Pollution*; Springer Netherlands: Dordrecht, 2014; pp. 355–392.

(186) Goto, D.; Wallace, W. G. Relevance of intracellular partitioning of metals in prey to differential metal bioaccumulation among populations of mummichogs (*Fundulus heteroclitus*). *Mar. Environ. Res.* **2009**, *68*, 257–267.

(187) Wallace, W. G.; Lopez, G. R. Relationship between Subcellular Cadmium Distribution in Prey and Cadmium Trophic Transfer to a Predator. *Estuaries* **1996**, *19*, 923–930.

Acknowledgments

First and foremost, I would like to thank **Laura** for her supervision and support over the years. Laura, we often joke about this, but now I have to officially put it down in writing! Eight years ago you received an email from an unknown 20-year-old American student asking if you had any space in your lab for a summer internship. I still look back on the moment (after waiting anxiously for two weeks) when I received your email. To my amazement you invited me for the summer without knowing anything about me, and with that invitation you gave me an opportunity that literally changed the course of my life. Little did either of us know that a wonderful ten week summer internship would evolve into a Bachelors, Masters, and now finally the Ph.D. thesis. You have contributed work of great significance to the field of aquatic chemistry and, as your last Ph.D. student, I hope that I can continue to carry forward all the unfinished work, bringing meaningful findings to the field as you have done.

First day at Eawag (or maybe the second if it was a Monday), I met a woman filled with such incredible energy, fire, enthusiasm, and innate curiosity it was infectious. **Tati**, thank you for your co-supervision over these years when I, the chemist, had puzzling biological questions that needed to be worked out, for lots of laughs over morning coffee breaks, and interesting and spontaneous lunch discussions about the latest crazy results. However, what has touched me the most over these years is your genuine caring of the people around you. You have been there in support, not only with respect to work, but also during difficult personal times. For this, I sincerely thank you.

One day I had this crazy idea that it would be fun to use an incredibly abstract technique (to the biologist), on a complex biological sample (to the physicist), targeting a metal that is inherently a pain in the butt to measure (to the chemist). To my pleasant surprise **Maarten** said, "great, let's try to measure your algae that takes up lead!" Not sure if either of us knew the journey ahead (a common theme it seems). What started out as a hunch, a side project, and then a not-so-side project, coincidentally lead to an incredible piece of work in the end. Maarten, thank you for jumping into this project, bringing your invaluable ideas to the table, and having the patience and perseverance during these last two years. We certainly ended on a high note. Also huge thanks to **Jakub** for his incredible effort in the project, the data analysis, and his incredible humor through it all. Without your humor pointing to the insanity of this project, I don't think I would have come back for all those beamtimes.

A big thanks to **all the people in Utox** for creating a fun and open atmosphere. **Bettina**, you have been there right from the start helping me incredibly in my first few years. I will never forget our "Wettbewerb" to see how fast we could add EDTA to get a 5 second exposure time point. *Real science nerds*. You are a wonderful person and have been a wealth of knowledge. **David**, **Adi**, and **Ursi**, my metal-analyzing experts and helping hands. **Jacqueline** for her help with LC-OCD-OND, **Regula** for periphyton characterization, and **Irene B.** for CNS analysis. **Marc**, always being there for feedback, telling me the names of unknown birds, and able to answer almost every administrative question. **Franziska**, the wonder woman of making all logistical things possible. Blast from the past crew: **Stefanie**, **Ilona**, **Enrique**, **Miriam**, **Christian**, **Irene S.**, **Flavio** wherever you are now, thanks for the hikes and great laughs over the years. **Carmen**, my official periphyton scraping buddy. Shared lots of laughs in times of sheer agony and frustration over the insanity of working with complicated slime. **Alex,** for helping create a great VH setup, thus preventing certain death by electrocution or asbestos inhalation. **Smitha**, always was there for crazy experiments and conversations ranging from science, to life, to informing me of the gossip in the department (even though I am still always the last to know things). The F-stock crew, **Muris** – lots of laughs and good coffee, **Linn** – non-stop positive energy sharing some great times this year. **Anke,** for the excruciating process of translating way to complicated English sentences into German. **Kristin,** for your support and constant curiosity in the lab as well as outside. Looking forward to the years ahead.

Curriculum Vitae

Theodora J. Stewart

Department of Environmental Toxicology
Eawag: Swiss Federal Institute of Aquatic Science and Technology
Überlandstrasse 133
6800 Dübendorf, Switzerland

Date of Birth: 13 September 1985
Nationality: American
Languages: English (native); German (proficient); Spanish, French, Lithuanian (basic)

EDUCATION

MSc ETH Umweltnaturwissenschaften (2010) ETHZ, Zürich, Switzerland

B.A. Chemistry (2007) Wellesley College, Wellesley, MA

RESEARCH & WORK EXPERIENCE

ETHZ, Zürich, Switzerland. TA. 2012, 2013
    Supervisor: Dr. Laura Sigg
    Teaching assistance for bachelors course Aquatic Chemistry

Eawag, Dübendorf, Switzerland. Researcher. 2006, 2007.
    Supervisors: Dr. Laura Sigg and Dr. Renata Behra

GRANTS & AWARDS

Best Platform Presentation, CSC Environmental Division, 2013

Swiss National Science Foundation Research Grant, 2010

Excellence Scholarship & Opportunity Program (ETHZ), 2009

Magna Cum Laude, 2007

Phi Beta Kappa, 2007

Sigma Xi (National Science Honors Society), 2007

The Jean V. Crawford Prize in Chemistry, 2007

Jerome A. Schiff Fellowship for Honors Thesis, 2007

Howard Hughes Medical Institute (HHMI) Research Grant, 2006, 2007.

Woods Hole Oceanographic Institute Summer Internship Scholarship (declined), 2006.

PAPERS

Stewart, T. J, Behra, R., Sigg, L. Impact of chronic lead exposure on metal distribution and biological effects to periphyton. In submission to *Environmental Science and Technology*.

Stewart, T. J., and Szlachetko, J., Sigg, L., Behra, R., Nachtegaal, M. Tracking the temporal dynamics of intracellular metal speciation. In submission to *PNAS*.

Zhurov, K. O. & Stewart, T. J. Conference report CH analysis 2013. *Chimia (Aarau)* **68**, 331 (2014)

Stewart, T. J., Traber, J., Kroll, A., Behra, R. & Sigg, L. Characterization of extracellular polymeric substances (EPS) from periphyton using liquid chromatography-organic carbon detection-organic nitrogen detection (LC-OCD-OND). *Environ Sci Pollut Res Int* **20,** 3214–3223 (2013).

Stewart, T. J.; Yau, J. H.; Allen, M. M.; Brabander, D. J.; Flynn, N. T. Impacts of Calcium-Alginate Density on Equilibrium and Kinetics of Lead(II) Sorption onto Hydrogel Beads. *Colloid Polym. Sci.* **287**, 1033–1040 (2009)

"Chemical Characterization of the Periphyton Matrix"
    Thesis: ETH Zürich, Switzerland. July, 2010

"Investigation and Application of C. reinhardtii for the Removal of Lead(II) from Freshwater"
    Thesis: Wellesley College, MA. December, 2007

PRESENTATIONS

Tracking intracellular Pb speciation dynamics in the green alga C. reinhardtii
    Presentation: CHanalysis, Beatenberg, Switzerland. November, 2013

Determination of intracellular Pb speciation in the green alga C. reinhardtii Using High Energy Resolution Fluorescence Detected-Resonance Inelastic X-Ray Scattering
    Presentation: Canadian Chemistry Society (CSC), Québec, Canada. May 2013

Intracellular Speciation of Pb the in Green Alga C. reinhardtii using High Energy Resolution Fluorescence Detected X-ray Absorption Spectroscopy
    Presentation: SETAC North America, Long Beach, CA. November 2012.

Lead Binding to Periphyton Extracellular Matrix
    Presentation: Chemodynamics and Biointerfaces, Monte Verità, Switzerland. October 2011.

Characterization of Extracellular Matrix of Algal Biofilms
    Poster: SETAC Europe, Seville, Spain. May 2010

Investigation and Application of C. reinhardtii for the Removal of Lead(II) from Freshwater
    Poster: ACS, New Orleans, LA. April 2008